Clim. Past, 22, 1305–1362, 2026
https://doi.org/10.5194/cp-22-1305-2026

Climate of the Past
Open Access
EGU

Pleistocene benthic foraminifera bioevents in the Central Arctic Ocean: stratigraphic and paleoceanographic implications

Jutta E. Wollenburg and Jens Matthiessen

Alfred Wegener Institute Helmholtz Centre for Polar and Marine Research, Bremerhaven, 27570, Germany

Correspondence: Jutta E. Wollenburg (jutta.wollenburg@awi.de)

Received: 16 December 2025 – Discussion started: 29 December 2025
Revised: 13 May 2026 – Accepted: 29 June 2026 – Published: 21 July 2026

Abstract. Benthic foraminifera show distinct temporal and spatial distribution patterns in the Central Arctic Ocean (CAO) demonstrating their potential to provide robust age constraints and to address paleoceanographic change in the Pleistocene. Several benthic foraminifera bioevents have been previously reported from the Pleistocene that are critically evaluated here by studying three sediment cores from the Mendeleev and Lomonosov ridges and analysing published data sets. Based on these data bioevents are defined by using absolute abundances of species in the $> 63\,\mu m$ grain-size fraction, whereas relative abundances are considered not reliable because taphonomic processes such as disintegration and/or dissolution overprint the original assemblage composition. Bioevents are correlated to lithological horizons, and linked to marine isotope stages (MIS) based on available independent stratigraphic data.

Three calcareous bioevents can be defined in the Middle Pleistocene: (1) the highest common occurrence of *Bolivina arctica* (∼MIS 9), (2) the lowest common occurrence of *Oridorsalis umbonatus* (∼MIS 7), and (3) the acme of *Bulimina aculeata* (∼MIS 7) in water depths of less than ∼ 2000 m. The lowest common occurrence of *Oridorsalis umbonatus* is coeval with the base of the acme of *Bulimina aculeata* at shallow sites. Since the number of radiometric and biostratigraphic ages is limited, the proposed correlation of bioevents to marine isotope stages should be considered provisional.

Further benthic foraminifera bioevents may be useful for stratigraphic correlation on a regional to supra-regional scale but require evaluation of previous taxonomic identifications and additional sediment core studies. The extinct agglutinated species *Haplophragmoides obscurus* disappeared at the Lomonosov Ridge in the Middle Pleistocene but the complex taxonomy and the few data on the occurrence in Arctic sediment cores currently prohibits the application as biostratigraphic marker. The assemblage turnover from agglutinated to calcareous benthic foraminifera occurred close to the first downcore change of normal to reverse magnetic polarity at the Lomonosov Ridge and Morris Jesup Rise and might be a synchronous event in the eastern Arctic Ocean in middle Pleistocene sediments older than MIS 11. However, this fundamental change in assemblage composition is time-transgressive across the Arctic Ocean because it occurred in the Amerasian Basin in the Early Pleistocene.

The bioevents in the CAO are caused by a complex interplay of various biological processes. Apart from *B. arctica* and *H. obscurus* that likely evolved in the Arctic Ocean, *B. aculeata* and *O. umbonatus* must have invaded the Arctic Ocean from subpolar latitudes. Since an unrestricted exchange of intermediate to deep-water masses with subpolar latitudes is only facilitated through the Fram Strait and the Barents Sea, these intermediate to deep-water species had to be transported as juvenile specimens (propagules) by Atlantic Water to CAO sites during time periods favourable for their propagation. The maximum reachable location for settlement within the Arctic Ocean depended on the species, the local environmental conditions, and the strength of Atlantic Water advection. Environmental conditions, in particular the availability of food, played then a major role for the successful colonization at a particular site, not only for the invading species but also for the species endemic to the CAO (*H. obscurus*, *B. arctica).* These sites must have faced a high (*H. obscurus*, *B. arctica*, *O. umbonatus*) or significantly higher particulate organic carbon export to the sea floor than today (*B. aculeata*). Such environmental conditions must have occurred basin-wide to trigger the synchronous and coincident changes in assemblage compositions. Moreover, ex-

ternal forcing may have triggered environmental change. A massive discharge of detrital dolomite-rich ice-rafted debris might have induced the abrupt collapse of a *Bolivina arctica* dominated fauna and imminent disappearance of *Haplophragmoides obscurus*. The most conspicuous change in the environment is expressed in the turnover from a predominance of agglutinated to calcareous benthic foraminifera which was either caused by a fundamental change in food supply and its quality or by corrosive bottom waters. In general, due to selective dissolution of thin-shelled epifaunal taxa, assemblages are enriched in robust epifaunal and/or infaunal calcareous species, or may consist only of an agglutinated taphocoenosis.

1 Introduction

The Pleistocene biostratigraphy and paleoceanography of the Arctic Ocean is rather challenging because ecologic and taphonomic processes such as temperature gradients, dissolution and degradation in the water column and sediments limit the applicability of the routinely used planktic microfossil groups in the Pleistocene. Calcareous microfossils (coccoliths, foraminifera) are more prominent than biosiliceous and organic-walled microfossils but assemblages have a low diversity and taxa are only discontinuously present (e.g., Herman, 1974; Herman et al., 1989; Cronin et al., 2008; Backman et al., 2009; Razmjooei et al., 2023). Biosiliceous microfossils are largely absent in Pleistocene sediments while organic-walled palynomorphs (e.g. dinoflagellate cysts) are sparse and occur only in certain stratigraphic intervals (e.g., Mudie, 1985; Herman et al., 1989; Matthiessen et al., 2018).

In the CAO the long polar night and, except for occasional leads, the permanent ice cover results in a low primary production that varies over time and by region (e.g., Mar, 2014). Together with the very low surface water temperatures, these factors are critical for many fossilizable planktic organisms such coccolithophores, foraminifera, and dinoflagellates which generally prefer warmer open-waters rather than Arctic conditions. In planktic foraminifera, maximum adaptability to this harsh environment results in net catches under the permanent ice cover consisting of $> 90\,\%$ of the polar species *Neogloboquadrina pachyderma*, the only species reproducing under perennial sea ice, whereas accessory species are advected from further south (e.g., Carstens and Wefer, 1992; Vermassen et al., 2025). Since *N. pachyderma* also has the thickest shell of all planktic foraminifera encountered, thin-shelled subpolar species usually disintegrate during descent, and dissolve at the sediment surface, resulting in relative abundances of $> 98\,\%$ *N. pachyderma* in sediment samples (Herman, 1964; Eynaud et al., 2009; O'Regan et al., 2019).

In contrast, benthic foraminifera are the most diverse and widespread microfossil group in the Arctic Ocean, and approximately 400 living and dead calcareous and agglutinated species have been recorded from the different environments (e.g., Lagoe, 1977; Scott and Vilks, 1991; Wollenburg, 1992; Bergsten, 1994; Ishman and Foley, 1996; Hald and Korsun, 1997; Wollenburg and Mackensen, 1998a, b; Wollenburg and Kuhnt, 2000; Polyak et al., 2002; Saidova, 2011; Husum et al., 2015; Kniazeva and Korsun, 2019). Due to their adaption to different ecological niches in outer estuarine to deep-sea sediments, benthic foraminifera have a strongly variable spatial and temporal distribution and depict pronounced changes in assemblage composition in the Arctic Ocean. Based on summer field data, the distribution of living benthic foraminifera and their abundance in the Arctic Ocean are mainly determined by food availability and competition, although additional ecological aspects such as currents and temperature are also relevant for some species (Wollenburg and Mackensen, 1998a; Wollenburg and Kuhnt, 2000; Husum et al., 2015).

Benthic foraminifera species have not been thoroughly utilized as biostratigraphic and paleoceanographic proxy in the Pleistocene Arctic Ocean although O'Neill (1981) already demonstrated by analysing a set of sediment cores that benthic foraminifera have distinct stratigraphic ranges and form different benthic biofacies in the Amerasian Basin. The biostratigraphic applicability is limited by the low evolutionary turnover of deep-sea benthic foraminifera (Van Morkhoven et al., 1986; Thomas, 2007; Mckinney, 1987) generally leading to few appearances and extinctions of taxa in the Pleistocene (e.g., Buzas and Culver, 1989; Kawagata et al., 2005, 2007; Hayward, 2001; Hayward et al., 2007; Mancin et al., 2013; Kender et al., 2016). Therefore, most species previously used for Arctic Ocean biostratigraphy have a long stratigraphic range on a global scale (e.g., *Pullenia bulloides*, *Epistominella exigua*, *Bulimina aculeata*, *Oridorsalis umbonatus*, Holbourn et al., 2013). On the Pleistocene time scale, however, benthic records from the adjacent Norwegian-Greenland Sea up to the Barents Sea continental shelf show that abundance maxima may be useful stratigraphic bioevents if these were calibrated to an independent time scale. Here, acmes of *Siphotextularia rolshauseni* and *Pullenia bulloides* mark certain time intervals in MIS 2 and 5, respectively (e.g., Nees and Struck, 1994; Haake et al., 1992; Wollenburg et al., 2001b). In the CAO, stratigraphic occurrences of selected species have been frequently used to assign isotope stages to foraminifer-rich intervals and to correlate such layers across the Arctic Ocean (e.g., Ishman et al., 1996; Backman et al., 2004; Polyak et al., 2004, 2013; Nørgaard-Pedersen et al., 2007a, b; Adler et al., 2009; Cronin et al., 2013, 2014, 2019a; Lazar and Polyak, 2016; Zhao et al., 2022; Hanslik et al., 2013; Kaufman et al., 2008; Xiao et al., 2020). However, faunal counts and quantitative data are rarely reported and therefore compilations exclusively based on presence/absence data may lead to rather inconsis-

tent occurrences in different sediment cores (e.g., *Bulimina aculeata*, Alexanderson et al., 2014). Moreover, previous age assignments of such events are now outdated because of recent progress in $^{230}Th_{xs}$ dating and coccolith biostratigraphy (Hillaire-Marcel et al., 2017; Song et al., 2023; Razmjooei et al., 2023). Despite these limitations, calcareous benthic foraminifera may generally provide valuable tie points for stratigraphic correlation between Lomonosov, Mendeleev, and Northwind ridges (e.g., Backman et al., 2004; Polyak et al., 2004; Cronin et al., 2014). Benthic foraminifera bioevents have the potential to improve the still imprecise Pleistocene Arctic Ocean chronostratigraphy if these events were defined based on stratigraphic ranges and abundance patterns of individual species, and their regional/supra-regional synchroneity tested by calibration to an independent chronology.

The paleoceanographic applicability is strongly hampered by the variable preservation of species often leading to the enrichment of robust thick-shelled taxa (Loubere and Rayray, 2016). Moreover, agglutinated taxa are often excluded from benthic foraminifera analysis although agglutinated species dominate in lower Pleistocene sediments (O'Neill, 1981; Scott et al., 1989; Evans and Kaminski, 1998; Cronin et al., 2008). This may result in a lower number of species, with increased relative abundance, lowered specimen numbers per sample weight and the loss of any faunal information on samples devoid of calcareous taxa. In practice, only a few species are often used for paleoceanographic interpretations, regardless of their proportion of the total assemblage.

Here, we primarily evaluate the potential of the calcareous benthic foraminifera *Bolivina arctica*, *Bulimina aculeata, Cassidulina neoteretis*, *Epistominella arctica*, *E. exigua*, *Oridorsalis umbonatus* and *Pullenia* spp. and the agglutinated foraminifera *Haplophragmoides obscurus* as biostratigraphic and paleoceanographic markers in the Pleistocene based primarily on absolute (specimens/gram dry sediment in the size fraction $> 63\,\mu m$) and secondly on relative abundances. Since previous benthic foraminifera research has mainly focused on sediment cores retrieved from relatively shallow water depths (500–< 1900 m) (e.g., Scott et al., 1989; Ishman et al., 1996; Jakobsson et al., 2001; Backman et al., 2004; Polyak et al., 2004; Cronin et al., 2008, 2013, 2014; Lazar and Polyak, 2016), we used the relatively well-studied core PS2185-6 from the Lomonosov Ridge (1073 m water depth) as reference core for such sites (Fig. 1, Table 1). However, as the Lomonosov Ridge represents a barrier to deep water exchange > 1870 m between the Eurasian Basin and Amerasian Basin (Björk et al., 2007), deep-water sites must be considered for a reconstruction of paleo-deep water circulation/change within the Arctic basins and to assess the applicability of benthic bioevents. To take this into account, we also studied sediment cores PS72/396-5 and PS72/340-5 retrieved from ∼ 2300 and ∼ 2700 m water depth, respectively, at the western Mendeleev Ridge (Fig. 1). Moreover, the three selected sediment cores also cover a range of average sedimentation rates on the order of ca. 1 to 10 mm kyrs^{-1}. Bioevents in these cores are compared with published data to assess the spatial and temporal relationship between bioevents in the western and eastern Arctic Ocean. The individual bioevents are calibrated to independent chronostratigraphic data and lithological marker beds to reveal a possible synchroneity on a regional or supra-regional scale. Finally, ecological and taphonomic processes are discussed that may have caused the formation of these bioevents and influence their applicability for paleoceanographic reconstructions.

2 Material and Methods

2.1 Sediment cores

Benthic foraminifera have been studied in sediment cores PS72/340-5 and PS72/396-5 from the Amerasian Basin west of the southern Mendeleev Ridge and in core PS2185-6 from the central Lomonosov Ridge (Fig. 1). Primarily, the uppermost core sections that are characterized by normal magnetic polarity (Brunhes Chron, Frederichs, 1995; Bazhenova, 2012; Elkina et al., 2023) were studied because this interval comprises the foraminiferal events used previously for stratigraphic correlation (e.g., Backman et al., 2004; Polyak et al., 2004). The sediment cores were sampled at variable depth intervals in 1 cm-thick slices at the *Polarstern* Core Repository in Bremerhaven (Germany) depending on the expected foraminifera content. The mid-depth of the sample is used in this study. The brown layers were sampled at a higher resolution because these layers are usually more productive for foraminifera (e.g., Polayk et al., 2004; Adler et al., 2009). All sediment cores referred to in the text are shown in Fig. 1 and the meta data are listed in Table 1.

2.2 Foraminifera analysis

2.2.1 Sample preparation

The samples of the sediment cores were freeze-dried to determine the number of specimens per gram dry sediment. Freeze-drying and wet-sieving is preferred to oven drying because simple oven drying of sediments can lead to alterations in shell-based proxies in organic-rich sediments due to dissolution or artificial precipitation on calcareous foraminifera (Sperling et al., 2002). Saraswat et al. (2020) reported significant faunal loss in dead foraminifera shells in their modern estuarine samples when results from wet-sieved samples were compared with those of freeze-dried samples. If present, loosely agglutinated foraminifera disintegrate soon after depth within the first 2–4 cm, leaving just robust agglutinated taxa in fossil assemblages. In contrast to Saraswat et al. (2020) we do not observe fragmentation of thin-shelled calcareous taxa (e.g. Fig. 2) when applying freeze-drying. Thus, sediment samples of the three Kastenlot cores were freeze-dried as routinely done in many other studies on foraminifera faunas (e.g., Devendra et al., 2023;

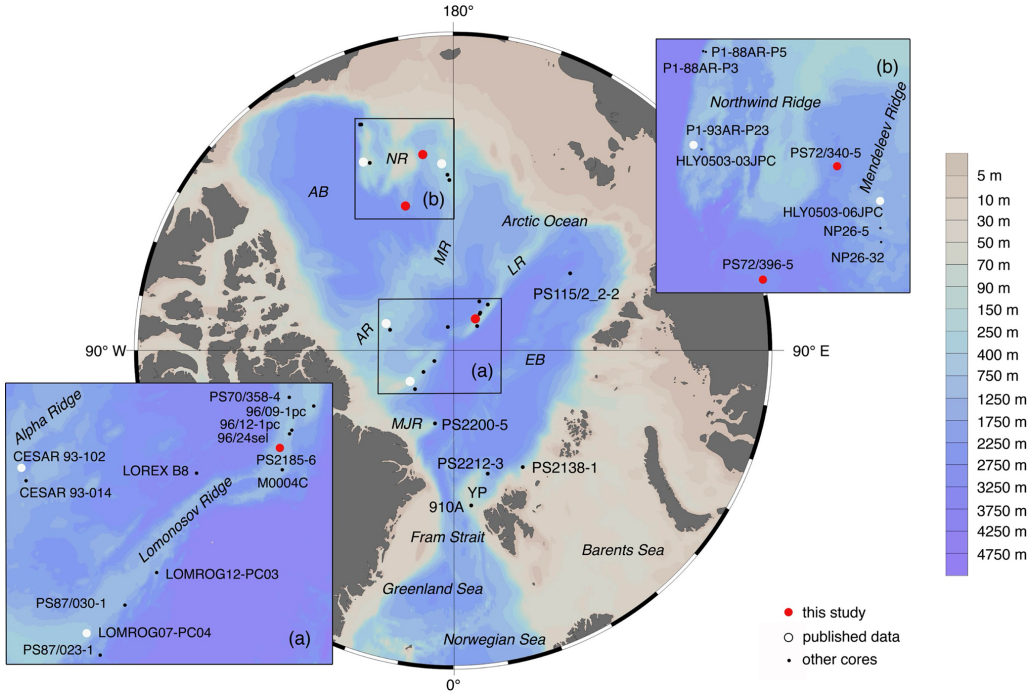

Figure 1. Location of sediment cores. Inset maps: **(a)**, sediment cores from the western Lomonosov and Alpha ridges. **(b)**, sediment cores from the western Mendeleev and Northwind ridges. AB: Amerasian Basin; AR: Alpha Ridge; EB: Eurasian Basin; MJR: Morris Jesup Rise; MR: Mendeleev Ridge; NR: Northwind Ridge; YP: Yermak Plateau. The map bases were drawn in Ocean Data View (Schlitzer, 2022).

Devendra et al., 2022). The good preservation of loosely agglutinated *Rhizammina algaeformis* in core PS72/340-5 indicates that agglutinated foraminifera experienced no significant artificial loss. Despite different preparation techniques, the abundance, diversity, species composition and abundance of agglutinated foraminifera in core PS2185-6 correspond to those previously recorded for this core by Evans and Kaminski (1998) who applied wet-sieving without freeze-drying and plotted their data versus a "mean wet weight".

In our cores dry weight was determined after freeze-drying (mean freeze-dried sample weight is 75, 89, and 96 g for cores PS72/396-5, PS72/340-5, and PS2185-6, respectively). Thereafter, samples were washed with tap water over > 2 mm and > 63 µm sieves and oven dried at 50 °C. The dried sand-size fraction (< 2000–> 63 µm) was split into a small-size fraction > 63–< 125 µm (sf) and large-size fraction > 125–< 2000 µm (lf) using a 125 µm-mesh. All size fractions were weighed and the dry weight-% of each grain size fraction calculated.

Benthic foraminifera were picked and identified from both sf and lf separately. With aid of a micro-splitter, grain-size fractions were split to obtain ∼ 100 and 300 specimens picked from the whole sample splits of the sf and lf, respectively. Fragments of a particular taxon were also counted and included in the counts if the sum of fragments resulted in complete specimens (Wollenburg, 1995). A cut off of 100 specimens in low-diverse samples was applied for sf because picking small foraminifera is extremely time-consuming.

For the calculation of absolute (number of specimens per gram dry weight $=$ no g^{-1} dry weight) and relative (dry weight-%) abundances in the sand-size fraction (> 63 µm) of a sample, foraminifera counts per sample split were first extrapolated to 100 % of the size fraction, then the counts of both size fractions were added, and abundances calculated.

$$\frac{\text{sfnos}}{\text{sfp}} \cdot 100 + \frac{\text{lfnos}}{\text{lfp}} \cdot 100 = \text{tsfnos}$$

$$\frac{\text{tsfnos}}{\text{tdw}} = \text{tsf}\frac{\text{nos}}{\text{g dry weight}}$$

sfnos = foraminifera counts per split of the total fraction $> 63 < 125$ µm

lfnos = foraminifera counts per split of the total fraction < 2 mm > 125 µm

tsf = extrapolated total number of specimens in the size fraction > 63 µm

sfp = split size of the sf-fraction in %

lfp = split size of the lf-fraction in %

tdw = total dry weight of the sample

Table 1. Sediment cores referred to in this study. GC: gravity corer; KAL: Kastenlot corer; PC: Piston Corer; HPC: Hydraulic Piston Corer; SEL: SelCorer.

Station	Type	Longitude	Latitude	Water Depth (m)	Recovery (m)	Reference
PS2138-1	SL	30.8762	81.5377	862	6.34	Wollenburg et al. (2001a)
PS2185-6	KAL	144.1662	87.5293	1073	8.10	this study
PS2200-5	KAL	−14.0220	85.3277	1073	7.70	Evans and Kaminski (1998)
PS2212-3	KAL	15.6723	82.0237	2531	8.02	Wollenburg et al. (2001c)
PS70/358-4	KAL	152.1462	86.5263	1462	7.90	Stärz (2008)
PS72/340-5	KAL	−171.4933	77.6038	2351	8.14	this study
PS72/396-5	KAL	−162.3179	80.5778	2723	7.87	this study
PS87/023-1	KAL	−44.8997	86.6372	2445	6.98	Elkina et al. (2023)
PS87/030-1	KAL	−61.5420	88.6620	1277	6.28	Stein (2015)
PS115/2_2-2	KAL	123.4839	81.2441	3669	7.64	Stein et al. (2025)
LOREX B8	GC	−167.1305	88.4953	4225	1.48	Morris et al. (1985)
CESAR 83-014	GC	−108.3600	85.8467	1370	4.40	Scott et al. (1989)
CESAR 83-102	GC	−111.1183	85.6350	1495	1.18	Scott et al. (1989)
NP26-5	GC	−178.1500	78.9783	1435	1.48	Ishman et al. (1996), Polyak et al. (2004)
NP26-32	GC	−178.6667	79.3233	1610	1.00	Ishman et al. (1996), Polyak et al. (2004)
P1-88AR-P5	PC	−157.8840	74.6225	1089	4.76	Poore et al. (1994), Ishman et al. (1996)
P1-88AR-P3	PC	−157.6598	74.5933	1909	5.81	Poore et al. (1994), Ishman et al. (1996)
P1-93AR-P23	PC	−155.0650	76.9550	951	5.72	Polyak et al. (2013), Lazar and Polyak (2016)
Hole 910A	HPC	6.5900	80.2647	567	24.26	Wollenburg (unpublished data)
96/09-1pc	PC	143.4395	86.4087	927	2.70	Frank et al. (2008)
96/12-1pc	PC	144.7703	87.0918	1003	7.81	Jakobsson et al. (2001), Backman et al. (2004)
96/24-1sel	SEL	144.6060	87.1830	980	4.00	Jakobsson et al. (2003)
HLY0503-03JPC	PC	−156.0625	77.1000	594	7.25	Polyak et al. (2013), Dipre et al. (2018)
HLY0503-06JPC	PC	−176.9862	78.2938	800	12.1	Lazar and Polyak (2016)
LOMROG07-PC04	PC	−53.7700	86.7000	811	5.23	Hanslik et al. (2013), Lazar and Polyak (2016)
LOMROG12-PC03	PC	−54.4253	87.7247	1607	3.73	West et al. (2023)
M0004C	HPC	136.1897	87.8678	1288	25.60	Cronin et al. (2008)

If benthic foraminifera counts were less than 100 specimens per sample, only absolute abundances of calcareous and agglutinated foraminifera were calculated. Actual specimen counts per sample, sample dry weight, the number of specimens per g/dry weight, and relative abundances of the individual taxa are archived in the data repository PANGAEA® (Wollenburg and Matthiessen, 2026a, b, c). The foraminifera of each sample split were picked and stored in plastic microslides which are archived in the *Polarstern* Core Repository.

Planktic foraminifera in the lf were also enumerated in cores PS72/340-5 and PS72/396-5 because their abundance is used to characterize brown layers in the Arctic Ocean (e.g., Polyak et al., 2004). Hereby, depending on the diversity ∼ 100–300 specimens were picked from sample splits of the lf. Planktic foraminifera data of the size fraction > 125–< 500 µm from core PS2185-6 have been reported by Spielhagen et al. (1997b).

Foraminifera were picked and identified by the senior author under a ZeissSteREO Discovery.V8 stereomicroscope, equipped with a PlanS 1.0× FWD81 mm objective, and WPL 10×/23 Bf. foc. oculars, allowing for a magnification range of 10–80×, if needed oculars were changed to PL16×/16 Bf. foc. oculars allowing a maximum magnification of 128×. All stereomicroscope images are stacked digital images taken under a Zeiss Axio Zoom.V16 microscope equipped with 16×/16 Br. foc. oculars and the objectives PlanNeoFluar Z 1.0× (numerical aperture 0.25, FWD 56 mm, magnification 11×...179× with eyepieces PL 16×/16; object field in mm 23...1.4), and Apo Z 1.5× (numerical aperture 0.37, magnification 10.5...168× with eyepieces PL 16×/16; object field in mm 15...0.95). The numerical aperture is 0.25, and the microscope used the ZEISS ZEN 2.3 (blue edition) imaging software. Images were taken with a ZEISS Axiocam 506 colour microscope camera. Scanning electron microscopy (SEM) images are performed by means of a JEOL JSM-IT100 InTouchScope™ Scanning Electron Microscope. Samples mounted on aluminium stubs using conductive double-sided carbon tape are analysed without conductive coating in low vacuum mode. Shell thickness measurements were performed on SEM pictures of the broken last chamber of the respective species using the software ImageJ (Schneider et al., 2012).

A sound taxonomy is the prerequisite for the application of species in biostratigraphy and paleoceanography. Therefore, the taxonomic status of the selected species was restudied before bioevents were defined. The taxonomy follows the original descriptions deposited in the Ellis and Messina Catalogues (Ellis and Messina, 1940–2025), and deviating generic classification as described in The World Foraminifera

Database (Hayward et al., 2025). A total of 236 species was identified in the sediment cores (Table A1). Specimens that could not be identified to species level are recorded under the respective genus or are listed as unidentified benthic foraminifera. White, dull or fragmented tests of calcareous foraminifera, often with enlarged pores, are interpreted as indication of progressive corrosion of calcareous shells (Poirier et al., 2021; Wollenburg et al., 2023a). Fragments of agglutinated shells are indicative of progressive Fe-mobilisation and degradation of organic cement (Murray and Alve, 2011; Schroeder, 1988). Taxonomic notes and images of the stratigraphically relevant species are included in the Appendix A. The characteristic morphological features and ecological preferences of the selected species are listed in Appendix B. Here, we report only the specimen counts of the taxa relevant for this stratigraphic study (Wollenburg and Matthiessen, 2026a, b, c), whereas all other taxa and unidentified specimens are listed as other benthic foraminifera.

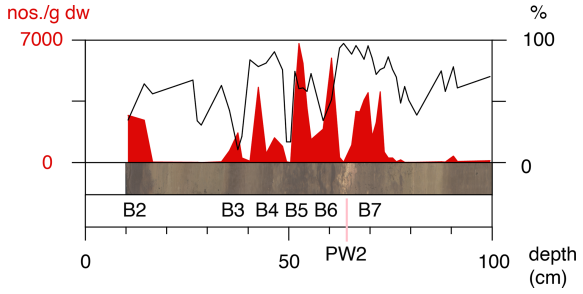

Figure 2. Digital image of core PS72/396-5 and relative (%) and absolute (no g^{-1} dw) abundances of *Stetsonia horvathi*. This species dominates in most assemblages but only shows distinct absolute abundance maxima in the brown layers. Please note that bioturbation has blurred the clear distinction between foraminifer-rich brown and foraminifer-poor grey layers, making distinction of specific brown layers difficult. Brown layer terminology after Polyak et al. (2004) and Stein et al. (2010b).

2.2.2 Definition of bioevents

The bioevents were described based on absolute abundances rather than relative abundances and presence/absence data. Absolute abundance maxima are often more distinct and confined to shorter intervals and distinct lithological units than relative abundances (Fig. 2; e.g., Jakobsson et al., 2001; Polyak et al., 2004). Moreover, the relative abundance of a species, generally used in Arctic studies (Adler et al., 2009; Polyak et al., 2013; Lazar et al., 2016; Chauhan et al., 2014, 2015; Hanslik et al., 2013), is influenced by the variable abundances of all other taxa counted in an assemblage.

The definition of bioevents follows the concept of biostratigraphic datums used by De Schepper and Head (2008). The in-situ stratigraphic occurrence of a taxon is marked by the lowest (LO) and highest (HO) occurrence. The highest and lowest sample in a sediment core in which a particular taxon is noticeably abundant, indicates the highest common occurrence (HCO) and lowest common occurrences (LCO), respectively. A particular taxon may occur in very low numbers above and below this stratigraphic level. Bell-shaped curves may indicate that bioturbation has blurred distinct absolute abundance maxima. Thus, species may have high relative abundances above and below absolute abundance maxima in sediments that originally had low benthic foraminifera contents (Fig. 2). Therefore, an LCO, HCO, and acme, based on absolute abundances appear to be more useful than LO and HO when sedimentation rates are on the order of mm $kyrs^{-1}$. Chronological information was compiled from various sources to assess the ages of the bioevents in the individual cores. The bioevents were assigned to the Pleistocene subseries of the Quaternary system (Head et al., 2021) and tentatively to marine isotope stages.

2.2.3 Comparison with published records

Published benthic foraminifera data of Arctic sediment cores were compiled to obtain a broader geographic coverage of the bioevents (Fig. 1). Comparison with previous studies is complicated by the fact that there is no common agreement on the grain-size fraction to be used in Arctic foraminifera analyses. Early studies applied the CLIMAP cut off of > 150 or > 125 µm (Poore et al., 1994; Adler et al., 2009; Hanslik et al., 2013) although it was realized that smaller benthic foraminifera may account considerably to the assemblages. Schroeder et al. (1987) emphasize the importance of smaller sized species such as *Alabaminella weddellensis* or abundant small-sized offspring such as *Epistominella exigua* in benthic foraminifera assemblages. Thus, smaller specimens (> 63–< 125 µm) may be by one order of magnitude more abundant in samples from Arctic Ocean cores than larger benthic foraminifera (> 125 µm) (Wollenburg and Mackensen, 1998a; Wollenburg et al., 2001b; Lazar and Polyak, 2016). Nevertheless, different grain-size fractions are still used to obtain smaller foraminifera (e.g. > 63 µm, > 100 µm; Ishman et al., 1996; Polyak et al., 2004, 2013; Chauhan et al., 2014; Lazar and Polyak, 2016). Usually, only the relative abundances of marker species are shown, and their corresponding maxima are often found in specimen-poor samples. Such samples may indicate an allochthonous origin of specimens, e.g. by bioturbation into deeper sediments or are often depleted in especially thin-shelled species like *Stetsonia horvathi* or *Epistominella arctica* (Lazar and Polyak, 2016). It is usually not stated whether analyses were limited to a certain set of taxa making it difficult to assess relative abundances.

Here, we analyzed the > 63 to < 2000 µm size fraction to obtain a record of the smaller sized, and usually dominant, benthic foraminifera, and compare the absolute abundance data with those records obtained from the same size fraction (Scott et al., 1989; Lazar and Polyak, 2016). It must be noted

that Lazar and Polyak (2016) did not include agglutinated species which may lead to some bias in relative abundances compared to the new data.

2.3 Lithostratigraphy at Mendeleev and Lomonosov Ridges

Arctic Ocean sediments are characterized by a pronounced lithological variability and previous studies revealed that the stratigraphic occurrence of calcareous foraminifera is related to specific lithological layers (e.g. Polyak et al., 2004; Adler et al., 2009). Therefore, the lithostratigraphic schemes used for stratigraphic correlation in the Arctic Ocean are shortly reviewed. For the western Arctic Ocean, Clark et al. (1980) proposed thirteen lithostratigraphic units (standard arctic lithostratigraphic units A to M) based on grain size composition and presence of detrital carbonate-rich pink-white layers. This scheme has been routinely applied in subsequent studies and slightly modified for cores from Alpha Ridge (Minicucci and Clark, 1983; Mudie, 1985; Darby et al., 1989; Clark et al., 1990; Poore et al., 1993, 1994; Ishman et al., 1996; Phillips and Grantz, 1997; Stein et al., 2010a, b). In the past years, a simplified lithostratigraphy has been preferred for visual core description counting downcore the alternation of brown, calcareous foraminifer- and manganese-rich and coarser-grained grey to olive, foraminifer- and manganese-poor layers (Polyak et al., 2004). These layers were termed brown beds B1 to B7 and grey beds G1 to G6, and are interpreted to reflect interglacials/interstadials and glacials/stadials, respectively. In the western Arctic Ocean, lithological Unit M comprises brown beds B1 to B6, whereas the top of Unit L is marked by brown bed B7 (Figs. 3, 4). This scheme was extended downcore into older sediments but the number of brown layers in specific stratigraphic intervals varies between cores (Stein et al., 2010b; Wang et al., 2018; Dong et al., 2020; Park et al., 2020). März et al. (2011) note that diagenetic processes may lead to post-depositional dissolution and/or formation of Mn-rich brown layers. Therefore, they emphasize that these layers should not be used for stratigraphic correlation without independent age control.

The combination of the standard lithostratigraphic units and colour stratigraphy has been applied on cores from southern Mendeleev Ridge including PS72/340-5 and PS72/396-5 (Figs. 3, 4) (Stein et al., 2010a, b). However, the link between brown layers and calcareous foraminifera abundances is not straightforward because when sedimentation is extremely slow (mm $kyrs^{-1}$) as at site PS72/396, brown beds are difficult to distinguish because of extensive bioturbation blurring the record (Fig. 3) (Stein et al., 2010b). Moreover, brown bed B 5 is barren of calcareous foraminifera and contains only agglutinated foraminifera in core PS72/340-5 (Fig. 4). This is also a common feature in Northwind Ridge cores (Poore et al., 1993,1994; Ishman et al., 1996; Phillips and Grantz, 1997; Yurco et al., 2010).

Thin layers enriched in pink-white and whitish lenses or clasts of detrital dolomite (white and pink-white layers) may be useful for stratigraphic correlation in the western Arctic Ocean but the relative high number of these layers in sediment cores from the Northwind and Mendeleev ridges make an unequivocal correlation difficult (Clark et al., 1980; Mudie and Blasco, 1985; Minicucci and Clark, 1983; Poore et al., 1993; Poore et al., 1994; Phillips and Grantz, 1997; Polyak et al., 2004; Adler et al., 2009; Stein et al., 2010a; Stein et al., 2010b; Cronin et al., 2014; Bazhenova et al., 2017). These diamictons reflect synchronous rapid sedimentation events from melting icebergs. These icebergs had calved at the grounding line of the Laurentide ice sheet, at the Arctic margin, then drifted with prevailing currents across the Arctic basins and released predominantely calcareous debris while melting (Darby et al., 2002; Polyak et al., 2004; Matthiessen et al., 2010; Stein et al., 2010a, b; Bazhenova et al., 2017).

The lithostratigraphic scheme of Clark et al. (1980) cannot be applied on Lomonosov Ridge sediments (Sellén et al., 2008) and a separate lithostratigraphic scheme has not been developed yet for Eurasian Basin cores. Non-destructive physical property records, such as magnetic susceptibility (ms) and wet bulk density (wbd) enable correlation within similar depositional environments (Sellén et al., 2010; O'Regan et al., 2019; Vermassen et al., 2021; Razmjooei et al., 2023). Thus, Razmjooei et al. (2023) used wbd maxima of two diamictons in the upper part of sediment cores from the western Lomonosov Ridge for stratigraphic correlation, including core PS2185-6 (Fig. 5).

Since foraminifer-rich brown layers are also widespread in the eastern Arctic Ocean (e.g., Jakobsson et al., 2001; Backman et al., 2004; Polyak et al., 2004; Löwemark et al., 2014), these may be applicable for a basin-wide lithostratigraphic correlation if they were coeval across the Arctic Ocean. Visual inspection of sediment core images revealed that some intervals in core PS2185-6 with high planktic foraminifera concentrations (Spielhagen et al., 1997a, 2004) and increased manganese contents (Schoster, 2005) have a brown colour (Grobe and Fütterer, 2003), comparable to those in adjacent core 96/12-1pc (Jakobsson et al., 2001; Backman et al., 2004).

There are possibly some lithological marker sequences that may be used for stratigraphic correlation across the Arctic Ocean. In the Mendeleev Ridge area, the base of lithological Units M and J are marked by the dolomite-rich pink-white diamictons PW 2, and PW 1, respectively (Figs. 3, 4; Clark et al., 1980; Poore et al., 1993; Polyak et al., 2004; Adler et al., 2009; Stein et al., 2010a, b; März et al., 2011). Pink-white layer PW 2 is interbedded in two brown layers which were correlated to foraminifer-rich brown layers in core 96/12-1pc on Lomonosov Ridge (Backman et al., 2004; Polyak et al., 2004). A similar sequence may be observed in core PS2185-6 where detrital carbonates in the 125–500 µm size fraction (Spielhagen et al., 1997b) may represent fine-grained

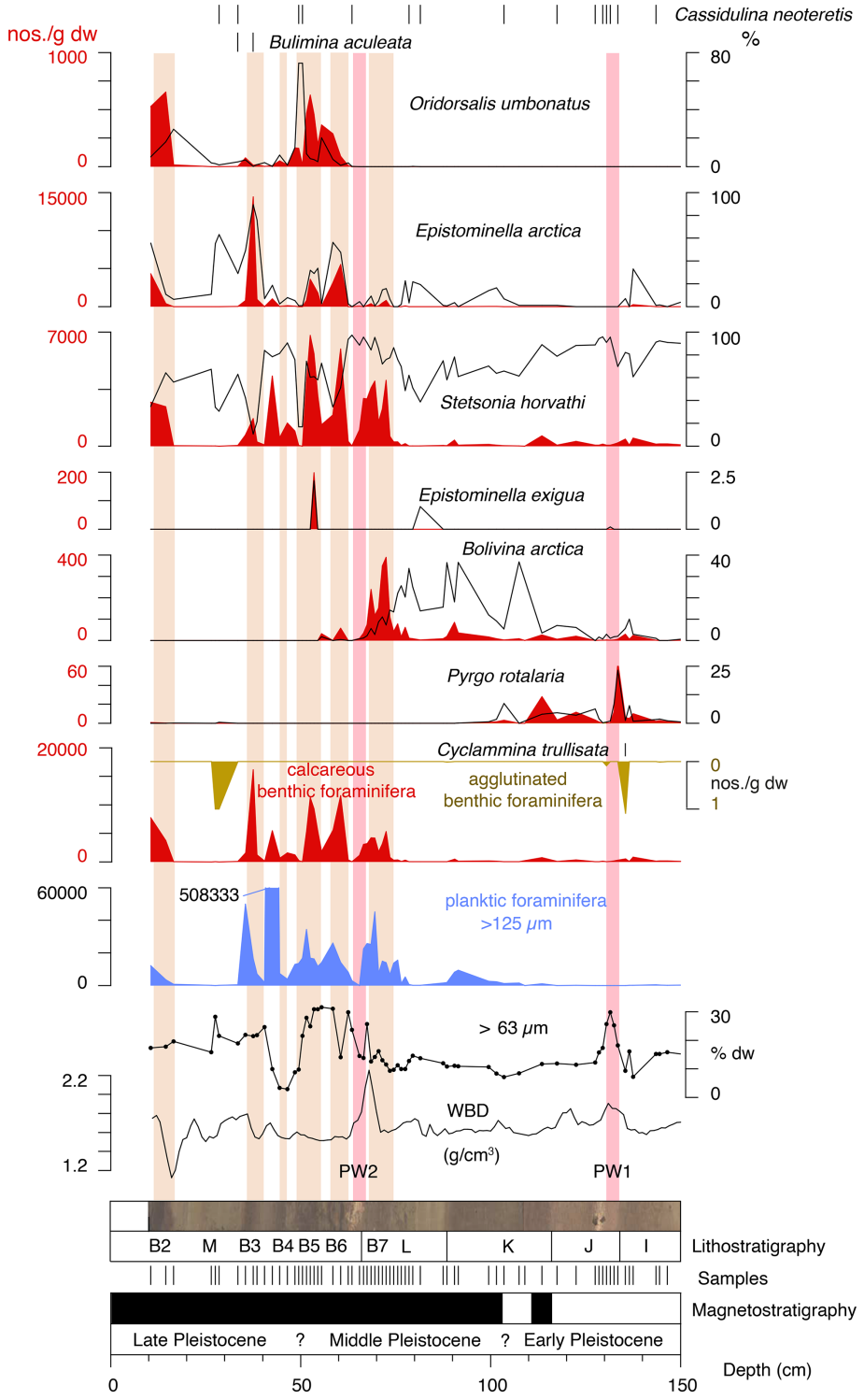

Figure 3. Stratigraphic distribution of selected benthic foraminifera (> 63 µm) in sediment core PS72/396-5 from the western Mendeleev Ridge area. Only the presence of *Bulimina aculeata* and *Cassidulina neoteretis* is noted because of consistently low relative abundances (< 2 %). The first downcore change in magnetic polarity is assigned to the Brunhes/Matuyama boundary (Elkina et al., 2023) which is supported by $^{230}Th_{ex}$ data (Geibert et al., 2021). The Pleistocene is tentatively subdivided into subseries. The standard lithostratigraphic units M to I of Clark et al. (1980) were identified by Stein et al. (2010b). Brown (B) and pink-white layers (PW) are labelled according to Polyak et al. (2004) and Stein et al. (2010b). Line scan images are from Matthiessen (2013b). Wet bulk density data (wbd) are from Niessen (2010b). Please note that brown bed B 1 was not recovered at the core top due to coring disturbance. %: relative abundances; no g^{-1} dw: absolute abundances.

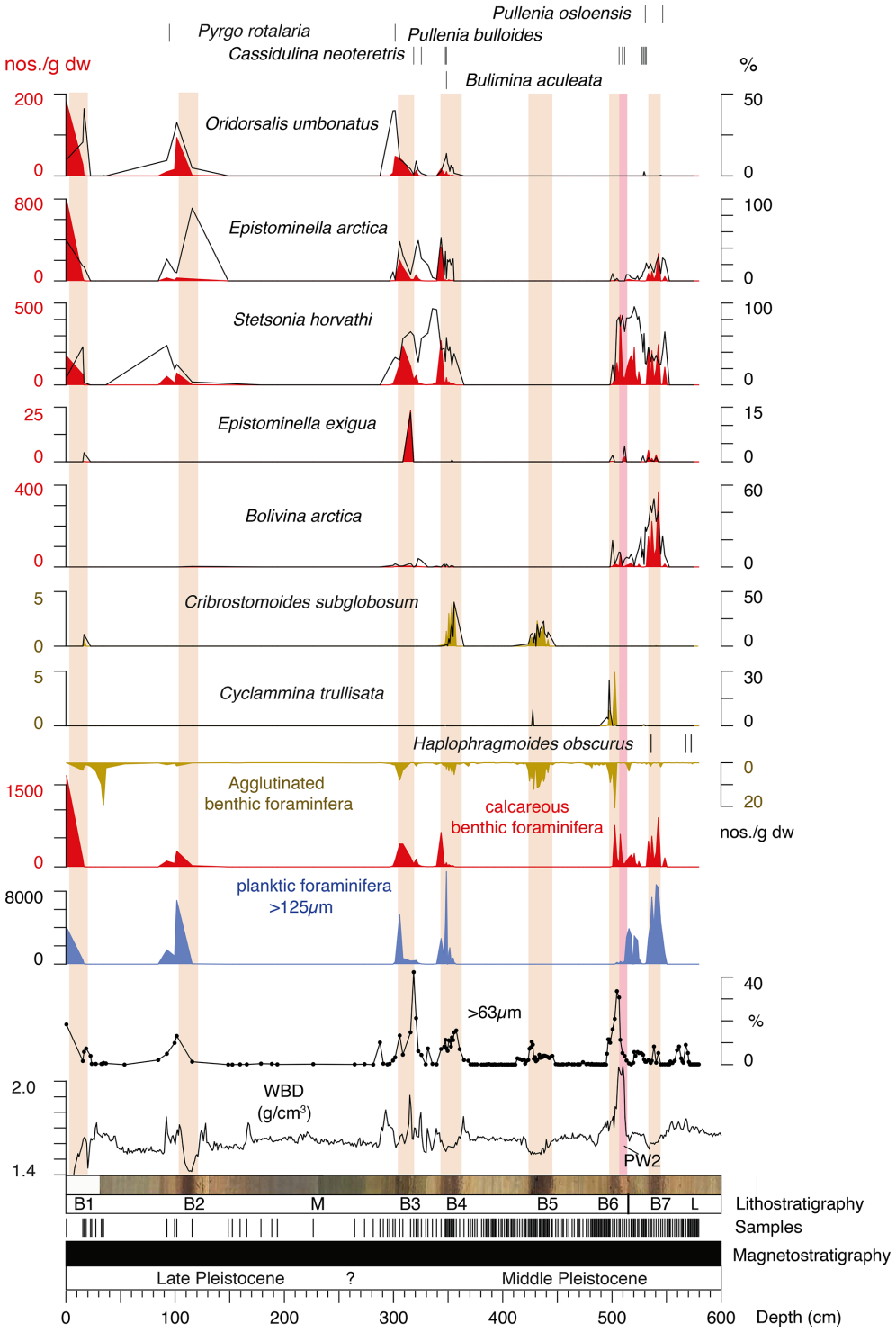

Figure 4. Stratigraphic distribution of selected benthic foraminifera in sediment core PS72/340-5 from the western Mendeleev Ridge area. Only the presence of *Bulimina aculeata*, *Cassidulina neoteretis*, *Pullenia bulloides*, *Pullenia osloensis* and *Pyrgo rotalaria* is noted because of consistently low relative abundances ($< 2\,\%$). The studied core interval was deposited during the Brunhes Chron (Bazhenova, 2012). The standard lithostratigraphic units M and L of Clark et al. (1980) were identified by Stein et al. (2010b). Brown (B) and pink-white layers (PW) are labelled according to Polyak et al. (2004) and Stein et al. (2010b). Line scan images are from Matthiessen (2013a). Wet bulk density (wbd) data are from Niessen (2010a). %: relative abundances; no g^{-1} dw: absolute abundances.

detrital dolomites between two foraminifer-rich brown layers in the lower part of the uppermost interval with normal polarity (Fig. 5). Pink-white clasts in a diamicton in adjacent core PS70/358-4 (Stärz, 2008) were used by Stein et al. (2010a, Fig. 9) to tentatively infer the presence of diamicton PW 2. Based on this correlation, Stein et al. (2010b) suggest that brown bed B7 must be present below this layer in cores PS70/358-4 and PS2185-6. At about the same stratigraphic level, Kaparulina et al. (2016) observed a maximum of dolomite in the heavy mineral fraction $> 63\,\mu m$ in core 96/12-1pc, interbedded into two brown layers. Previously, Morris et al. (1985, p. 904) used the presence of whitish blotches at the base of the Theta member of their Makarov Basin Formation in LOREX core B8 to infer the presence of the base of Unit M (see also Sellén et al., 2008). These observations suggest that sediments equivalent to the base of Unit M and the top of Unit L may also be recorded in the central Lomonosov Ridge area.

However, sedimentation on the shallow Lomonosov Ridge may be disrupted by glacial erosion and/or slow sedimentation during times of extensive glacial ice cover (e.g., Jakobsson et al., 2001, 2010; Frank et al., 2008) complicating the construction of age models. Thus, an erosional unconformity is observed below a pink layer in core 96/09-1pc that is correlated by wbd and ms to core PS2185-6 (Jakobsson et al., 2001; Razmjooei et al., 2023). This correlation suggests that this pink layer is synchronous with the inferred pink-white layer PW 2 above brown bed B 7 in PS2185-6 (Fig. 5).

3 Results

3.1 Foraminifera occurrence and lithology

The discontinuous occurrence of foraminifera in the studied cores is related to the lithology (Figs. 3–5). Planktic and calcareous benthic foraminifera show absolute abundance maxima rather in brown layers than in the grey to olive layers, as it has been previously observed (e.g., Polyak et al., 2004; Backman et al., 2004; Adler et al., 2009). Core PS72/396-5 has lower sedimentation rates and thus comprises older sediments in the lower core section than core PS72/340-5. Below brown bed B 7 absolute abundances of calcareous foraminifera are much lower in brown layers than in younger sediments. On Lomonosov Ridge, only some brown layers in the uppermost interval with normal magnetic polarity are rich in calcareous foraminifera. The few calcareous shells in the grey to olive layers of the three cores may be bioturbated from the brown layers, as indicated by extensive brown mottling (see digital images and x-radiographs; Fütterer and Grobe, 2003; Matthiessen and Stein, 2008a, 2008b; Matthiessen, 2013a, b), or may be of allochthonous origin (Geibert et al., 2021). Coarse-grained intervals, such as the diamictons in core PS2185-6 are barren (Fig. 5).

Planktic foraminifera assemblages are almost exclusively composed of *Neogloboquadrina pachyderma* (not shown) in cores PS72/340-5 and PS72/396-5. In most benthic foraminifera assemblages in the intervals with calcareous taxa *Stetsonia horvathi* contributes more than 50 % to the assemblages (Figs. 3-5), whereas stratigraphically important taxa such as *Bolivina arctica* exceed only in a few samples more than 50 %. Calcareous foraminifera bioevents occur in Unit M and in the upper part of Unit L in brown bed B 7.

Agglutinated benthic foraminifera do not show a consistent distribution in the three cores. Where calcareous and agglutinated foraminifera are preserved, absolute abundances of agglutinated foraminifera are generally two orders of magnitude lower than those of the calcareous taxa. Brown layers in the lower part of core PS2185-6, and brown bed B5 in core PS72/340-5 comprise exclusively agglutinated foraminifera. In core PS72/340-5 the thick interbedded grey to olive layers comprise few to no calcareous foraminifera but sometimes low abundances of agglutinated foraminifera. Core PS72/396-5 is almost devoid of agglutinated taxa.

3.2 Stratigraphic occurrence of benthic foraminifera

Species of *Pullenia* are present at different stratigraphic levels in the studied sediment cores. *Pullenia bulloides* only occurs in the *B. aculeata* acme of core PS2185-6 (Fig. 5), and in core PS72/340-5 in brown bed B 3 (Fig. 4). *Pullenia quinqueloba* and *P. osloensis* are sporadically present in cores PS2185-6 and PS72/340-5, respectively. *Pullenia bulloides* shows a variable distribution in sediment cores from the Arctic Ocean (Fig. 7).

Benthic taxa which are potentially important for biostratigraphy and ecology are shown in Figs. 3, 4, and 5. Additionally, the stratigraphic occurrence of these taxa in cores from Alpha Ridge, Northwind Ridge, Mendeleev Ridge, and Lomonosov Ridge (Fig. 1; this study; Scott et al., 1989; Lazar and Polyak, 2016) is compiled in Figs. 6 to 11 to evaluate their distribution across the Arctic Ocean.

The agglutinated benthic foraminifera *Siphotextularia rolshauseni*, a stratigraphic marker for MIS 2 in Norwegian-Greenland Sea sediments, has not been observed in the sediment cores from the CAO but it occurs sporadically in the Fram Strait area and at the adjacent Barents Sea continental slope (Wollenburg et al., 2001b). This species has not been observed in any other study on agglutinated foraminifera from the Arctic Ocean (e.g., O'Neill, 1981; Scott et al., 1989; Evans and Kaminski, 1998).

Bulimina aculeata is abundant only in core PS2185-6 where an absolute abundance maximum is restricted to a short interval in a brown layer (Fig. 5). It is present in very low numbers at the deep-water sites, in a single sample in brown bed B 4 in core

PS72/340-5, and in two samples in brown bed B 3 in core PS72/396-5 (Figs. 3, 4). This species occurs at different stratigraphic intervals in sediment cores and a distinct maximum of absolute abundances has been only observed in cores from relatively shallow water depths ($<\sim 2000$ m), oc-

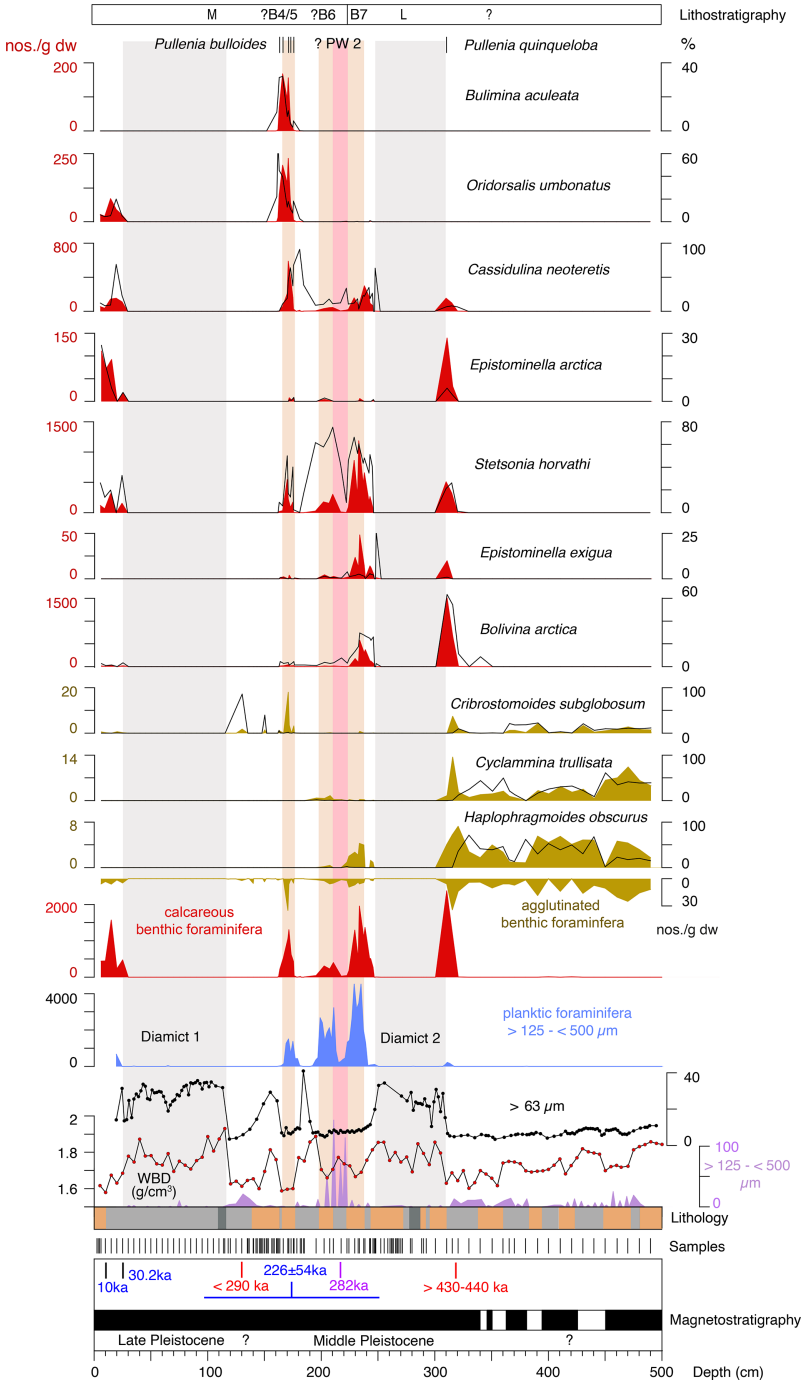

Figure 5. Stratigraphic distribution of selected benthic foraminifera in sediment core PS2185-6 from Lomonosov Ridge. Only the presence of *Pullenia bulloides* and *P. quinqueloba* is noted because of consistently low relative abundances (< 2 %). The numerical ages (blue colour) in the interval with normal magnetic polarity (Frederichs, 1995) are based on two AMS ^{14}C ages at the core top (selected from a radiocarbon data set of Wollenburg et al., 2023a) and a $^{230}Th_{xs}$ extinction age (depth range is depicted by a bar; Song et al., 2023). This core is correlated to adjacent cores by distinct wbd maxima (Bergmann, 1995) representing diamict 1 and 2 enabling to transfer ages of coccolith events (red colour) to core PS2185-6 (Razmjooei et al., 2023). The pink age is assigned to a detrital carbonate-rich interval based on the correlation to pink-white layer PW 2 (Stein et al., 2010b, 2025). The simplied lithology characterized by brown, olive grey, and grey layers is taken from photographic images (Grobe and Fütterer, 2003). Lithostratigraphic units are tentatively assigned to M and L, and brown beds to B4 to B7. Planktic foraminifera concentrations, relative abundance of coarse sediment fraction, and detrital carbonate contents (no > 125–< 500 µm) are from Spielhagen et al. (1997b). %: relative abundances; no g^{-1} dw: absolute abundances.

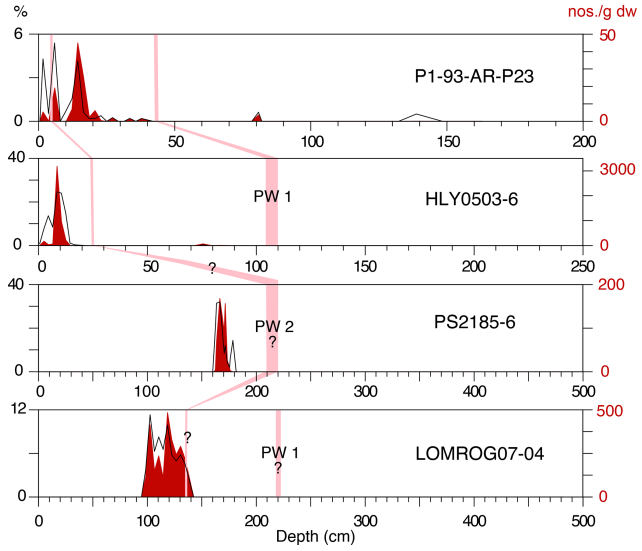

Figure 6. Stratigraphic occurrence of *B. aculeata* across the Arctic Ocean. A distinct acme is observed above PW 2 in all cores from relatively shallow water depths, except for core P1-93-AR-P23. Core locations are shown in Fig. 1. Absolute abundances (> 63 µm) of cores P1-93-AR-P23, HLY0503-6, and LOMROG07-04 are from Lazar and Polyak (2016). The depth intervals of the pink-white layers in these cores are from Cronin et al. (2014). %: relative abundances; no g^{-1} dw: absolute abundances.

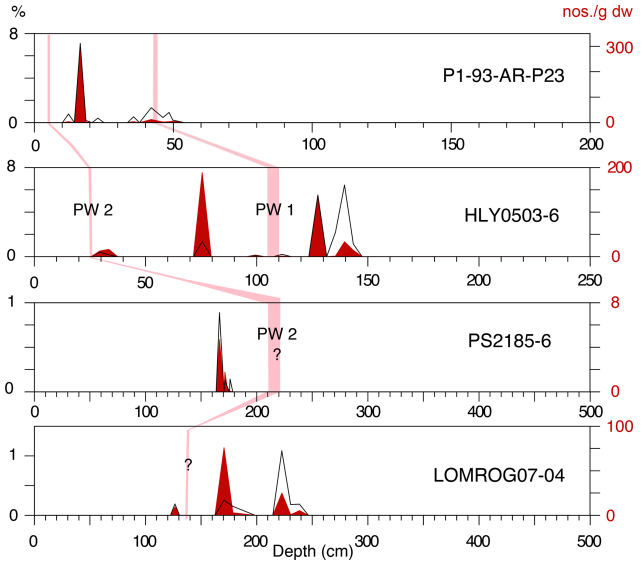

Figure 7. Stratigraphic occurrence of *P. bulloides* across the Arctic Ocean. Core locations are shown in Fig. 1. Absolute abundances (> 63 µm) of cores P1-93-AR-P23, HLY0503-6, and LOMROG07-04 are from Lazar and Polyak (2016). The depth intervals of the pink-white layers in these cores are from Cronin et al. (2014). %: relative abundances; no g^{-1} dw: absolute abundances.

curring usually above pink-white layer PW 2 in lithological Unit M in the western Arctic Ocean (Fig. 6).

Species of *Pullenia* are present at different stratigraphic levels in the studied sediment cores. *Pullenia bulloides* only occurs in the *B. aculeata* acme of core PS2185-6 (Fig. 5), and in core PS72/340-5 in brown bed B 3 (Fig. 4). *Pullenia quinqueloba* and *P. osloensis* are sporadically present in cores PS2185-6 and PS72/340-5, respectively. *Pullenia bulloides* shows a variable distribution in sediment cores from the Arctic Ocean (Fig. 7).

Oridorsalis umbonatus (often referred to *O. tener*, see Appendix A) has a distinct lowest maximum of absolute abundances above PW 2 in a brown layer across the Arctic Ocean (Figs. 3, 4, 5, 8). A distinct relation to a specific brown layer is not observed in the western Arctic Ocean where the oldest maximum occurs in brown beds B 3 and B 6 in cores PS72/340-5 and PS72/396-5, respectively. However, brown beds B 4, B 5 and B 6 are difficult to distinguish in core PS72/396-5 because of intensive bioturbation, and at site PS72/340 brown bed B 5 is barren in calcareous foraminifera. The oldest abundance maximum coincides with that of *B. aculeata* in cores from shallow water depths (Figs. 5, 8) as it has also been observed in the size fraction > 150 µm in cores 96/12-1pc and the composite record of cores NP26-5 and NP26-32 (as *O. tener*; Jakobsson et al., 2001; Polyak et al., 2004). Below the oldest maximum, *O. umbonatus* can be present but never reaches high absolute abundances.

Cassidulina neoteretis occurs in certain brown layers in core PS2185-6 and is particularly abundant in the *B. aculeata* acme above the lowest maximum of absolute abundances of *O. umbonatus* (Fig. 5). A comparable assemblage has been observed in the composite record of cores NP26-5 and NP26-32 and core 96/12-1pc (as *C. teretis*; Jakobsson et al., 2001; Polyak et al., 2004). In cores PS72/340-5 and PS72/396-5 from deeper waters, *C. neoteretis* is only rare in some intervals (Figs. 3, 4). This species might be a good additional marker for the *B. aculeata* acme in shallow water cores, but *C. neoteretis* has not been consistently distinguished from *C. teretis* making it currently difficult to assess its stratigraphic potential (Appendix A).

Epistominella arctica and *E. exigua* do not show a consistent stratigraphic occurrence in the studied sediment cores (Figs. 3–5). *Epistominella arctica* is more abundant than *E. exigua* and occurs with variable absolute and relative abundances in certain brown layers. Hereby, *E. arctica* is more frequent above PW 1, and *E. exigua* below PW 2 (Figs. 9, 10).

Bolivina arctica occurs in variable absolute and relative abundances through the cores (Figs. 3–5). Absolute abundance maxima are generally restricted to the lower part of the interval with normal magnetic polarity. The youngest pronounced absolute abundance maximum is terminated by a pronounced decline to low abundances. This is located at the top of Unit L in brown bed B7 just below pink-white layer

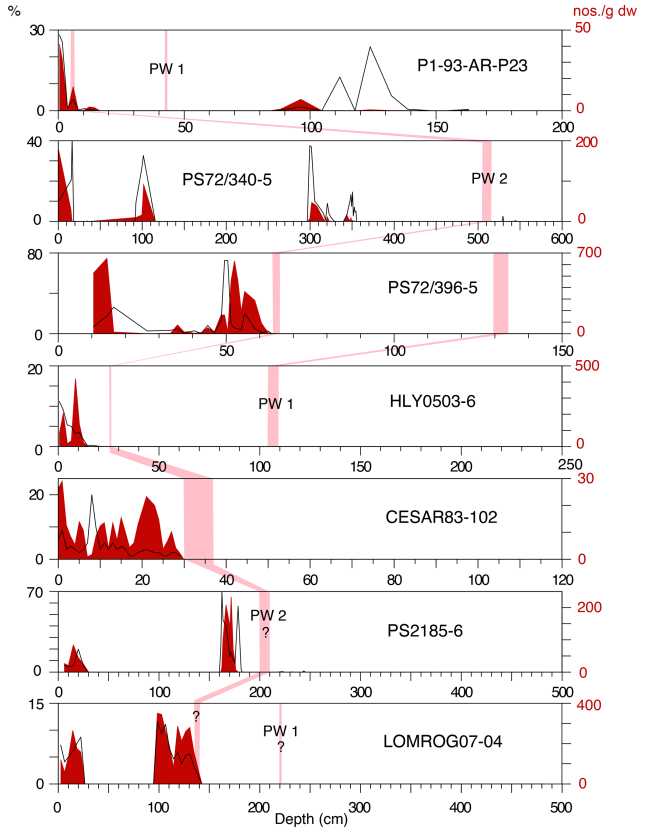

Figure 8. Stratigraphic occurrence of *O. umbonatus* across the Arctic Ocean. This species consistently shows absolute abundance maxima above PW 2. Core locations are shown in Fig. 1. Absolute abundances (> 63 µm) of cores P1-93-AR-P23, HLY0503-6, and LOMROG07-04 are from Lazar and Polyak (2016), and CESAR83-102 from Scott et al. (1989). The depth intervals of the pink-white layers in these cores are from Cronin et al. (2014) and Scott et al. (1989). %: relative abundances; no g^{-1} dw: absolute abundances. Absolute abundances in core CESAR83-102 are numbers/10ccm wet sample (Scott et al., 1989).

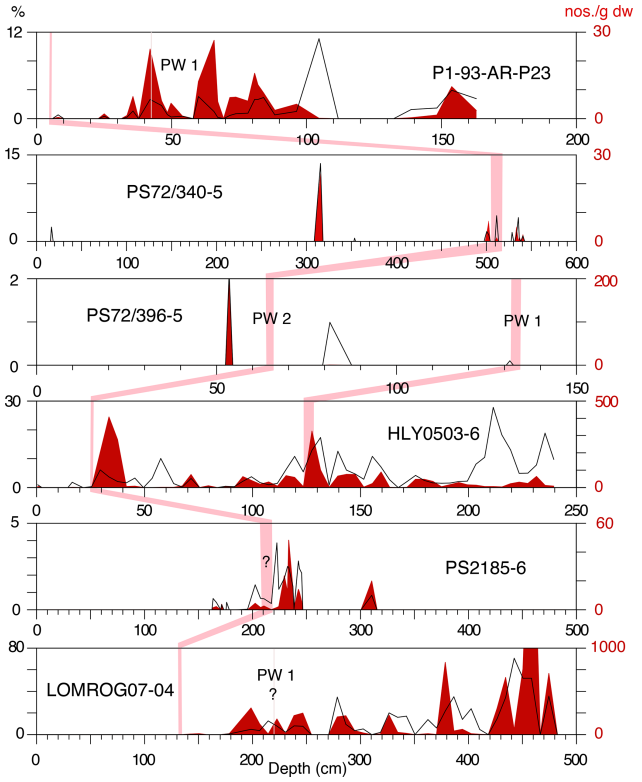

Figure 9. Stratigraphic occurrence of *E. exigua* across the Arctic Ocean. Core locations are shown in Fig. 1. Absolute abundances (> 63 µm) of cores P1-93-AR-P23, HLY0503-6, and LOMROG07-04 are from Lazar and Polyak (2016). The depth intervals of the pink-white layers in these cores are from Cronin et al. (2014). %: relative abundances; no g^{-1} dw: absolute abundances.

PW 2 in the western Arctic Ocean, and at the same stratigraphic level on Lomonosov Ridge based on the proposed lithostratigraphic correlation (Fig. 11, Stein et al., 2010b).

The extinct agglutinated foraminifera *Haplophragmoides obscurus* dominates the benthic assemblages in the lower part of core PS2185-6 (Fig. 5) and disappears above the top of the youngest absolute abundance maximum of *B. arctica*. This species is only observed in traces in PS72/340-5 (Fig. 4). In core PS72/396-5 *H. obscurus* is absent but likely the stratigraphic occurrence of the extant *Pyrgo rotalaria* is comparable with that of *H. obscurus* (Fig. 3).

The changeover in predominance from agglutinated to calcareous benthic foraminifera has been observed in core PS2185-6 slightly above the change to normal magnetic polarity (Fig. 5). This substantial decline of agglutinated foraminifera has been previously described for this core (Evans et al., 1995; Evans and Kaminski, 1998). Below the changeover, assemblages only comprise foraminifera firmly agglutinated with high iron content in the cement (Schröder, 1988; Hedley, 1963; Bender, 1989). These include taxa accessory in recent assemblages (*Cribrostomoides subglobosus*, *Glomospira* spp., *Rhabdammina* spp., *Jaculella* spp., *Hyperammina* spp., *Saccammina socialis*, *S. sphaera*, *Psammosphaera fusca*, *Reophax* spp.), and *H. obscurus* and *Cyclammina trullissata* that are unknown from the modern Arctic benthic foraminifera fauna. *Cyclammina trullissata* disappeared in core PS2185-6 in a brown layer above the proposed pink-white layer PW 2, and in core PS72/340-5 in brown bed B 5. In younger sediments above the HOs of *H. obscurus* and *C. trullisata* the agglutinated fauna is dominated by modern taxa, and predominantly firmly agglutinated *Cribrostomoides subglobosus* occurs sporadically in certain intervals. Agglutinated foraminifera are almost absent in the studied interval of core PS72/396-5 whereas in core PS72/340 brown layers and some laminated interbedded sequences comprise predominantly agglutinated tubular taxa.

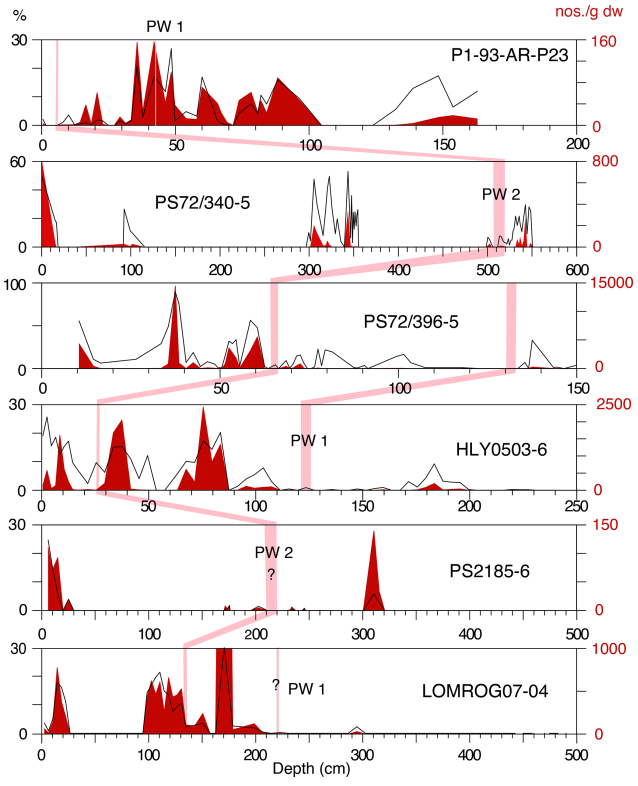

Figure 10. Stratigraphic occurrence of *E. arctica* across the Arctic Ocean. Core locations are shown in Fig. 1. Absolute abundances (> 63 µm) of cores P1-93-AR-P23, HLY0503-6, and LOMROG07-04 are from Lazar and Polyak (2016). The depth intervals of the pink-white layers in these cores are from Cronin et al. (2014). %: relative abundances; no g^{-1} dw: absolute abundances.

4 Discussion

4.1 Chronostratigraphy of studied sediment cores

A robust chronostratigraphic framework for Pleistocene sediments in the CAO has not been developed yet, and beyond the range of radiocarbon dating there are few chronological tie-points because of discontinuous microfossil and sparse radionuclide records. Moreover, variable accumulation of sediments and stratigraphic breaks at the Arctic Ocean sea-floor hamper linear interpolation between tie-points and thus calculation of numerical ages for bioevents (Hillaire-Marcel et al., 2017; Matthiessen et al., 2018).

Since the turn of the century the Pleistocene chronostratigraphy in the western Arctic Ocean primarily relied on stratigraphic correlation to the central Lomonosov Ridge (e.g., Backman et al., 2004; Polyak et al., 2004; Spielhagen et al., 2004; Adler et al., 2009; Park et al., 2024). Three brown layers that comprise absolute abundance maxima of planktic foraminifera interbedded in two diamicts (diamict 1 and 2 sensu Razmjooei et al., 2023) in cores PS2185-6 (Fig. 5) and 96/12-1pc have been dated to MIS 5 by coccolith biostratigraphy and optical stimulated luminescence (OSL) ages (Jakobsson et al., 2000, 2003; Spielhagen et al., 2004). These ages served with AMS ^{14}C dates as backbone for the Arctic Ocean MIS 1 to 6 chronostratigraphy (e.g., Jakobsson et al., 2001; Jakobsson et al., 2003; Backman et al., 2004; Spielhagen et al., 2004). New radiocarbon, coccolith, amino acid razemisation and radiometric data from various Lomonosov Ridge cores now require a substantial revision of these age assignments (Hillaire-Marcel et al., 2017; Geibert et al., 2021; Razmjooei et al., 2023; Song et al., 2023; West et al., 2023; Wollenburg et al., 2023a).

Chronological tie points for core PS2185-6 are now radiocarbon ages for the Holocene to late glacial interval (MIS 1–3) and a $^{230}Th_{xs}$ extinction age for the Middle Pleistocene (Wollenburg et al., 2023a; Song et al., 2023). These ages confirm that the uppermost interval with normal magnetic polarity in core PS2185-6 corresponds to the Brunhes Chron (Fig. 5).

Although the extinction age has large uncertainties with respect to the stratigraphic interval and age (ca. 226 ± 54 ka (MIS 7) at 174 ± 76 cm, Song et al., 2023), the core section with the three foraminifera maxima between 160 and 240 cm is older than MIS 6 even if the true extinction age is close to the youngest possible $^{230}Th_{xs}$ age (Fig. 5). The previous coccolith biostratigraphy of Spielhagen et al. (2004) for core PS2185-6 based on the presence of *Emiliania huxleyi* (assigned to *Geophyrocapsa huxleyi* by Bendif et al., 2023) in these foraminifera maxima could not be confirmed by a detailed taxonomic restudy (Razmjooei et al., 2023).

The new age constraints complicate the identification of MIS 5 in Lomonosov Ridge sediments. The radiocarbon and $^{230}Th_{xs}$ extinction ages are supplemented by correlating coccolith bioevents from sediment cores on the western Lomonosov Ridge to core PS2185-6 by means of wbd (Razmjooei et al., 2023). This correlation suggests that *E. huxleyi* must have appeared below diamict 1 in core PS2185-6 indicating an age younger than the MIS 8/9 transition based on its global first appearance (290 ka, Backman et al., 2012; Anthonissen and Ogg, 2012), which agrees with the extinction age below this possible LO (Fig. 5). Amino acid razemization data on *N. pachyderma* and *C. wuellerstorfi* indicate a MIS 6–9 age for the LO of *E. huxleyi* in core LOMROG12-PC03 (West et al., 2023). In contrast, the extinction age of $^{231}Pa_{xs}$ of 140 ka below the correlated LO in core PS87/030-1 indicates an age younger than MIS 6 (Hillaire-Marcel et al., 2017; Razmjooei et al., 2023). Thus, *E. huxleyi* might have appeared in the Arctic Ocean not before MIS 5 (Razmjooei et al., 2023) but this datum should be calibrated in a core with a detailed independent chronostratigraphy.

Unfortunately, the interval between the base of diamict 1 and the foraminifera maximum at 170 cm is barren of calcareous microfossils in core PS2185-6. In contrast, a foraminifera-bearing layer has been recognized in adjacent core 91/12-1pc at the stratigraphic level of the proposed LO of *E. huxleyi* (Jakobsson et al., 2001; Backman et al., 2004; Razmjooei et al., 2023) that might correspond to MIS 5.

The top of the lower foraminifera-rich layer at ca. 220 cm, tentatively assigned to brown bed B 7, may be of late MIS 9 age if the detrital carbonate maximum in core PS2185-6 is equivalent to a pink-white layer in core PS115/2-2-2 dated to 282 ka based on $^{230}Th_{xs}$ data (Fig. 5; Stein et al., 2010a, 2025).

Based on the wbd correlation the coccolith *Pseudoemiliania lacunosa* must have disappeared slightly below diamict 2 in core PS2185-6 (Fig. 5; Razmjooei et al., 2023), the former MIS 6 (Spielhagen et al., 2004). This stratigraphic level might be placed at the absolute abundance maximum of foraminifera at ca. 310 cm that has been previously assigned to MIS 7 (Spielhagen et al., 2004). However, the disappearance of *P. lacunosa* indicates an age older than uppermost MIS 12 (ca. 430–440 ka) for this stratigraphic level (Backman et al., 2012; Anthonissen and Ogg, 2012). Razmjooei et al. (2023) suggest that *P. lacunosa* disappeared in MIS 13 (> 478 ka) because they assume that this coccolithophore was not present in the Arctic Ocean in a glacial period such as MIS 12. However, a pronounced temperature decline in a glacial stage might have been a more likely trigger for extinction than a relatively warm interglacial. The correlated HO of *P. lacunosa* in core PS2185-6 indicates that the first downcore change in magnetic polarity occurred in the early Middle Pleistocene, and is older than MIS 11 but probably younger than the Brunhes/Matuyama boundary (Fig. 5).

The new stratigraphic data appear to be rather consistent for the central Lomonosov Ridge. In particular, the revised coccolith biostratigraphy now aligns much better with the $^{230}Th_{xs}$ data. However, this calls into question the interpretation of the OSL ages from core 96/24-1sel located close to core 96/12-1pc (Fig. 1; Jakobsson et al., 2003) that apparently disagrees with the new chronology.

The chronostratigraphy of the western Arctic Ocean cores is more debatable. Magnetostratigraphy provides the basic age model for cores PS72/340-5 and PS72/396-5 (Bazhenova, 2012; Elkina et al., 2023). The entire studied interval in core PS72/340-5 is assigned to the Brunhes Chron supported by radiocarbon ages (Fig. 4) (Bazhenova, 2012; Elkina et al., 2023) while $^{230}Th_{xs}$ data (Geibert et al., 2021) suggest that the change to reverse magnetic polarity in core PS72/396-5 corresponds to the Brunhes/Matuyama boundary, located in the middle part of Unit K, while the Jaramillo Subchron is placed at the transition of Unit K to J (Fig. 3, Elkina et al., 2023). This agrees with the correlation of lithological units to the magnetic polarity pattern based on the re-analysis of paleomagnetic data obtained on sediment cores recovered from ice island T-3 in the Mendeleev Ridge area (Jones, 1987). Song et al. (2023) used the $^{230}Th_{xs}$ data to tentatively propose a MIS 5e/late Termination II age at ca. 28 cm, and an age older than MIS 7 and younger than MIS 9 at ca. 65 cm in core PS72/396-5. At the latter stratigraphic level the diamicton PW 2 has been dated to 282 ka (top MIS 9) based on the correlation to a pink-white layer in core PS115/2-2-2 (Stein et al., 2025). Both age estimates are quite close indicating a MIS 9 age for the biogenic carbonate-bearing brown bed B7. In contrast, the interval which may have a MIS 5e/late Termination II age (Song et al., 2023) is barren of foraminifera in core PS72/396-5 (Fig. 3).

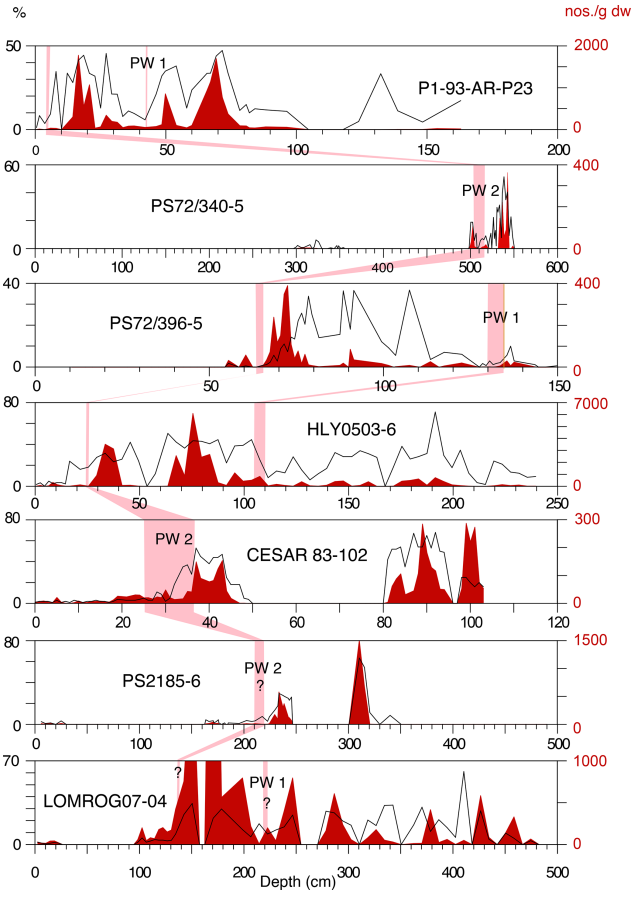

Figure 11. Stratigraphic occurrence of *B. arctica* across the Arctic Ocean. Core locations are shown in Fig. 1. Absolute abundances (> 63 µm) of cores P1-93-AR-P23, HLY0503-6, and LOMROG07-04 are from Lazar and Polyak (2016), and CESAR83-102 from Scott et al. (1989). The depth intervals of the pink-white layers are from Cronin et al. (2014) and Scott et al. (1989). %: relative abundances; no g^{-1} dw: absolute abundances. Absolute abundances in core CESAR83-102 are numbers/10ccm wet sample (Scott et al., 1989).

4.2 Foraminifera biostratigraphy

Here, we critically discuss the benthic foraminifera bioevents to select those that are useful for stratigraphic correlation in the CAO. These bioevents are tentatively calibrated to independent lithological and chronological data. We refrain from assigning numerical ages or marine isotope substages to bioevents because of a lack of a robust independent chronostratigraphy. We rather stick to marine isotope stages that imply a certain duration and not a single definite age. This

leaves some degree of freedom for chronostratigraphic interpretations based on other proxies.

4.2.1 Changeover in benthic foraminifera assemblages

A conspicuous change in benthic foraminifera assemblages occurred across the Arctic Ocean in the Pleistocene when the predominance of agglutinated benthic foraminifera was replaced by calcareous foraminifera (Fig. 5) (O'Neill, 1981; Scott et al., 1989; Evans and Kaminski, 1998; Backman et al., 2004; Polyak et al., 2004; Cronin et al., 2008). Cronin et al. (2008) compile data from various sediment cores and suggest that this turnover may have occurred across the Arctic Ocean in MIS 7 to 9, but they note that the age control is based on sites from the central Lomonosov Ridge. However, the new age tie-points of core PS 2185-6 rather suggest an older age, and the evaluation of previously published data of cores from the Amerasian Basin (see below) suggest a time-transgressive change in the benthic foraminifera assemblages across the CAO.

The stratigraphic level of the turnover is located close to the first downcore change from normal to reverse magnetic polarity on the western Lomonosov Ridge in cores PS87/023-1, PS2185-6, 96/12-1pc and IODP Hole M0004C (Figs. 1, 5, Frederichs, 1995; Evans and Kaminski, 1998; Jakobsson et al., 2001; Backman et al., 2004; Spielhagen et al., 2004; Cronin et al., 2008; OŔegan et al., 2008; Stein, 2015; Elkina et al., 2023). Frequent polarity changes occurred below this stratigraphic level where assemblages in most cores are almost exclusively composed of agglutinated benthic foraminifera. The HO of *Pseudoemiliania lacunosa* correlated to core PS2185-6 suggests an age older than MIS 11 for this stratigraphic level (Fig. 5).

Semi-quantitative shipboard data of core PS87/030-1 suggest that agglutinated foraminifera increased downcore from an indurated carbonate layer at ca. 218–222 cm core depth (Stein, 2015). The wbd correlation between cores PS87/030-1 and PS2185-6 (Razmjooei et al., 2023) indicates that the changeover from agglutinated to calcareous foraminifera and the indurated carbonate layer are almost coeval with the first downcore change from positive to negative magnetic polarity. Based on the age tie-points of core PS2185-6, a MIS 11 or older age for this layer is likely. Interestingly, a carbonate hardground of comparable age has been dredged on the Alpha Ridge being probably not older than 400 ka (MIS 11, Bingham-Koslowski et al., 2025).

Formation of hardgrounds are linked to sedimentation breaks suggesting the presence of a hiatus or a condensed stratigraphic interval in core PS87/030-1. Neither an indurated layer nor an unconformity has been described for core PS2185-6 (e.g. Svindland and Vorren, 2002) but a significant increase in coarse fraction content ($> 63\,\mu m$) occurred slightly above this stratigraphic level (Fig. 5). Unconformities formed by glacial erosion have been observed frequently on Lomonosov Ridge (e.g., Jakobsson et al., 2001, 2010; Polyak et al., 2001; Frank et al., 2008) complicating the establishment of age models for sediment cores. The considerable thickness of lower to middle Pleistocene sediments younger than 1.8 Ma in ACEX Hole M0004C (O'Regan et al., 2008; Frank et al., 2008) rather suggests a more continuous sedimentation in deeper waters close to site PS2185.

A comparable relation to the magnetic polarity change can been observed on Morris Jesup Rise in core PS2200-5 where planktic foraminifera abundances decrease while agglutinated foraminifera abundances increase downcore at the base of the uppermost interval with normal magnetic polarity (Evans and Kaminski, 1998; Frederichs, 1995; Spielhagen et al., 2004). It might be likely that the substantial change in benthic foraminifera assemblages at the sites in the eastern Arctic Ocean was coeval and occurred in the Middle Pleistocene older than MIS 11.

In the western Arctic Ocean, there is some variability in the age of the turnover but it is apparently older than on Lomonosov Ridge. On Northwind Ridge the changeover occurred in core PI-88AR-P5 in the uppermost Early Pleistocene close to the base of the Jaramillo Subchron (ca. 1.1 Ma; Poore et al., 1993; Backman et al., 2004). At the Mendeleev Ridge, the new sediment cores have not been studied down to the turnover of calcareous to agglutinated foraminifera but preliminary shipboard data suggest that it occurred below the Jaramillo Subchron (Stein et al., 2010b; Elkina et al., 2023). This is comparable to Clark et al. (1990) who observed this change at approximately 1.5–2 Ma. At the Alpha Ridge, the turnover occurred in core CESAR 83-14 within or at the top of the Olduvai Chron (ca. 1.77–1.93 Ma; Scott et al., 1989; Aksu, 1985).

4.2.2 HCO of *Bolivina arctica*

According to the current knowledge, *Bolivina arctica* evolved in and is endemic to the Arctic Ocean. The species likely appeared in the Late Pliocene (HLY0505-03JPC; Polyak et al., 2013; Dipre et al., 2018) and eventually evolved from *Virgulopsis pygmeus* which was described from Oligocene sediments in the Beaufort-Mackenzie basin (McNeil, 1997) (Appendix A). *Bolivina arctica* is today only a rare component of living assemblages, e.g. at site PS2185 (Wollenburg and Mackensen, 1998; Wollenburg and Kuhnt, 2000). It is rare in upper Pleistocene sediments and increases to strongly variable relative and absolute abundances downcore from the lower part of the uppermost interval with normal magnetic polarity (Herman, 1973; Scott et al., 1989; Pak et al., 1992; Ishman et al., 1996; Wollenburg et al., 2001a, b, c, d; Polyak et al., 2004, 2013; Cronin et al., 2014; Lazar and Polyak, 2016) and occurs from the top of lithological Unit A to top of Unit M in the western Arctic Ocean (O'Neil, 1981; Scott et al., 1989).

At the deep-water sites PS72/340 and PS72/396 the youngest maximum of absolute abundance is observed in a lithological sequence consisting of two brown layers in-

terbedded with sediments enriched in detrital dolomite which is visible on split core surfaces at the Mendeleev Ridge (Figs. 3, 4). This sequence is assigned to brown beds B 6 and B 7 and pink-white layer PW 2 (Stein et al., 2010b). A pronounced decrease of the absolute abundance occurred close to the base of PW 2 at the top of a brown layer on Northwind, Mendeleev and Alpha ridges (Fig. 11; Scott et al., 1989; Cronin et al., 2014; Lazar and Polyak, 2016). The lithostratigraphic correlation suggests that the HCO on the Lomonosov Ridge is located at comparable stratigraphic level, the base of the potential pink-white layer PW 2 in core PS2185-6 (Fig. 5).

Therefore, the HCO of *B. arctica* (> 63 µm size fraction) can be defined for sediment cores from 800 to 2700 m water depth, at the top of the youngest absolute abundance maximum, corresponding to the top of brown bed B7 and the base of the diamicton PW 2. Absolute abundances of *B. arctica* are consistently low above this stratigraphic level (Fig. 11). Moreover, this bioevent marks the top of lithological Unit L. This offers the possibility to test whether certain sedimentary layers characteristic for Unit M in the Mendeleev Ridge area may also be found on Lomonosov Ridge. It must be noted that high relative abundances may occur above this stratigraphic level but if absolute abundance were calculated these are low (e.g., Scott et al., 1989, 2009).

Previously, this stratigraphic level was assigned on Lomonosov Ridge in core PS2185-6 to MIS 5.5 (Jakobsson et al., 2003; Spielhagen et al., 2004; Backman et al., 2004) but this is untenable because the $^{230}Th_{xs}$ extinction age of 224 ± 56 ka above the HCO is older than MIS 6 (Fig. 5). At the northern Barents Sea continental margin *B. arctica* is rare in Hole 910A, cores PS2212-3 and PS2138-1 in MIS 6 to MIS 2 sediments (Wollenburg et al., 2001a, b, c, d; Wollenburg, unpublished data) supporting an age older than MIS 6 for the HCO. The HCO is located above the correlated HO of *P. lacunosa* (Razmjooei et al., 2023) which confirms a Middle Pleistocene age, being older than MIS 6 and younger than MIS 12 (Fig. 5). A pink-white layer in core PS115/2-2-2 from the Laptev Sea continental margin that has been dated to 282 ka (Stein et al., 2025) might be coeval with the layer rich in detrital carbonates (PW 2) at the top of the HCO in core PS2185-6. This age perfectly fits into the stratigraphic sequence, suggesting that the HCO has a MIS 9 age (Fig. 5).

At the southwestern Mendeleev Ridge, a tentative interpretation of the $^{230}Th_{ex}$ data (Song et al., 2023) suggests an age older than MIS 7 and younger than MIS 9/late Termination IV for the HCO in core PS72/396-5 (Fig. 3). If the correlation of a pink-white layer from the Eurasian Basin to the Mendeleev Ridge PW 2 layer holds true (Stein et al., 2025), then an upper MIS 9 age of the HCO of *B. arctica* appears likely for the entire Arctic Ocean.

The calibration of this bioevent cannot be improved in the subarctic realm because records of *B. arctica* from the North Atlantic (Scott et al., 1989; Kaminski et al., 1989; Hull et al., 1996; Collins et al., 1996; Wang et al., 2021) are not thoroughly documented to assess a subpolar occurrence.

4.2.3 HO of *Haplophragmoides obscurus*

The HO of the extinct agglutinated *Haplophragmoides obscurus* might be a useful bioevent in the eastern Arctic Ocean in the Middle Pleistocene but a definite datum cannot be defined with the available data. It disappeared slightly above the HCO of *B. arctica* in a calcareous foraminifera-rich brown layer in core PS2185-6 (Fig. 5), and a few specimens were observed at the top of Unit L in deep-water core PS72/340-5 (Fig. 4). In ACEX Hole M0004C, *H. obscurus* (as *Cyclammina pusilla*) occurs up to the top of the interval with dominant agglutinated benthic foraminifera but specimens were not determined to species level above the changeover to calcareous foraminifera (Cronin et al., 2008; O'Regan et al., 2008) preventing to define the HO. The HO of *H. obscurus* (as *Cyclammina pusilla*) in core PS2200-5 from Morris Jesup Rise is in a planktic foraminifer-rich interval in the Brunhes Chron which may correspond to that in core PS2185-6 (Evans and Kaminski, 1998; Spielhagen et al., 2004).

In cores from the western Arctic Ocean the HO of *H. obscurus* has been recorded mainly from lower Pleistocene sediments. (O'Neill; 1981; Jones, 1987) On Alpha Ridge *H. obscurus* (as *Cyclammina pusilla*) disappeared in core CESAR 93-014 close to the top of the Olduvai Subchron (ca. 1.8Ma; Aksu 1985; Scott et al., 1989). This species occurs sporadically up to the top of the youngest lithological unit M in Northwind Ridge cores PI88-AR-3 and PI88-AR-5 (Poore et al., 1994; Ishman et al., 1996) but these young occurrences may have been reworked.

4.2.4 *Pullenia bulloides*

The occurrence of the genus *Pullenia* spp. or *Pullenia bulloides* has been previously used as stratigraphic marker for MIS 7 in the CAO (Jakobsson et al., 2001; Backman et al., 2004; Nørgaard-Pedersen et al., 2007a, b; Hanslik et al., 2013). However, *P. bulloides* is not restricted to a single stratigraphic interval in Pleistocene sediments from shallow submarine highs in the CAO and at the northern Barents Sea continental margin (Fig. 7; Scott et al., 1989; Poore et al., 1994; Wollenburg et al., 2001a, b, c, d; Chauhan et al., 2014, 2015; Lazar and Polyak, 2016). This species has been used in the Norwegian-Greenland Sea and Fram Strait as a stratigraphic marker for MIS 5a but in cores located in less than 2000 m water depth, maxima in relative abundance occur during various time intervals in the Late Pleistocene. A single maximum has only been observed in cores from water depths > 2000 m (e.g., Haake et al., 1992; Struck, 1997; Wollenburg et al., 2001). The stratigraphic application is further complicated by the co-occurrence of three closely related *Pullenia* species (*P. bulloides*, *P. quinqueloba*, *P. osloensis*) in the CAO (Figs. 4, 5; Appendix A). These species must

be unequivocally distinguished before any of these taxa can further be applied as stratigraphic marker.

4.2.5 *Epistominella exigua* and *E. arctica*

Absolute abundances of *E. exigua* are usually lower than those of *E. arctica* in Arctic Ocean cores from shallow water depths and *E. exigua* is only sporadically present at the deep-water sites PS72/396 and PS72/340 (Figs. 3, 4). In the upper Pleistocene a time-transgressive changeover from *E. exigua* to *E. arctica* is observed between PW 1 and PW 2 (Figs. 9, 10; Lazar and Polyak, 2016). In sediments younger than the latter stratigraphic level *E. exigua* is generally rare.

The stratigraphic occurrence is, on the one hand, influenced by the preferential dissolution of thin shells of epifaunal to shallow infaunal taxa (Appendix Table B; Fig. 12). Often the last and largest chamber of *E. arctica* is lost and specimens may be then found preferentially in the size fraction < 63 µm. Selective dissolution of thin-shelled and small (< 100 µm) Arctic benthic foraminifera may lead to overrepresentation of robust and/or infaunal species such as *Bulimina aculeata* and *Bolivina arctica*.

On the other hand, *E. exigua* may also be difficult to distinguish from *Eilohedra vitrea* (Appendix A). Since *E. exigua* and *E. arctica* differ in their ecological requirements, probably defining a different stratigraphic occurrence, both species must be unequivocally distinguished. Both species are feeding on phytodetritus, but *E. arctica* is adapted to the Arctic, whereas *E. exigua* is an invasive Atlantic species, demanding a higher, possibly also more frequent particulate organic carbon transfer to depth and eventually higher temperatures (Appendix Table B). Differentiation between *E. exigua* and *E. vitrea* is also essential as only *E. exigua* is a deep-water phytodetritus species, whereas *E. vitrea* is more common at shallower sites and a reproduction following phytodetritus blooms is not mandatory (Appendix Table B).

The turnover from *E. exigua* to *E. arctica* might be a useful stratigraphic event but the age assignment must be evaluated after detailed taxonomic studies were conducted to unequivocally distinguish *E. arctica* and *E. exigua* from *Stetsonia horvathi* and *Eilohedra vitrea*, respectively (Appendix A).

4.2.6 LCO of *Oridorsalis umbonatus*

A range bottom of *O. umbonatus* (as *O. tener)* based on the size fraction > 125 µm has been previously defined at the base of a foraminifer-rich brown layer in cores 96/12-1pc, NP26-5 and PI88-AR-P5 and dated to MIS 5.1 (Backman et al., 2004; Polyak et al., 2004). However, this species also occurred sporadically in older sediments (Fig. 8; Clark et al., 1990; Pak et al., 1992; Ishman et al., 1996; Polyak et al., 2004; Hanslik, 2011; Lazar and Polyak, 2016). In contrast, a distinct oldest absolute abundance maximum can be observed across the CAO in a brown layer above pink-white layer PW 2 (Fig. 8). In sediment cores from shallow submarine highs (< 2000 m water depth) this stratigraphic level coincides with the acme of *B. aculeata* (see below) on Lomonosov Ridge (Fig. 5, PS2185-6; 96/12-1pc, LOMROG07-PC04; Jakobsson et al., 2001; Lazar and Polyak, 2016) and on Mendeleev Ridge (NP26 composite of cores NP 26-5 and 26-32, HLY0503-6JPC; Polyak et al., 2004; Lazar and Polyak, 2016). Therefore, based on absolute abundances in the size fraction > 63 µm, the LCO of *O. umbonatus* is defined, coeval with the base of the *Bulimina aculeata* acme in sediment cores from water depths shallower than 2000 m. Since *O. umbonatus* generally increases above the HCO of *B. arctica*, it is assumed that the LCO of *O. umbonatus* in both cores PS72/396-5 and PS72/340-5 is coeval with that in core PS2185-6. The LCO is located in core PS2185-6 (Fig. 5) slightly below the $^{230}Th_{xs}$ extinction age of 226 ± 54 ka and distinctly above the correlated $^{230}Th_{xs}$ age of 282 ka (Stein et al., 2025) suggesting an age older than top of MIS 7 and younger than MIS 9. At the southwestern Mendeleev Ridge, the LCO is located slightly above pink-white layer PW 2 in core PS72/396-5 (Fig. 3). This layer has been assigned an age of 282 ka (uppermost MIS 9) (Stein et al., 2025), and was tentatively dated to older than MIS 7 and younger than MIS 9/late Termination IV by Song et al. (2023). Based on these age constraints, the LCO is probably of MIS 7 age. The LCO is not unequivocally linked to a specific brown layer at Mendeleev and Northwind ridges. The lowest distinct absolute abundance maximum is associated with brown beds B5 and B4 in the composite record of cores NP26-5 and NP26-32 (Polyak et al., 2004). The maximum in B5 is linked to high relative abundances reflecting possibly post-depositional enrichment of this robust species due to selective dissolution of thin-shelled associated species. Comparably, relatively high relative abundances occur in cores PI-88-AR-3 and -5 at the top of brown bed B5 to B4 (Poore et al., 1994; Ishman et al., 1996). Absolute abundances of *Oridorsalis umbonatus* increase in brown bed B4 in core PS72/340-5 (Fig. 4). An even older LCO cannot be excluded because laminated sediments and absence of calcareous foraminifera in brown bed B5 indicate carbonate-aggressive bottom/pore water conditions at this site. In core PS72/396-5, the LCO occurred at the base of brown bed B6. These differences indicate that an unequivocal correlation of many brown layers is dubious. This may be caused by extensive bioturbation at sites with slow sedimentation (mm ka^{-1}) such as PS73/396 which is indicated by extensive brown mottling in greyish sediments, the absence of calcareous benthic foraminifera over long intervals at sites such as PS72/340-5 (Fig. 4) and possibly post-depositional changes of redox conditions leading to formation or dissolution of Mn-rich layers (März et al., 2011) causing a variable record of brown layers between sites (see also Stein et al., 2010b).

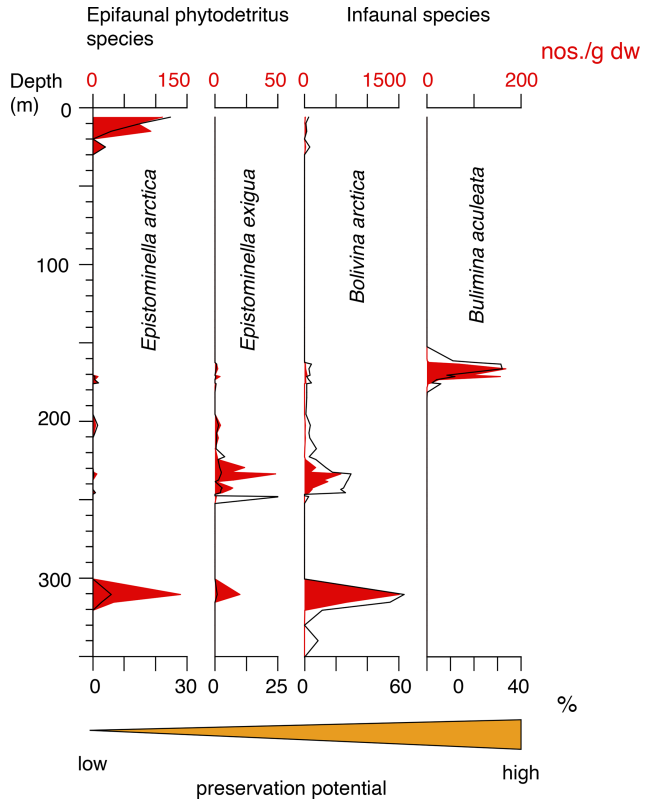

Figure 12. Influence of the preservation potential (qualitative assessment based on Appendix B: Ecology, shell characteristics, and preservation of main calcareous taxa) of *Epistominella arctica, E. exigua, Bolivina arctica* and *Bulimina aculeata* on the formation of absolute abundance maxima in core PS2185-6. The more robust species are successively enriched with increasing selective dissolution.

4.2.7 Acme of *Bulimina aculeata*

The acme of *Bulimina aculeata* in a short stratigraphic interval in Pleistocene Arctic Ocean sediments, corresponding to the *B. aculeata* assemblage zone of Ishman et al. (1996), has previously been used as stratigraphic marker for MIS 5.1 (e.g., Jakobsson et al., 2001; Polyak et al., 2004; Nørgaard-Pedersen et al., 2007a, b; Cronin et al., 2014; Xiao et al., 2020). Despite its possible stratigraphic importance this bioevent is rather poorly defined, and often only the occurrence of *B. aculeata* is noted (e.g., Hanslik et al., 2013; Alexanderson et al., 2014; Cronin et al., 2014; Xiao et al., 2020). Moreover, the stratigraphic interpretation is complicated by sporadic occurrences at other stratigraphic levels in the Pleistocene (Fig. 6; Herman et al., 1989; Scott et al., 1989; Poore et al., 1993, 1994; Ishman et al., 1996; Osterman, 1996; Jakobsson et al., 2001; Polyak et al., 2004; Lazar and Polyak, 2016).

In contrast to relative abundances, absolute abundances depict a distinct single maximum in cores from less than ~ 2000 m water depth across the Arctic Ocean in the Middle Pleistocene (Fig. 6; Jakobsson et al., 2001; Polyak et al., 2004; Lazar and Polyak, 2016). This abundance maximum is located in many cores above a pink-white layer which is assigned to PW 2 (see also Polyak et al., 2004). In core P1-93-AR-P23 from Northwind Ridge the acme is observed even below the inferred PW 2 layer at the HCO of *B. arctica* (Fig. 6) close to the core surface, probably caused by mixing of sediments due to coring disturbance. In contrast, in adjacent cores P1-88-AR-3 and -5, a single maximum in relative abundances occurs distinctly above the HCO of *B. arctica* (Ishman et al., 1996). The maximum is associated with a brown layer that has been assigned to brown bed B 4 in the composite record of cores NP26-5 and NP26-32 on Mendeleev Ridge (Polyak et al., 2004). A common feature in many records is the absence of *B. aculeata* in sediments younger than the acme (Fig. 6).

The *Bulimina aculeata* acme is here defined based on a pronounced maximum in absolute abundances in the $>$ 63 µm size fraction, associated with brown bed B 4 on Mendeleev Ridge. This acme is restricted to cores from moderate water depths (~ 2000 m) corresponding to the modern habitat depth (200 to 1500 m) of the closely related *B. marginata* which is usually lumped with *B. aculeata* in studies on Norwegian-Greenland Sea sediments (Mackensen et al., 1985; Höglund, 1947; Husum and Hald, 2004; Feyling-Hanssen, 1964; Spezzaferri et al., 2013). *Bulimina aculeata* occurs only sporadically beyond its habitat in deeper waters (Fig. 4). The acme is associated with an absolute abundance maximum of *Cassidulina neoteretis* and *Oridorsalis umbonatus* on the shallow submarine highs (Fig. 5) which can be also recognized in the $>$ 150 or $>$ 125 µm grain-size fractions (Jakobsson et al., 2001; Polyak et al., 2004; Lazar and Polyak, 2016).

The $^{230}Th_{xs}$ extinction age of 226 ± 54 kyrs suggests a MIS 7 age for the base of the acme in core PS2185-6 (Fig. 5). The stratigraphic correlation of the LO of *E. huxleyi* to PS2185-6 (Razmjooei et al., 2023) which is located above the acme indicates an age certainly older than MIS 5 for the top of the acme. Hillaire-Marcel et al. (2017) observe that the maximum of *B. aculeata* at 70–90 cm in the shipboard data set of core PS87/030-1 ($>$ 125 µm size fraction, Stein, 2015) is located between the extinction ages of $^{231}Pa_{xs}$ of ~ 140 kyrs at about 70 cm and of $^{230}Th_{xs}$, of $\sim 250 \pm 19$ kyrs at ~ 109 cm ± 44 cm (Song et al., 2023). These authors assume that the base of the event is located at the MIS8/7 transition and in early MIS 7. Therefore, the acme may have occurred in MIS 7, which corresponds to the age for the LCO of *O. umbonatus*. Despite a clear relation to lithology being absent, the LCO in combination with the *B. aculeata* acme appears to be a robust stratigraphic datum in shallow water cores.

4.3 Ecological and taphonomic processes determine the formation of bioevents

Since evolutionary turnover does not play a role in the stratigraphic occurrence of most benthic foraminifera species in the Pleistocene of the Arctic Ocean, the composition of assemblages is determined by the complex interaction of ecologic requirements and taphonomic processes (Appendix Table B). Thus, the formation of bioevents is controlled by a set of factors rather than a single environmental variable (Martin, 2003; Loubere et al., 1993; Loubere and Rayray, 2016).

The spatial distribution of living benthic foraminifera and their preference for specific bathyal water depths is essentially controlled by their food and oxygen requirements (Jorissen, 2003; Jorissen et al., 1995). To a lesser extent competition, grain size of sediments, current activity, bottom water pH, and hydrostatic pressure determine the bathyal faunal composition (Gooday and Jorissen, 2012; Wollenburg et al., 2015).

However, foraminifera do not exclusively live at the sediment surface but can also survive at significant sediment depths if labile organic matter and oxygen is still available (Jorissen, 2003). Mean modern carbon export in the permanently ice-covered CAO is considered amongst the lowest in the world's oceans (Honjo et al., 2008; Nowicki et al., 2022) resulting in particulate organic carbon (POC) fluxes of 0.17–1 $g\,C\,m^{-2}\,yr^{-1}$ at depths > 1000 m (Harada, 2016; Roca-Martí et al., 2016). The low amount of POC reaching the seafloor in the CAO is usually immediately consumed at the sediment surface and not buried to sustain living foraminifera below the surface centimeter under a permanent ice cover (Wollenburg and Mackensen, 1998b). Moderate to deep-infaunal living taxa like *Melonis zaandami* and *Nonionellina labradorica* are only sustained where food flux is seasonally high in the seasonally ice-free areas. Species with an even higher food-demand like *Bulimina aculeata* (Jorissen et al., 1995) are absent from the modern Arctic Ocean (Wollenburg and Mackensen, 1998a, b; Wollenburg and Kuhnt, 2000; Husum et al., 2015).

Benthic foraminifera have been used to reconstruct past sea ice conditions (Cronin et al., 2008; Polyak et al., 2013; Seidenkrantz, 2013). However, benthic foraminifera are only indirectly linked to sea-ice conditions because primary production and sedimentation of organic matter is related to light-penetration through sea ice, upwelling processes at the ice margin and release of ballast material from melting sea ice (Anderson et al., 2003; Mar, 2014; Swoboda et al., 2024). The ice-covered bathyal Arctic Ocean is characterized by opportunistic shallow-infaunal and epilithic/-phytic foraminiferal taxa adapted to low to very moderate carbon flux (Wollenburg and Kuhn, 2000). In seasonally ice-free areas the surplus of labile organic matter provided by export from algae blooms (Swoboda et al., 2024) at the ice edge cause an increase in the number of species that dwell on the sea floor in the accumulated phytodetritus (Faiezieva et al., 2026). Such species rapidly reproduce after algae export events and are termed phytodetritus species (Gooday, 1988; Gooday and Lambshead, 1989; Thomas et al., 1995; Wollenburg and Kuhnt, 2000; Wollenburg et al., 2001b, 2004; Moodley et al., 2002; Polyak et al., 2013).

Among the taphonomic processes, dissolution strongly affects benthic foraminifera assemblages in the Arctic Ocean and its marginal seas (Hunkins et al., 1971; Herman et al., 1989; Steinsund and Hald, 1994; Wollenburg and Kuhnt, 2000; Wollenburg et al., 2001b, 2004; Loubere and Rayray, 2016). Thus, Hunkins et al. (1971, p. 234) assume that foraminifer-poor intervals in CAO sediments indicate conditions more favourable for complete dissolution of calcareous material. In our cores the abundance of thin-shelled specimens and the preservation status of more robust shells indicate when dissolution had a significant impact on the assemblage composition in a specific sample. Many epifaunal taxa, in particular phytodetritus species, which form a major component of living benthic foraminifera in the Arctic Ocean (Wollenburg and Mackensen, 1998a), are thin-shelled and are therefore susceptible to dissolution. These taxa are often lost in the bioturbated uppermost 5 to 10 cm sediments (Loubere and Rayray, 2016). Consequently, the Arctic fossil record usually consists of infaunal and occasional thick-shelled epifaunal taxa (e.g. Cibicides-types). In contrast, high percentages of epifaunal taxa like *Epistominella exigua* are unusual and cannot be explained with modern geochemical processes in near-surface sediments (Loubere and Rayray, 2016). The extensive loss of thin-shelled epifauna species is often caused by massive sedimentation of labile organic matter after algal blooms (Wollenburg and Kuhnt, 2000). The oxidization of this labile organic matter often leads to lowered pH and carbonate aggressive conditions in near-surface sediments and pore water resulting in a dominance of agglutinated taxa even in the living fauna (Scott and Vilks, 1991; Wollenburg and Mackensen, 1998a; Wollenburg and Kuhnt, 2000; Seidenkrantz, 2013).

If the bottom water pH drops seasonally or periodically to values ≤ 7.8, thin-shelled epifaunal foraminifera shells dissolve first. Therefore, assemblages enriched in robust infaunal species such as *Bolivina arctica*, *Oridorsalis umbonatus*, and especially *Bulimina aculeata* reflect a significant taphonomic loss in associated thin-shelled epi- and shallow-infaunal species (Figs. 12–13). Such dissolution-affected assemblages are common in the brown layers especially during the transition from glacial to interglacial conditions. Here the whitish and edged shells of thick-shelled calcareous infaunal taxa are accompanied only by shell fragments of a diminishing number of thin-shelled *Stetsonia horvathi* and *Epistominella arctica* in the small size fraction (Fig. 12).

The identification of MIS 5, especially the last interglacial MIS 5e, is a controversial issue, and the respective foraminifera fauna might have been lost by diagenetic processes in some cores from Lomonosov Ridge. The last interglacial was significant warmer than today, and on the north-

ern Barents Sea continental slope this resulted in primary and export production exceeding todays values (Matthiessen and Knies, 2001; Wollenburg et al., 2001). The degradation of labile organic matter at the sea floor causes a drop in pH at the sediment-water interface (Steinsund and Hald, 1994; Wollenburg and Kuhnt, 2000) and is the main reason for the partial or complete dissolution of calcareous foraminifera at sites of high primary and export production in the modern and marginal Arctic Ocean (Steinsund and Hald, 1994; Wollenburg and Kuhnt, 2000; Wollenburg et al., 2001, 2007). We may thus presume also at site PS2185-6 a sea-ice cover being only seasonal and/or thinner and enabling a higher MIS 5e primary and export production than today. In such a scenario all calcareous foraminiferal shells were likely dissolved and not just a significant proportion as on the northern Barents Sea continental slope (Wollenburg et al., 2001). In core PS2185-6 we observe a few agglutinated *C. subglobosus* at $\sim$ 125 cm that could indicate interglacial or interstadial conditions, but this remains speculative until supported by additional data.

In the CAO calcareous foraminifera are usually restricted to Quaternary sediments, and were rarely reported from the Pliocene. Often sediments older than the Brunhes Chron exclusively comprise agglutinated foraminifera (O'Neill, 1981; Mullen and McNeil, 1995; Cronin et al., 2008b; Kaminski et al., 2009; Kender and Kaminski, 2013). Modern assemblages composed exclusively of agglutinated foraminifera occur only where carbonate dissolution is prevalent, in the deep-sea below the CTD, mud-flats or deep shelves (Murray and Alve, 2011; Murray, 2014). Nonetheless, these are residual assemblages resulting from post-depositional dissolution of calcareous shells in an originally mixed assemblage due to carbonate-aggressive past bottom- and/or pore water pH values (Murray and Alve, 2011). The transition from agglutinated assemblages or wide-spread barren core sections to predominantly calcareous faunas is characterized by the absence of thin-shelled and corrosion traces on more robust taxa (Figs. 12, 13).

The modern CAO benthic foraminifera fauna is rich in loosely agglutinated taxa like *Crithionina* spp., *Rhizammina* spp., and *Aschemonella* spp. that disintegrate soon after death, and robust agglutinated taxa (Wollenburg and Mackensen, 1998). Robust species, firmly agglutinated with ferruginous cement and often thicker shells like *Rhabdammina* spp., *Saccammina* spp., *Psammosphaera fusca*, *Adercotryma glomerata*, *Glomospira* spp., *Reophax* spp., *Cribrostomoides subglobosus*, *Cyclammina* spp. (Bender, 1989; Schröder, 1988), and the extinct *Haplophragmoides obscurus*, are often the only foraminifera preserved in residual sediment core assemblages. It is assumed that the preservation of agglutinated foraminifera is favoured by a rapid burial and/or exposure of sediments to reducing pore waters. Under oxidizing conditions, the iron in the cement is mobilized and shells disintegrate (Schröder, 1988). High organic-bound iron content (Gooday et al., 2008a) is further suggested to be responsible for preservation of organic-walled *Placopsilinella aurantiaca* down to $>$ 400 cm sediment depth in core PS2185-6 and in Alpha Ridge core CESAR 83-014 (Scott et al., 1989). As *H. obscurus* possess firmly agglutinated thick-shelled tests, we presume that it is the least vulnerable taxon susceptible to disintegration (e.g. this study, Scott et al., 1989) explaining their predominance in the intervals with exclusively agglutinated foraminifera. The fact that the original agglutinated residual assemblage with abundant *H. obscurus* had a higher diversity is obvious in samples where associated agglutinated species are observed. Accordingly, the absence of agglutinated foraminifera in core PS72/396-5 can likely be explained by sedimentation rates being too low to prevent iron mobilization from agglutinated shells. The occurrence of *Saccorhiza ramosa*, e.g. in laminated sediments of PS72/340-5, can be explained by its preference for moderate turbiditic water (Schröder, 1988). It is a dominant species in troughs of the Kara Sea where it is positively related to organic- and natural radionuclide-rich sediments (Domanov et al., 2017), indicating a preferred preservation at sites/times with increased sedimentation rate. Secondary enrichment by hydrodynamic sorting as it has been observed in distal turbidites on abyssal plains of the Northwest Atlantic, may have happened.

4.4 Recolonization

Environmental conditions changing with time may also have caused the formation of benthic foraminifera-rich intervals. The observed abundance maxima often occurred after intervals that are barren or contain only a few individuals. Even if one assumes that episodically most foraminifera were lost due to carbonate dissolution or disintegration of agglutinated foraminifera, recolonization must also have occurred after times of adverse living conditions that have caused the partial or total death of faunas. Dispersal of foraminifera following e.g. anoxia or extinction is usually rapid on geological time scales (Buzas and Culver, 1991; Alve, 1999; Murray, 2006), however, to restore the full faunal biodiversity after disturbance may take several millennia indicating different species-dependent capabilities of dispersal (Schmiedl et al., 2003). Based on studies on shallow-water foraminifera and occasional net catches, it is assumed that the dispersal and recolonization of foraminifera in the deep realm occurs via propagules, juvenile individuals smaller than 32 µm (Alve and Goldstein, 2010; Alve and Goldstein, 2003; Murray, 2006; Gooday and Jorissen, 2012). The possible time span of a viable transport of propagules is different for different species and up to two years (Alve and Goldstein, 2014; Alve and Goldstein, 2010). As Fram Strait (sill depth $\sim$ 2500 m) is the only deep-water connection of the Arctic to the world's ocean, any recolonization has and had to occur through Fram Strait. Propagules are advected by inflow of waters from subpolar latitudes, then circulating anticlockwise as Atlantic

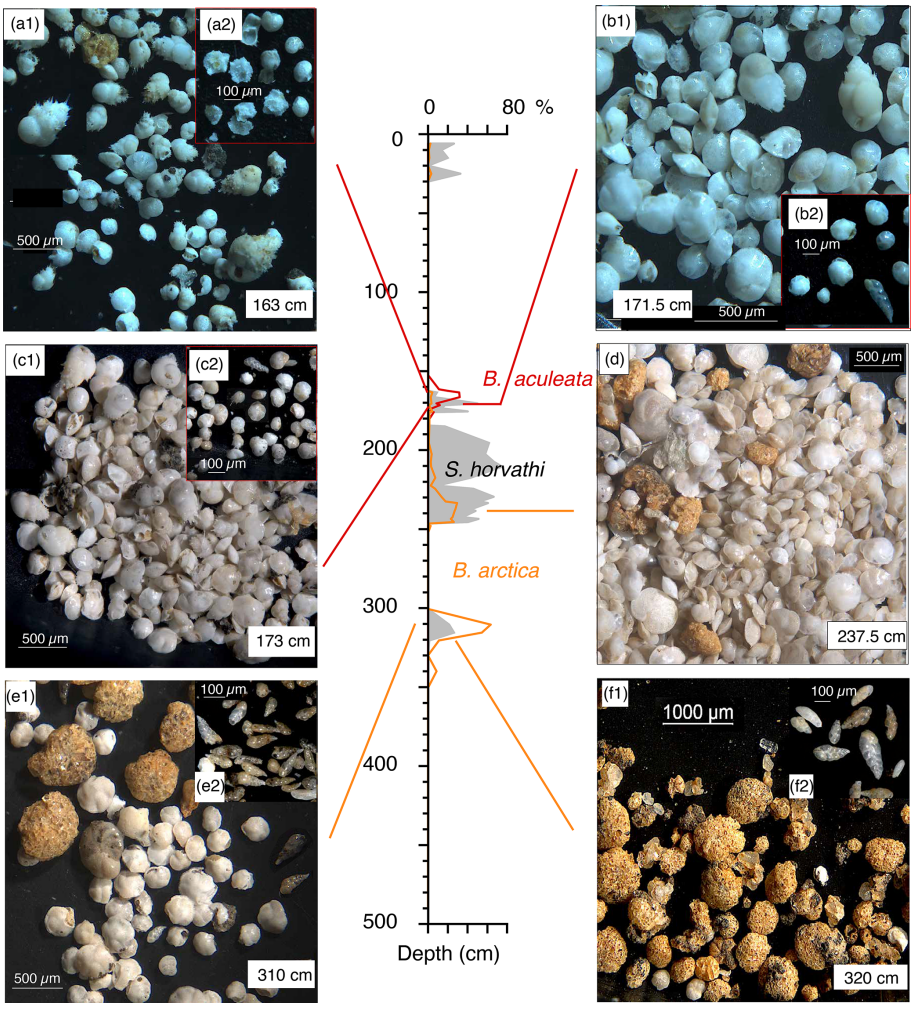

Figure 13. Exemplified preservation of benthic foraminifera in core PS2185-6. Relative abundances of *Bolivina arctica* and *Bulimina aculeata* are plotted vs. *Stetsonia horvathi*. **(f)** 320 cm, lower *B. arctica* maximum. (f1) lf dominated by *H. obscurus*. (f2) mostly well-preserved *B. arctica* in the sf, few corroded calcareous shallow-infaunal specimens, thin-shelled *S. horvathi* almost absent. **(e)** 310 cm, *B. arctica* well preserved, with associated shallow-infauna (e.g. *C. neoteretis*, *S. horvathi*) affected by minor to moderate dissolution (white and partly edged tests), lf (e1) and sf (e2). **(d)** 237.5 cm, below HCO of *B. arctica*, sf and lf shells mostly well preserved, partly hyaline, epifaunal species like *L. wuellerstorfi* present. **(c)** 171.5 cm base of *B. aculeata* acme, almost all shells are whitish but edging in the lf (c1) is minor, in the sf (c2) edging is significant, *S. horvathi* becomes rare. **(b)** 173 cm, peak of *B. aculeata* acme. Shells are progressively affected by dissolution incl. edging (b1), number of *S. horvathi* in the sf (b2) diminished. **(a)** 163 cm, top of *B. aculeata* acme. (a1) cf shells are heavily etched and thin-shelled taxa are extremely rare. (a2) sf consists mainly of shell fragments.

Water (~ 200–600 to 850 m) and Upper Polar Deep Water (Rudels and Carmack, 2022; Timmermans and Marshall, 2020). The fact that Atlantic Water advection is a main factor controlling the distribution of certain foraminiferal species in the Arctic Ocean has been previously suggested based on the restricted distribution of certain taxa in areas close to the Atlantic water inflow (Wollenburg and Kuhnt, 2000). Combined sediment and water DNA analyzes around western and northern Svalbard now support these observations and indicate effective foraminiferal propagule dispersal by Atlantic Water (Nguyen, 2022; Nguyen et al., 2025). From entrance to exit the mean transit time of modern Atlantic Water circulation in the Arctic Ocean is 15–55 years for a full circle (Wefing et al., 2021). In the past the maximum reachable location for a settlement of Atlantic-derived foraminifera species within the Arctic Ocean depended on the species, the local environmental conditions, and the strength of Atlantic water advection during that time. In particular the availability of food played then a major role for the successful colonization at a particular site, not only for the invading species but also the species endemic to the CAO (*H. obscurus*, *B. arctica*).

The modern Arctic Ocean shares the majority of foraminiferal species with the Norwegian-Greenland Sea (Lagoe, 1977; Mackensen et al., 1985; Scott and Vilks,

1991; Bergsten, 1994; Struck, 1995; Wollenburg and Mackensen, 1998a; Wollenburg and Kuhnt, 2000; Rasmussen et al., 2003b; Rasmussen and Thomsen, 2008; Husum et al., 2015). In pre-Brunhes sediments this was different, e.g. *Oridorsalis umbonatus* occurred in Late Miocene sediments on the Vøring Plateau (Osterman and Qvale, 1989) but likely much later in the Arctic Ocean. As other calcareous taxa like *E. exigua*, that possess a thinner shell than *O. umbonatus* or *C. teretis/neoteretis* with an approximately similar shell-thickness, are preserved in much older sediments, this indicates that living propagules of *O. umbonatus* had not been successfully advected to the investigated sites for considerable time before the event.

4.5 Paleoceanographic implications of bioevents

4.5.1 Changeover of agglutinated to calcareous benthic foraminifera

A fundamental change in benthic foraminifera assemblages occurred in upper Pliocene to middle Pleistocene sediments in the CAO (Cronin et al., 2008; this study). This change may be comparable to that observed during the Mid-Pleistocene Transition (MPT) in lower latitudes that was likely driven by a substantial change in food quality and supply (Hayward et al., 2010, 2012; Mancin et al., 2013). Species adapted to a more continuous food supply, with a long life-span and low number of offspring (k-strategists) (Hayward, 2002; Kawagata et al., 2005; Hayward et al., 2012; Kender et al., 2016) were replaced by opportunistic species adapted to more seasonal primary production and able to immediately react with large offspring to food fluxes (r-strategists) (Thomas, 2007; Hayward et al., 2012; Mancin et al., 2013; Kender et al., 2016). None of the MPT extinction-group taxa are observed in the Arctic Ocean (O'Neill, 1981; Osterman, 1996) but the shift from a k-strategy to r-strategy dominated foraminiferal assemblage is likely reflected in the change from large-sized agglutinated taxa (considered to be k-strategist, Hottinger, 1983; Linke, 1992) including the dominant *Haplophragmoides obscurus* in core PS2185-6 (Fig. 5) and the miliolid *Pyrgo rotalaria* (Linke, 1992) in core in PS72/396-5 (Fig. 3), to faunas dominated by calcareous r-strategists. Evans et al. (1995) presume that the abundance maxima composed of agglutinated infaunal species with a detritivore life style reflect interglacial conditions, supporting their interpretation as k-strategist species. The fact that agglutinated foraminifera with ferruginous cement can only be preserved in reducing sediments may be indicative of increased past labile organic matter deposition supporting such interpretations.

However, the interpretation is complicated by the unknown loss in calcareous and agglutinated benthic foraminifera in the intervals with dominant agglutinated foraminifera. In core PS72/396-5, agglutinated taxa are rarely present, and we assume the common occurrence of *P. rotalaria* below the HCO of *B. arctica* being partly synchronous with the common occurrence of *H. obscurus* at site PS2185. *Pyrgo rotalaria* is a k-strategist, which is able to ingest large amounts of algae during export events, and to live on its own cytoplasm during periods of starvation (Linke, 1992). It is a long-living species without spontaneous reproduction in response to export events (Linke, 1992; Linke and Lutze, 1993; Linke et al., 1995; Faizieva et al., 2026). *Pyrgo rotalaria* is common in modern northern high latitude foraminifera faunas (size fraction $> 125\,\mu m$) dominated by calcareous species such as *Lobatula wuellerstorfi*, *C. neoteretis* or *O. umbonatus* plus the associated agglutinated species *Cribrostomoides subglobosus* (Mackensen et al., 1985; Thies, 1991; Nees, 1997; Wollenburg and Mackensen, 1998a, b). At first glance, this fossil assemblage could be regarded as just a modern-analog assemblage affected by dissolution of calcite and disintegration of agglutinants, however, the preservation potential of *P. rotalaria* is described as being lower than that of *L. wuellerstorfi* and *O. umbonatus* (Corliss and Honjo, 1981). Therefore, the dominance of the k-strategist *P. rotalaria* over the r-strategist *L. wuellerstorfi* and *O. umbonatus* in the $>$ 125-fraction is not caused by calcite dissolution but likely reflects a different paleo-export production scenario than today. *Cribrostomoides subglobosus* ingests freshly accumulated phytodetritus within 1-3 days after deposition (Altenbach, 1992; Linke, 1992; Linke and Lutze, 1993; Enge et al., 2011), hereby doubling its cytoplasmic volume in this time span. As no food-triggered reproduction is reported, this species can be considered a k-strategist that already occurred in some of the oldest sediments of PS2185-6 and at the Alpha Ridge, but till today is a common faunal component and among the agglutinated species with highest preservation potential.

4.5.2 Massive supply of IRD as potential trigger for the decrease of *Bolivina arctica* abundance

The youngest absolute abundance maximum of *Bolivina arctica* is terminated by the deposition of the detrital dolomite-rich layer PW 2 in the Arctic Ocean (Figs. 3–5). This represents a massive supply of iceberg-/sea-ice transported material from the Canadian Arctic (e.g. Bazhenova et al., 2017) that might have triggered a fundamental change in the Arctic Ocean ecosystem, possibly linked to grounding of glacial ice on the Lomonosov Ridge. Prior to the HCO the assemblages contain well-preserved intermediate thin-shelled specimens of shallow-infaunal *Cassidulina neoteretis* and sometimes of the even more dissolution susceptible, thin-shelled *Stetsonia horvathi* indicating that preservation did not significantly affect these assemblages (Fig. 12). Benthic foraminifera are absent in PW 2 suggesting that the sea floor was recolonized after this event by species from subpolar latitudes. Since *B. arctica* and *H. obscurus* are endemic species, their abundance was strongly reduced during this event, and they never regained significant abundances when environmental conditions improved after deposition of the PW 2 diamicton.

4.5.3 The *Bulimina aculeata* acme

The assemblages are characterized by the predominance of robust infaunal species such as *B. aculeata* and *O. umbonatus*. In contrast, especially thin-shelled specimens (*E. arctica*, *E. exigua*), episodically also *S. horvathi* and *C. neoteretis* are thoroughly corroded, indicating extensive dissolution and preservation of only a residual assemblage. Moreover, iron-manganese coatings on shells show that these assemblages were exposed for extended times to sea water, reflecting slow sedimentation during this event. *Bulimina aculeata* is adapted to high carbon fluxes and tolerates a high O_2 depletion (Fontanier et al., 2002; Mackensen et al., 1990; Kaithwar et al., 2020). It is as a deep infaunal living foraminifera restricted today to the seasonally ice-free areas, usually at lower latitudes, water depths < 1000 m and high carbon fluxes (Holbourn et al., 2013; Koho et al., 2015; Mackensen et al., 2000). In contrast to *B. aculeata*, the associated fauna primarily consists of typical Arctic foraminiferal species with normal to slightly increased nutritional requirements (Appendix B). Therefore, this mixed assemblage is caused by enrichment of robust species and by specific ecological conditions. Nevertheless, the sudden increase of *Oridorsalis umbonatus* within this event indicate a substantial ecological change, invasion of the respective species and likely competition.

5 Conclusions

Benthic foraminifera bioevents that were previously used to correlate Pleistocene sediments across the central Arctic Ocean were evaluated by studying three sediment cores from the Lomonosov Ridge and the Amerasian Basin west of the southern Mendeleev Ridge, and by comparing the results with published records. A standardized methodology and a stable taxonomy are prerequisites for any biostratigraphic and palecologic interpretation of bioevents. Therefore, the taxonomy of previously used taxa is restudied to select those species that can be unequivocally identified. A detailed taxonomic discussion including light and scanning microscope images are provided in the appendix. Published descriptions of some species are controversial and complicate distinguishing *Epistominella exigua* from *Eilohedra vitrea*, *Stetsonia horvathi* from *Epistominella arctica*, *Cassidulina teretis* from *Cassidulina neoteretis*, and different agglutinated taxa. The only taxa that are relatively well-defined are *Bolivina arctica*, *Bulimina aculeata*, species of *Pullenia*, *Oridorsalis umbonatus* and the agglutinated species *Haplophragmoides obscurus*.

If possible, a minimum of 300 specimens were counted in the size fraction of larger than 125 µm to smaller than 2 mm and depending on diversity $>$ 100–300 in the size fraction larger than 63 to smaller than 125 µm in each sample to achieve robust results. The definition of bioevents is based on absolute abundances, i.e. number of specimens per gram dry weight sediment. Relative abundances calculated as dry weight-% are less reliable because taphonomic processes such as bioturbation, dissolution and disintegration overprint assemblage composition.

Based on absolute abundances, we consider the acme of *Bulimina aculeata*, the lowest common occurrence of *Oridorsalis umbonatus*, and the highest common occurrence of *Bolivina arctica* as robust bioevents in the Middle Pleistocene of the central Arctic Ocean. These bioevents are tentatively assigned to marine isotope stages, MIS 7 for *B. aculeata* and *O. umbonatus*, and MIS 9 for *B. arctica*. The proposed correlation to marine isotope stages should be considered provisional and subject to modifications as additional age tie-points become available. So far numerical ages for these bioevents are too imprecise due to the limited number of biostratigraphic and radiometric ages.

Propagules of *B. aculeata* and *O. umbonatus* must have been advected to the CAO over longer distances from subpolar latitudes, and adequate environmental conditions must have prevailed coeval on a basin-wide scale to form these synchronous bioevents. In contrast, *B. arctica* likely evolved in the Arctic Ocean and the conspicuous decrease in absolute abundances may have been triggered by a massive supply of detrital dolomite-rich ice-rafted debris dominated fauna leading to a considerable change in environmental conditions.

Other species such as *Epistominella exigua* are restricted to a specific water depth and areas with seasonal production pulses.

Agglutinated benthic foraminifera and the turnover of agglutinated to calcareous benthic foraminifera may be additionally useful for stratigraphic correlation in the Arctic Ocean. Based on available data the turnover occurred time-transgressive across the Arctic Ocean. *Haplophragmoides obscurus* is probably the only species that became extinct in the Middle Pleistocene of the CAO.

The recorded bioevents are characterized by extensive taphonomic changes. Robust epifaunal and/or infaunal calcareous species are generally enriched in the assemblages because of selective dissolution and disintegration of thin-shelled epifaunal and agglutinated taxa; ultimately assemblages consist only of agglutinated foraminifera. The predominance of agglutinated to calcareous benthic foraminifera might have been caused either by a fundamental change in food supply and its quality, or was linked to corrosive bottom waters.

The proposed bioevents require thorough testing in sediment cores that have a robust independent chronostratigraphy, e.g. provided by a sequence of radiometric ages (e.g., ^{14}C, ^{231}Pa, ^{230}Th), to accurately calculate numerical ages. The Fram Strait and Yermak Plateau may be ideal areas, where biogenic carbonate-bearing sediments have the potential to add a relatively continuous stable isotope stratigraphy. In the CAO, the upper slope of submarine highs below the possible level of glacial erosion ($>$ ca. 1300 m water depth)

where higher sedimentation rates should be expected may provide more complete sections.

Appendix A: Taxonomy of selected benthic foraminifera (J. Wollenburg)

The taxonomy follows the original descriptions as recorded in the Ellis and Messina Catalogues (Ellis and Messina, 1940–2025), and further revisions described in The World Foraminifera Database at the date of submission (Hayward et al., 2025). A total of 236 species were identified in the sediment cores (Table A1). Species relevant to this study are described in more detail in this Appendix.

Before turning to taxonomy, it is necessary to comment on the shell structure of calcareous species described and illustrated in the work of Herman (1973) and Lagoe (1977). Even at shallow sediment depth or right at the sediment surface the majority of calcareous foraminiferal shells are postmortem affected by authigenic calcite overgrowth resulting in a rough surface texture (Wollenburg et al., 2023a). This overgrowth may consist of idiomorphic crystallites or crystals (e.g. the glendonite resembling crystals which grow from the coalescence of idiomorphic crystallites of an overgrowth coating on *Bolivina arctica* in Plate A1, panel (c) or, likely due to secondary partial dissolution of authigenic calcite crystallites, an assembly of porous crystallite-remains is left (e.g. Pl. A1, panel (c2)), see also Wollenburg et al. (2023b).

The "surface samples" described by Lagoe (1977) comprise the uppermost three cm of piston cores collected from ice island T3. Since the uppermost part of these cores were often lost during coring operations (Clark et al., 1980), most samples may represent an unknown time interval. Lagoe (1977) observed common occurrences of *B. arctica* and illustrated extensive overgrowth on shells indicating that these samples are substantially older than recent. Authigenic overgrowth seen on SEM images of Lagoe (1977):

Pl. no.	Fig. no.	Species
2	2	Lagena sp.
2	10	*Esosyrinx?*
3	9	*Parafissurina* sp.
3	20–21	*Buliminella hensoni* as *B. elegantissima hensoni*
3	23–24	*Parafissurina* sp.
4	2, 6	*Bolivina arctica*
4	3	*Alabaminella weddellensis* as *Buccella arctica*
4	9, 13, 18	*Nonionella iridea* as *Valvulineria arctica*
4	14, 15, 19	*Epistominella arctica*
4	22	*Stetsonia horvathi*
5	8	*Chilostomella elongata*
5	13	*Ioanella horvathi* as *Eponides tumidulus* subsp. *horvathi*
5	16	*Cassidulina neoteretis* as *C. teretis*
5	17–18	*Islandiella norcrossi* as *C. norcrossi*
5	19–21	*Seabrockia earlandi as C. norcrossi*

***Bolivina arctica* Herman, 1973 emend.**

Pl. A1, panels (a)–(d)

Bolivina cf. *B. inflata* Vilks 1969, Pl. 3, Fig. 10a–b.

Bolivina arctica Herman, 1973, Text-Fig. 3, Pl. 1, Figs. 1–7

Bolivina arctica Lagoe, 1977, Pl. 4, Figs. 2, 6.

Bolivina arctica Wollenburg, 1992, Pl. 15, Fig. 3.

A1 Original description (Herman, 1973)

Test small, elongate, about twice as long as broad. Greatest width formed by the last pair of chambers; initial test narrow and twisted. Chambers are biserial, inflated, and increase gradually in size; they are broad and low in the initial part becoming higher in the last 3 to 4 pairs. The sutures are distinct, and slightly oblique and the aperture is elliptical extending from the base of the final chamber. The wall is calcareous, perforate, composed of numerous closely packed, tapering, hollow tube-like structures illustrated in the scanning electron micrographs. This is the first time that such tube-like structures have been reported in benthic foraminifera to my knowledge. Dimensions: Length of holotype 0.20 mm, greatest width 0.12 mm, greatest thickness 0.90 mm. Paratypes length range 0.30–0.18 mm, greatest width range 0.14–0.10 mm, greatest thickness range 0.07–0.10 mm. Stratigraphic range: Pliocene – Pleistocene.

A2 Emended description

Test biserial either straight throughout or the juvenile test is twisted, test small, elongate, two to three times as long as broad. Up to 10 pairs of chambers have been observed; chamber height and width increase rapidly in size and especially ontogenetic old chambers are often very much inflated. The sutures are depressed and oblique, but each new pair of chambers overlap the previous one slightly creating a ribbon-like suture (Pl. A1, panel (b3)). Well-preserved tests are translucent (Pl. A1, panel (a1)), corroded tests or tests affected by calcite overgrowth opaque to white (Pl. A1, panels (c1), (d1), (e1)). Wall smooth and shiny, with irregularly distributed pores (Pl. A1, panels (a2)–(b3)), wall thickness 1 to 2 µm. Aperture very variable, sometimes a broad arch (Pl. A1, panels (c1)–(c2)) but more often an elongated basal loop extending within a depression up the apertural face of the last chamber with a serrated bordering lip, internal toothplate missing. Apertural surface covered with tubercles, some tubercles of older apertural surfaces may still be recognizable in the sutures (Pl. A1, panel (c2)).

Dimensions: 20 specimens measured in the size fraction > 63 µm: Length mean 200 µm (100–300 µm), largest width 70–400 µm, largest thickness 50–200 µm.

A3 Discussion

In this study, well-preserved specimens lack the closely packed, tapering, hollow tube-like structures, observed by Herman (1973, Pl. 1, Figs. 5–7). These features on the shell surface represent authigenic overgrowth and were included in the original description of *Bolivina arctica* by Herman (1973). The majority of Pleistocene *B. arctica* specimens (Pl. A1, panels (c)–(e)) are indeed covered with authigenic calcite overgrowth (Wollenburg et al., 2023a). However, well-preserved specimens are thin-shelled, and have a smooth shell surface and splendid pores (Pl. A1, panels (a)–(b)). Therefore, the original description must be emended to include the description of the shell surface of specimens not affected by post mortem precipitation of calcite.

Authigenic overgrowth cover the whole *B. arctica* tests either by a porous sheet (Pl. A1, panels (c1)–(c3)), as has been described by Herman (1973), or in form of solid idiomorphic crystallites (Pl. A1, panels (d)–(e)). In extreme cases authigenic crystallites grow to large crystals (Pl. A1, panels (d1)–(d2)).

The first two whorls of some specimens are rather triserially than twisted biserially arranged (Pl. A1, panels (a1)–(b1), (c1)–(c2)). Except for their shorter triserial test part, their general appearance and their aperture, these specimens resemble *Virgulopsis pygmeus* (3–4 triserial whorls) described from Oligocene sediments in the Beaufort-Mackenzie basin (McNeil, 1997). This may indicate an evolutionary relation of *B. arctica* to *Virgulopsis pygmeus*.

A4 Comparison to other studies

Specimens of *B. arctica* covered by authigenic overgrowth may be easily misidentified as *Siphotextularia rolshauseni* (Wollenburg et al., 2001) or vice versa because of the white agglutinated test with rough surface texture (Pl. A2, panel (a)) of the latter species. Wang et al. (2021) observed abundant *B. arctica* during MIS 2 in sediment core ARC5-BB01 from the Norwegian Sea. This core is located close to a series of sediment cores which contain abundant *S. rolshauseni* during early MIS 2 but not *B. arctica* (Nees and Struck, 1994). Therefore, it is likely that Wang et al. (2021) assigned specimens of *S. rolshauseni* to *B. arctica*. Scott et al. (2008) illustrated specimens as *B. arctica* (Pl. 5, Figs. 2–9) that may be assigned to the agglutinated taxon *Pseudobolivina antarctica* (Pl. 5, Figs. 2, 3, 6, 7), and the calcareous species *Bolivina pseudoplicata* possessing a rough surface texture (Figs. 8, 9) and *Fursenkoina complanata* (Figs. 4, 5). *Bolivina arctica* (Lazar and Polyak, 2016) was described in many Arctic sediment cores without documenting the identification by images (Scott et al., 1989; Wollenburg, 1995a; Wollenburg and Mackensen, 1998c; Mullen and McNeill, 1995; Polyak and Solheim, 1994; Polyak et al., 2013; Adler et al., 2009; Cronin et al., 2014). Given its stratigraphic distribution in these cores, confusion with other species is ruled out here.

A5 Stratigraphic range

?Pliocene to recent, *B. arctica* became a progressively rare faunal component after the youngest absolute abundance maximum.

A6 Geographic distribution

Arctic Ocean, occurrences outside the Arctic Ocean cannot be validated as respective studies lack images.

A7 Bathymetric comments

Continental slope and ridges, more common at lower mesopelagic to bathyal pelagic (600–4000 m) (Lagoe, 1977; Wollenburg and Mackensen, 1998c, a; Wollenburg and Kuhnt, 2000).

***Bulimina aculeata* d'Orbigny, 1826**

Pl. A2, panels (b)–(d)

Bulimina aculeata d'Orbigny, 1826,

Polymorphium pineïformium Soldani, 1791, p. 119, pl. 269, Fig. 1; pl. 130, Fig. vv.

Bulimina aculeata Parker, Jones and Brady, 1871, p. 172, Pl. 11, Fig. 128.

Bulimina aculeata Fornasini, 1902, p. 152, Fig. 4.

Bulimina pupoides var. *spinulosa* Williamson, 1858, p. 62, Pl. 5, Fig. 128.

Bulimina aculeata Brady, 1884a, p. 406, Pl. 51, Figs. 7–9.

Bulimina marginata Goës,1894 in parts., Pl. 9, Fig. 444.

Bulimina aculeata van Morkhoven et al., 1986, p. 31, Pl. 7.

Bulimina marginata Höglund, 1947, Figs. 205–209, 215–216.

Bulimina sp. O'Neill, 1981, Pl. 3, Fig. 7.

Bulimina aculeata Chauhan et al., 2015, Pl. C, Fig. 3.

Bulimina marginata Chauhan et al., 2015, Pl. C, Fig. 2.

A8 Original description d'Orbigny, 1826

No descriptions and figures were provided. Instead *Bulimina marginata* was illustrated in his work on recent sediment samples from the Adriatic Sea. In the respective study he also provided a new name, *B. aculeata*, for *Polymorphium pineïformium* Soldani 1791.

Parker, Jones and Brady (1871) later stated that the species would be "similar to *B. marginata*, but having a series of long spines fringing the outer margins of the chambers in place of the finely serrate edges exhibited by that species".

A9 Taxonomic remarks (Holbourn et al., 2013)

Test forms an elongate, triserial series; tapered in outline and subcircular in cross-section, with an acute initial portion, and a rounded apertural end; widest in the last whorl. The inflated chambers increase rapidly in height and are separated by distinct, depressed sutures. Chamber walls are calcareous, finely perforate, and often partially translucent and smooth, except at the outer margins of the basal chambers, which are fringed by sturdy spines. These spines may extend halfway up the test. Well-preserved specimens may also have a prominent basal spine. The primary aperture is a loop-shaped opening bordered by a lip and extending up from the base of the final chamber; with an internal toothplate. Geographic distribution: Worldwide. Stratigraphic range: Early Miocene to recent. Bathymetric distribution: Bathyal to abyssal. Dimension: 0.65 to 0.75 mm (Cushman and Parker, 1947).

A10 Discussion

Although *B. aculeata* and *B. marginata* are genetically separated (Tsuchiya et al., 2008), their morphology is extremely variable and intermediate morphotypes often dominate the assemblages. Collins (1989) and Burgess and Schnitker (Burgess and Schnitker, 1990) considered *B. aculeata* and *B. marginata* as distinct species, with an intermediate morphotype representing a morphological variation of *B. marginata*. In contrast, Höglund (1947) suggested that *B. marginata, B. aculeata* and *B. gibba* are morphotypes of the same species. Smith (1964) reported that the number of spines of *B. marginata* f. *denudata* was related to water depth, and loss of spines occurred in relation to increasing water depth. The number and length of spines is extremely variable (Van Morkhoven et al., 1986). Collins (1991) describes an increase in spine length with water depth at sites off Mexico, whereas in the Arctic Ocean specimens from lower deep bathyal water depth ($\sim$ 2500–3500 m in cores PS72/340-5 and PS72/396-5, this study; O'Neill, 1981) possess shorter but more numerous spines than those from upper bathyal to middle bathyal water depths (ODP Hole 910A, PS2185-6 (see PL. A1, panels (b)–(d))).. In the Arctic Ocean *B. aculeata* and *B. marginata* can be clearly distinguished from each other and usually *B. aculeata* is dominant.

A11 Stratigraphic range

Early Miocene to recent (Holbourn et al., 2013)

A12 Geographic distribution

Worldwide (Holbourn et al., 2013); absent from the modern Arctic Ocean

A13 Bathymetric comments

Upper bathyal to lower abyssal (200–10 000 m) (Holbourn et al., 2013).

Cassidulina neoteretis **Seidenkrantz, 1995**

Pl. A2, panels (e)–(i), Pl. A3

Cassidulina teretis Lagoe, 1977, Pl. 5, Figs. 15–16.

Cassidulina teretis Mackensen and Hald, 1988, Pl. 1, Figs. 5–15.

Cassidulina teretis Wollenburg, 1992, Pl. 15, Figs. 6–7.

Cassidulina teretis Wollenburg, 1995, Pl. 3, Figs. 12–13

Cassidulina neoteretis Seidenkrantz, 1995, Pl. 1, Figs. 1–6; Pl. 2, Figs. 1–14; Pl. 3, Figs. 1–8; Pl. 5, Figs. 1–3.

Cassidulina teretis Ishman and Foley 1996, Pl. 2, Fig. 4.

Cassidulina teretis Wollenburg & Mackensen, 1998a, Pl. 3, Figs. 12–13.

Cassidulina neoteretis Wollenburg and Mackensen, 2009, Figs. 3.10, 3.15.

Cassidulina neoteretis Chauhan et al. 2015, Fig. 3.3.

Cassidulina neoteretis Hanslik, 2011, Pl.1, Figs. 5–6.

Cassidulina neoteretis Lazar et al., 2016, Fig. 8.1–8.6.

Cassidulina teretis Cronin et al., 2019b, Pl. 1, Figs. 9–12.

Cassidulina neoteretis Cage et al., 2021, Fig. 2a, 2d–j, 2o.

For a more detailed list of synonyms see also Cage et al. (2021).

A14 Original description (Seidenkrantz, 1995)

Test lenticular, biconvex with an acute, slightly undulating, peripheral margin. Umbilical boss of milky semitranslucent shell material on each side. Eight to ten chambers (frequently 10) in the final whorl, biserial arranged in 4 to 5 alternating pairs, each chamber appearing large, rounded rhomboid to ovate and reaching to the umbilical boss on one side of the test, and small and subtriangular on the other side. Sutures distinct, thickened, but not limbate, slightly depressed and outlining the chamber. Wall calcareous, hyaline or opaque, and optically granular. Surface smooth with relatively small, rounded pores evenly distributed on the chamber walls but with no pores on the umbilical boss or along the sutures. Aperture an elongate, narrow slit extending from the base of the final chamber in a crescent paralleling the outer margin of

the chamber, reaching 2/3 to 3/4 the distance from the base of the chamber to the peripheral keel. A subtriangular apertural plate with a smooth edge, formed by the infolded chamber wall, lies along the inner margin and partly covers the aperture. Seldom few very small serrata on the apertural plate are developed. A narrow, serrate ridge lies adjacent to the outer margin of the aperture. Dimensions: greatest diameter: 230–410 µm (mean 300 µm), greatest thickness: 130–200 µm (mean 150 µm).

A15 Discussion

Cassidulina teretis differs from *C. neoteretis* by a usually narrower and crescentic rather than subtriangular-shaped apertural plate. The apertural plate is not almost smooth as in *C. neoteretis* but provided with densely packed serrata (Cage et al., 2021; Seidenkrantz, 1995). *Cassidulina teretis* (360–550 µm) has a larger test size than *C. neoteretis* (200–410 µm) (Cage et al., 2021). Well-preserved specimens may be identified under the light microscope, but SEM analyses may be required to eventually recognize serrata in corroded *C. teretis* specimens (Pl. A2, panel (i)). However, the majority of corroded *C. neoteretis* specimens can be identified by their broader prominent subtriangular apertural plate. This feature may support species assignment in diagenetically altered specimens even if the edge of the apertural plate has been affected by carbonate dissolution (Pl. A3). *Cassidulina teretis* occurs only in trace amounts in the deep-water cores examined in this study, while other species that are morphologically similar, such as e.g. *Paracassidulina neocarinata* are absent in all our cores. For a clear distinction between *C. neoteretis* and related species, the work by Cage et al. (2021) should be consulted. Tappan (1951) used only drawings in her original description of *C. teretis*. Neither photographs nor details of the apertural plate edge were shown or mentioned. Subsequently, all specimens resembling *C. teretis* were in studies on sub-Arctic to Arctic sediments assigned to *C. teretis*. Seidenkrantz (1995) later re-studied the *C. teretis* holotype and compared it to ∼ 2000 *Cassidulina* specimens with comparable morphology from high northern latitudes and described *C. neoteretis* as a new species. Yet, most Arctic studies did not differentiate between *C. neoteretis* and *C. teretis* until the early 2000s, and continued to assign all specimens to *C. teretis* (Polyak et al., 2004; Ishman and Foley, 1996; Ishman et al., 1996; Rasmussen and Sheldon, 2003; Rasmussen et al., 2003, 2014; Wollenburg and Mackensen, 1998a, b; Wollenburg and Kuhnt, 2000; Wollenburg et al., 2001, 2004). During her early studies the first author was searching for the change from *C. teretis* to *C.neoteretis* in calcareous microfossils-bearing sediments of core PS2185-6 that should have recovered the Brunhes/Matyama boundary (Spielhagen et al., 1997a). However, SEM analysis did not reveal a strongly serrate apertural plate in any of the roughly 100 specimens analyzed back then. With no significant differences in the toothplate (smooth or with only minor and narrow serrata) of all investigated specimens, the first author, as many others, sticked to *C. teretis* as the species name for specimens in her fossil and modern collection. Her first individuals with distinct serrata as indicative of *C. teretis* were observed in this study from the lowest calcareous foraminifera bearing sediments of core PS72/396-5. While Seidenkrantz describes the extinction of *C. teretis* and substitution by *C. neoteretis* in the Norwegian Sea at 700 ka, Lazar et al. (2016) report a long stratigraphic coexistence of both species in the Brunhes Chron on the Northwind Ridge and *C. teretis* specimens in almost every sample (Lazar et al., 2016). The images provided are of good quality and support their distinction of *C. teretis* and *C. neoteretis*. In contrast, in the new cores and surface and core samples the first author had previously worked on (older slides were revisited for this study) only *C. neoteretis* specimens were found. The first author analysed hundreds of specimens under the light microscope and conducted more than 100 SEM analyses on *C. neoteretis/teretis* specimens downcore in PS2185-6, and all specimens could be assigned to *C. neoteretis*. Similarily, in the deep-water cores PS72/340-5 and PS72/396-5 most analyzed specimens were assigned to *C. neoteretis*. Only in core PS72/396-5, at 130 cm sediments dated to the Matuyama Chron (Elkina et al., 2023) few *C. teretis* specimens could be identified. This stratigraphic interval is just below the stratigraphic change to *C. neoteretis* according Seidenkrantz (Seidenkrantz, 1995). In order to gain a better insight into a potential co-occurrence of *C. neoteretis* with *C. teretis* in modern to late Pleistocene sediments on the Mendeleev Ridge additionally well-preserved *C. neoteretis* specimens from the upper 5 cm of core PS72/413-3 (1263 m water depth) were analyzed by light microscope (100 specimens) and SEM (20 specimens). No *C. teretis* was observed in these samples. Probably Lazar et al. (2016) had also recorded reworked iceberg-rafted specimens in their analyses.

A16 Stratigraphic range

Cassidulina teretis was originally described from Pliocene to early Pleistocene sediments of Alaska (Tappan, 1951). It appeared in the Upper and Middle Miocene and became extinct in the North Atlantic shortly after the Gauss/-Matuyama boundary and in the Norwegian Sea shortly after the Brunhes/Matuyama boundary (Seidenkrantz, 1995). *Cassidulina neoteretis* had its first occurrence in the North Atlantic around 2.3–2.0 Ma and its first occurrence in the Norwegian Sea at ∼ 700 ka (Seidenkrantz, 1995). *Cassidulina neoteretis* obviously evolved from *C. teretis* and replaced the latter species at progressively younger times with increasing latitude until *C. teretis* finally disappeared after the Brunhes/Matyama boundary in the Norwegian Sea (Seidenkrantz, 1995). Due to the unclear differentiation of *C. teretis* and *C. neoteretis* the first and last occurrence of both taxa in the Arctic Ocean is unclear.

A17 Geographic distribution

Worldwide, common in the subarctic and Arctic (Holbourn et al., 2013)

A18 Bathymetric comments

Bathyal, in the Arctic Ocean most common at depths of 200–1400 m (Wollenburg and Mackensen, 1998c).

***Cribrostomoides subglobosus* (Cushman, 1910)**

Pl. A4, panels (a)–(b)

Haplophragmoides subglobosum Cushman, 1910, Figs. 162–163.

Lituola subglobosa Sars, M., 1868 (1869), p. 250.

Lituola subglobosa Sars, M., 1871 (1872), p. 253.

Haplophragmium latidorsatum Brady, 1884, Pl. 34, Figs. 8–10, not Figs. 7, 14) (Holbourn et al., 2013).

Haplophragmium latidorsatum Goës, 1894, Pl. 5, Figs. 102–123.

Labrospira subglobosa Høglund, 1947, Fig. 126, Pl. 2, Fig. 2.

Alveolophragmium latidorsatum Barker, 1960, Pl. 34, Figs. 7–8, 10, 14.

Cribrostomoides subglobosus Todd and Low, 1980, Pl. 1, Fig. 7.

Cribrostomoides subglobosum Scott and Vilks, 1991, Pl. 1, Figs. 19–20.

Cribrostomoides subglobosum Thies, 1991, Pl. 7, Figs. 4a–b, Pl. 10–11.

Cribrostomoides subglobosus Jones et al, 1993, Pl. 1, Figs 1–5; Pl. 2 Figs. 6–8; Pl. 3, Figs. 1-7.

Cribrostomoides subglobosum Wollenburg, 1995, Pl. 2, Figs. 10–11.

Recurvoides scitulus Ishman and Foley, 1996, Pl. 1, Fig. 11.

Cribrostomoides subglobosum Wollenburg and Mackensen, 1998, Pl. 2, Figs. 10–11.

A19 Original description (Cushman, 1910)

Test usually planispiral consisting of two or more coils, involute, depressed at the umbilici, chambers very broad and low, wall arenaceous somewhat roughened but variable, chambers usually seven or eight in the final coil, making the test as a whole subglobose, aperture a more or less elongated slit at the base of the apertural face, simple, colour: grey or brown; diameter 1–2.5 mm.

A20 Taxonomic remarks (Holbourn et al., 2013)

Test is involute, initially streptospiral, later planispiral with a subcircular outline and a rounded periphery. Chambers are low and broad, highly inflated, and separated by indistinct sutures. Chamber walls are agglutinated, non-calcareous, and usually smoothly finished. In early chambers the primary aperture is an oval to slit-like areal opening bordered by a narrow lip above the base of the last chamber. In later chambers the primary aperture may become more elongated and the lip may fuse to form multiple openings.

A21 Discussion

O'Neill (1981) described specimens from arctic sediments that are identical to *C. subglobosus* and/or *Cyclammina orbicularis* as *Alveolophragmium polarense* n.sp. but morphological differences to distinguish these species were not discussed. Evans and Kaminski (1998) stated that *A. polarense* from e.g. cores PS2185-6 and PS2212-3 resemble *C. subglobosus* but that alveols in the chamber wall and a planispiral coiling would place these species in *A. polarense*. Having worked on parallel samples from PS2212-3 (Wollenburg et al., 2001a, b, c) and PS2185 (this study), the new data suggest that they had assigned all quasi-planispiral *C. subglobosus*-resembling agglutinants to *A. polarense*. At least for core PS2212-3 and the upper 500 cm analyzed in core PS2185-6 this is a misjudgement since all respective specimens analysed under the SEM (> 10 from various depths) lack alveoles in their chamber wall, thus, have to be assigned to *C. subglobosus*. If we compare the poor SEM image of the chamber wall of *A. polarense* from Evans and Kaminski (1998) with the wall structure of *C. subglobosus* (Pl. 3 in Jones et al., 1993), it becomes apparent that a tight particle-packing in *C. subglobosus* cannot be observed or expected and that indeed Evans and Kaminski's specimen illustrated in their Pl. 2 Figs. (8–9) should be assigned to *C. subglobosus*. The wall structure of the *Alveolophragmium polarense* specimen shown in Pl. 4, fig. 1 of Kaminski et al. (2009) with a striking alveolar wall structure, however, is totally alveolar and resembles both in general appearance and wall structure *Cyclammina orbicularis* (Brady, 1884a), (see also their Pl. 1, Fig. (5a–b)). *Cyclammina orbicularis* is also found in our samples from PS2185-6 (Pl. A4, panel (c)). Considering the high morphological variability of *C. subglobosus* (e.g., Goës, 1894; Thies, 1991). The first author of this study also presumes that many specimens assigned by Evans and Kaminski to *Trochammina lomonosovensis* (Evans and Kaminski, 1998) in core PS2212-3, can be regarded as juvenile *C. subglobosus* specimens. Juvenile *C. subglobosus* tests are typically streptospiral coiled (Pl. 9 of Thies, 1991). and even the holotype SEM images for *T. lomonsovensis* can be regarded as strepto- rather than trochospiral coiled, compare with Evans and Kaminski (1998; Pl. 2, Figs. (7–9)) with the *C. subglobosus* illustrations. Moreover, in core PS2212-3 this

hypothesis is supported by the fact that adult *C. subglobosus* are almost exclsuively associated with small streptospiral individuals which are considered to be juvenile *C. subglobosus* rather than *T. lomonosovensis*. Planispiral juvenile *C. subglobosus* are very rare in the samples analysed. Only clear trochospiral tests co-occurring with *H. obscurus* are here assigned to *T. lomonosovensis.*

A22 Stratigraphic range

Upper Cretaceous to recent (Jones et al., 1993).

A23 Geographic distribution

Worldwide (Jones et al., 1993).

A24 Bathymetric comments

Shelf to abyssal (Jones et al., 1993), in the Arctic Ocean most abundant between 700 and 3000 m (Wollenburg and Mackensen, 1998c; Husum et al., 2015).

Cyclammina trullisata **(Brady, 1879)**

Pl. A4, panels (f1)–(f3).

Trochammina trullisata Brady, 1879, Pl. 5, Figs. 10a, b.

Cyclammina trullisata Barker, 1960, Pl. 40, Figs. 13a, b, 16.

Cyclammina bradyi Cushman, 1910, p. 113, Text-Figs. 174 a, b.

Cyclammina trullisata Schröder-Adams, Pl. 17, Fig. 17.

A25 Original description (Brady, 1879)

Test nautiloid, compressed, lenticular, somewhat excavated at the umbilicus; composed of about three convolutions, of which but little more than the latest is visible; peripheral margin acute or somewhat rounded. Segments about nine in each convolution. Septa marked by more or less sinuate lines, only slightly depressed. Exterior smooth, usually smooth, usually polished; interior surface often reticulate; colour brown. Aperture crescentic, situate on the face of the terminal chamber, close to the margin of the previous convolution. Diameter 1/20 inch (1.25 mm). The inner surface of the test of *C. trullissata* sometimes exhibits a slightly raised reticulation, but this in no case, so far as my observation goes, is more than a mere, superficial marking, and never comes to anything resembling the cancellated shelly growths that often nearly fill the chambers of *Cyclammina*. The distribution of the species is wide, but it is by no means abundant in any locality. The best "Challenger" specimens are from two stations in the North Atlantic and two in the South Atlantic, the depth of water varying from 390 to 2200 fathoms.

A26 Taxonomic remarks

The species has a fine-grained test with a smooth surface and an equatorial intermarginal aperture with an almost non-developed inner alveolar wall structure, very uncommon for the genus (Schröder-Adams et al., 1986). Diameter: 0.2–2 mm.

According to Schröder-Adams et al. (1986) who has studied deep-water agglutinated foraminifera of the North Atlantic Ocean in detail, Brady (1884 and collection) describes complete involute specimens and specimens in which up to 2 rarely 3 whorls can be observed. Like in her collection, this variability is also observed in the new cores.

A27 Geographic distribution

Arctic Ocean (O'Neill, 1981).

A28 Stratigraphic range Pliocene to recent (O'Neill, 1981).

A29 Bathymetric distribution

Seamounts, bathyal-abyssal.

Eilohedra vitrea **(Parker et al., 1953)**

Pl. A5, panels (d)–(f).

Epistominella vitrea Parker et al. 1953, Pl. 4; Figs. 34–36, 40–41.

Epistominella vitrea Feyling-Hanssen et al., 1983, Pl. 2, Figs. 7–8.

Epistominella vitrea Feyling-Hanssen and Ulleberg, 1984, Pl. 3, Figs. 25–27.

Epistominella vitrea Murray, 2003, Fig. 7.11–13.

Epistominella vitrea Pawlowsky et al., 2007, Figs. 1a–c.

A30 Original description (Parker et al., 1953)

Test small, convex on the dorsal side, depressed toward the umbilicus on the ventral side, periphery rounded, sometimes slightly lobulate, consisting of about three whorls; chambers slightly inflated, six in the last whorl; sutures very slightly depressed and slightly curved on the dorsal side, more depressed on the ventral side, the later ones slightly curved, earlier ones radial; wall smooth, translucent, very finely perforate; aperture long, narrow, slightly curved, with a narrow lip. Maximum diameter 0.27 mm, thickness 0.11 mm.

A31 Taxonomic remarks

The species has a bilamellar shell and an aperture composed of a short extension starting at the base of the chamber from the umbilical side of the periphery to its center then it bends and continues as a slit in the chamber wall (Pl. A5, Fig. (f)).

A32 Discussion

See under *E. exigua*.

A33 Geographic range

Worldwide except for the Mediterranean (Murray, 1991).

A34 Stratigraphic range

Eocene to recent (GaŸdzicki and Majewski, 2012).

A35 Bathymetric distribution

Predominantly shelf to upper bathyal, but also reports from abyssal depths (Pawlowski et al., 2007).

***Epistominella arctica* Green, 1959**

Pl. A4, panels (g)–(i)

Epistominella arctica Green, 1959, pp. 78–79, Pl. 1, Figs. 4a–b.

Epistominella arctica Green, 1960, Pl. 1, Figs. 4a–b.

Epistominella arctica Lagoe, 1977, Pl. 4, Figs. 14–16.

Epistominella? Lagoe, 1977, Pl. 4, 19–20, 22.

Stetsonia arctica Scott and Vilks, 1991, Pl. 3, Figs. 8–14, not Figs. 6–7.

Epistominella arctica Wollenburg, 1992, Pl. 18, Fig. 7.

Epistominella sp. 1 Wollenburg, 1992, Pl. 18, Figs. 8–9.

Epistominella sp. 2 Wollenburg, 1992, Pl. 18, Fig. 6.

Stetsonia arctica Bergsten, 1994, Pl. 2, Fig. 2, not Fig. 1.

Stetsonia arctica Mullen and McNeil, 1995, no images.

Stetsonia arctica Ishman and Foley, 1996, in parts, no images.

Stetsonia arctica Pak et al., 1992, no images.

Epistominella arctica Wollenburg and Mackensen 1998, Pl. 3, Figs. 16–17.

Epistominella AP. 1 Wollenburg and Mackensen 1998), Pl. 4, Figs. 2–3.

Epistominella AP. 2 Wollenburg and Mackensen 1998, Pl. 4, Figs. 4–5.

Epistominella arctica Wollenburg et al., 2001, 2004, 2007, no images.

Stetsonia arctica Adler et al., 2009, in parts, no images.

Epistominella arctica Polyak et al., 2013

Epistominella arctica Lazar and Polyak, 2016, no images.

Epistominella arctica Jennings et al., 2017, no images.

Epistominella arctica Jennings et al., 2020, Pl. 2, Figs. 8a–b.

Stetsonia horvathi https://byrd.osu.edu/research/groups/paleoceanography/projects/foram/gallery/stetsonia-horvathi (last access: 15 May 2026)

A36 Original description (Green, 1959)

Test minute, rotaloid, biconvex, last chamber greatly inflated, test opaque, small; edge broadly rounded; periphery lobate; all chambers slightly inflated, four to five chambers in the last whorl, two whorls visible on the dorsal side; suture depressed slightly; wall finely perforate; aperture elongate in the plane of coiling entrance recurved by an overgrowth of the dorsal wall at times pinching off the aperture before it reaches the base of the chamber leaving the aperture elevated in the face; however, the suture always extends to the base of the last chamber. Diameter of the holotype 0.070 mm, width of the holotype 0.03 mm.

A37 Taxonomic remarks

Different to the description by Green (1959), the shell of living or none-diagenetically altered specimens is fully translucent and not opaque. The specimens described and illustrated by Green were thus either affected by calcite dissolution or, authigenic overgrowth. Well-preserved shells are smooth, thin-shelled ($\sim 0.7\,\mu m$ shell-thickness) and possess irregularly distributed pores (Pl. A4, panels (h)–(i)). Green's description of the species includes two aperture morphotypes, one that reaches the base of the inflated chamber and another that is at distance to the suture elevated in the final chamber on the umbilical side. Following Wollenburg (1992) specimens with an inflated last chamber in which the aperture extended to the base of the chamber were counted as *E. arctica* sensu strictu. specimens in which the aperture had no connection to the base in the last inflated chamber were counted as *Epistominella* sp. 1, and specimens in which the aperture was situated within a depression extending from the periphery to the umbilical side were considered *Epistominella* sp. 2 (Wollenburg, 1992). These morphotypes were finally combined as

E. arctica sensu lato for faunal analyses and environmental/stratigraphic interpretations (Wollenburg, 1992, 1995b; Wollenburg and Kuhnt, 2000; Wollenburg et al., 2001, 2004, 2007; Wollenburg and Mackensen, 1998c). The inflated last chamber, is only expressed as the final chamber before reproduction. All previous ontogenetic stages, and thus the majority of specimens, are expressed by specimens in which the last chamber is completely depressed from the periphery to the umbilical side (Pl. A4, panel (i)). In this depression a round aperture is situated at the base of the last chamber. These none-terminal ontogenetic stages have been previously described as *Epistominella*? sp. (Lagoe, 1977) and as *Epistominella* sp. 2 (Wollenburg, 1992) (Pl. 18, Fig. 6).

A38 Discussion

Starting with Scott and Vilks (1991) *E. arctica* and the equally small but planispiral *Stetsonia horvathi* were for many years lumped as *S. arctica* (Bergsten, 1994; Adler et al., 2009; Polyak et al., 2010).

In some research groups foraminiferal analyses were or are still limited to the size fractions > 150 µm (Polyak et al., 2004; Adler et al., 2009) or > 100 µm (Chauhan et al., 2016, 2014; Rasmussen et al., 2007, 2014; Sztybor and Rasmussen, 2017). In these studies, the total abundance of the small-sized (mean test size approx. 100 µm) *E. arctica* and *S. horvathi* is not completely recorded.

A39 Geographic distribution

Arctic Ocean, Weddel Sea (Cornelius and Gooday, 2004).

A40 Stratigraphic range

?Pliocene, Pleistocene to recent (Müllen and Mcneil, 1995). Due to lumping with *Stetsonia horvathi* the first occurrence of *E. arctica* in the CAO is unclear.

A41 Bathymetric distribution

continental slope to abyssal (Wollenburg and Mackensen, 1998b).

***Epistominella exigua* (Brady, 1884)**

Pl. A5, panels (a)–(c).

Pulvinulina exigua Brady, 1884 (1884a), Pl. 103, Figs. 13–14.

Eponides exigua Cushman, 1931, P. 44, Pl. 10, Figs. 1–2.

Epistominella exigua Phleger, Parker and Peirson, 1953, PL. 9, Figs. 35–36.

Eponides exiguus Feyling-Hanssen, 1954, P.135, Pl. 2, Fig. 4.

Epistominella exigua Barker, 1960, Pl. 103, Figs. 13–14.

Epistominella exigua Wollenburg, 1992, Pl. 19, Fig. 1.

Epistominella exigua Jones, 1994, P. 103, Pl. 103, Figs. 13–14.

Not *Epistominella exigua* Hanslik, 2011, Pl. 1, Figs. 7–8 images show *E. vitrea* not *E. exigua??*

Epistominella exigua Kireenko et al., 2022, Pl. 4, Figs. 48a–b.

A42 Original description of (Brady, 1884a)

Test free, rotaliform; both faces convex, the inferior less so than the superior, periphery acute, lobulated; composed of three convolutions, of which the outermost has usually five segments. Sutures non-limbate; marked on the superior face by thickened lines of opaque-white shell-substance; on the inferior by slight depressions. Diameter, 1/65th inch (0.4 mm), or less.

A43 Taxonomic remarks (Holbourn et al., 2013)

Test forms a small trochospire; slightly lobulate in outline and unequally biconvex in cross-section, with an evolute, slightly convex spiral side, an involute, convex to nearly conical umbilical side, and an acute, lobulate periphery. The five moderately inflated chambers in the last whorl increase gradually in size, and are separated by flush, oblique, thickened sutures on the spiral side, and by curved, slightly depressed sutures on the umbilical side. Chamber walls are calcareous, finely perforate, and smooth. The primary aperture is an interiomarginal slit extending up the face of the final chamber on the umbilical side (Holbourn et al., 2013).

A44 Discussion

It is largely unknown that *E. exigua* co-occurs with the visually and genetically closely related *Eilohedra vitrea* (Parker, 1953) (Pl. A3, panels (a)–(b)) in the marginal Arctic Ocean (Barents Sea continental slope, Yermak Plateau) (Sirenko et al., 2001; Osterman, 1996). Due to the comparable chamber arrangement, *E. vitrea* is easily confused with *E. exigua.* The two species can be best differentiated by the larger chamber number in the last whorl of *E. vitrea* (6 compared to 5 in *E. exigua*), and the less depressed umbilicus in the latter (Pl. A5. panels (a)–(f)), and the rather umbilical than peripheral aperture. In detail the aperture of *E. exigua* also lacks the apertural extension along the periphery and its shell wall is monolamellar not bilamellar as in *E. vitrea*. There are many reports of *E. exigua* in sediment cores from the central Arctic Ocean, however, the only illustrated specimen has 6.5 chambers thus, is a *E. vitrea* (Hanslik, 2011). Therefore, the identification of *E. exigua* in other arctic records should be con-

sidered with care if these are not confirmed by images or taxonomic descriptions. Both species should be distinguished because *E. exigua* is a phytodetritus species and therefore regraded as indicative of seasonally ice-free conditions with increased carbon transfer to depth, similar observations have not been made for *E. vitrea* (Gooday and Lambshead, 1989; Gooday et al., 2008; Wollenburg et al., 2001).

Epistominella exigua is usually regarded as deep-water species, and also in the Arctic Ocean usually found at larger water depths > 900 m (Wollenburg et al., 2001). In contrast, *E. vitrea* is regarded as more common in shallow-water depths, e.g. on the Yermak Plateau in ODP holes 910C (Osterman, 1996) and 910A (own unpublished observations), here *E. exigua* is absent. However, shallower occurrences of *E. exigua* and much deeper occurrences of *E. vitrea* have also been reported (Pawlowski et al., 2007; Lecroq et al., 2009), and in the Arctic a broad bathymetric range where both species often coexist is found (own unpublished observation). For instance *E. vitrea* usually dominates at 600 m water depth but at site 276 (571 m) of the PS15 expedition of *Polarstern* in 1987 only *E. exigua* was found (Wollenburg, 1992).

A45 Geographic range

Worldwide except for the Mediterranean (Murray, 1991).

A46 Bathymetric comments

Predominantly lower bathyal to abyssal, but also reports from shallower bathyal depths (Holbourn et al., 2013).

A47 Stratigraphic range

Middle Eocene to recent (Holbourn et al., 2013).

Haplophragmoides obscurus **O'Neill, 1981**

Pl. A2, panel (i).

Haplophragmoides obscurus O'Neill, 1981, Pl. 2, Figs. 13, 17.

Cyclammina pusilla Evans et al., 1995, no images.

Cyclammina pusilla Evans and Kaminski, 1998, Pl. 1, Figs. 8–9.

Reticulophragmium pusillum Scott et al. 1989, no images.

Cyclammina pusilla Cronin et al., 2008, no images.

Reticulophragmium pusillum Kaminski et al., 2009, Pl. 4, Figs. 4, 6.

Haplophragmoides obscurus Hayward et al.2024

A48 Original description (O'Neill, 1981)

Test free, planispiral, involute, compressed, periphery rounded; chambers numerous approximately 10 in the final whorl, sutures indistinct; wall coarsely arenaceous consisting largely of angular quartz grains; aperture an arcuate interiomarginal slit; colour yellowish-brown.

Length of specimen 0.35–0.65 mm, maximum width of specimen 0.30–0.60 mm.

A49 Taxonomic remarks (this study)

The specimens chamber walls are thin and usually composed of one-layer of grains and a light brown coloration of the cement. In our specimens only quartz and light-coloured feldspar is used, dark minerals as described by Evans and Kaminski (1998), were not observed. We also observe neither pseudopores nor a labyrinthic wall structure. However, the individual chambers are developed as a high semi-acute arch with a low average height and very long flanks, therefore, in broken individuals, the side flanks of the chambers can be observed as punctiform depressions in the chamber wall.

A50 Discussion

Haplophragmoides obscurus was originally described from the Alpha Ridge where it is restricted to the Pliocene (O'Neill, 1981). Later Scott et al. 1989) (without illustrations,) Evans et al. 1995), Evans and Kaminski (1998) and Kaminski et al. (2009) (with illustrations) assigned respective specimens to *Cyclammina pusilla/ Reticulophragmium pusillum* (Brady, 1879). None of these authors discussed why they rejected O'Neill's species concept, but they mentioned that these arctic *C. pusilla* variants are constructed of much coarser grains than described for the species.

Reticulophragmium pusillum uses much smaller grains to construct their tests and is larger in size than *H. obscurus*.

A51 Geographic distribution

Arctic Ocean (O'Neill, 1981).

A52 Stratigraphic range

Pliocene to Pleistocene (O'Neill, 1981).

A53 Bathymetric distribution

bathyal to abyssal (O'Neill, 1981).

Oridorsalis umbonatus **(Reuss, 1851)**

Pl. A5, panels (g)–(k).

Rotalina umbonata Reuss, 1851, Pl. 5, Figs. 35a–c.

Truncatulina tenera Brady, 1884, Pl. 95, Fig. 11a–c.

Pulvinulina umbonata Brady, 1884, Pl. 105, Fig. 2.

Eponides tener Lagoe, 1977, Pl. 5, Figs. 3, 7.

Oridorsalis tenera Herman, 1989, no images.

Oridorsalis tener Belyaeva and Khusid, 1989, no images.

Oridorsalis umbonatus Scott and Vilks, 1991, Pl. 2, Figs. 15–16, Pl. 4, Figs. 4–5.

Oridorsalis umbonatus Bergsten 1994, Pl. 2, Figs. 17–18.

Oridorsalis tener Ishman and Foley 1996, Pl. 2, Fig. 9

Oridorsalis umbonatus Bornmalm 1997, Fig. 24J–k.

Oridorsalis tener Wollenburg and Mackensen 1998, Pl. 5, Figs. 6–8.

Oridorsalis umbonatus/tener Osterman et al., 1999, both names used in different graphs, no images.

Oridorsalis tener Wollenburg and Kuhnt 2000, no images.

Oridorsalis tener Wollenburg et al. 2001, no images.

Oridorsalis tener Wollenburg et al. 2004, no images.

Oridorsalis tener Polyak et al., 2004, no images.

Oridorsalis tener Polyak et al., 2013, no images.

Oridorsalis tener Husum et al., 2015, no images.

Oridorsalis tener Lazar and Polyak 2016, no images.

A54 Original description of *Rotalina umbonata* (Reuss, 1851)

Testa suborbiculata, depressa, subtus medio umbonate, superne convexa, margine lobato-carinata; anfractibus 3, internis obsoletis; loculis 5, subtus oblongis angustis, planis, superne triangularibus, convextusculis, superfiele laevi. Diameter = 0.35–0.45 mm.

A55 Original description of *Truncatulina tenera* (Brady, 1884a)

Test regularly rotaliform; both faces convex; peripheral edge acute and lobulated. Consisting of rather more than three convolutions of nearly equal width, the last of which is formed of five or six segments; sutures distinct, slightly depressed, marked on the superior face by nearly straight lines; aperture a curved fissure bordered by a thickened lip, situated at the inner margin of the final segment near the periphery. Diameter = 1/55th inch (0.46 mm).

A56 Discussion

There is a controversial discussion on the taxonomic status of *Oridorsalis tener* and *Oridorsalis umbonatus*. Subtle morphological differences distinguish *O. tener* from *O. umbonatus* and *O. tener* is often considered a junior synonym.

In the Challenger report Brady (1884a) illustrated *O. (Pulvinulina) umbonatus* and a new species *O. (Truncatulina) tenera*. He described that both taxa strongly resemble each other and that they are difficult to differentiate. However, the specimens in the Arctic Ocean with their very acute periphery and reduced shell height, resemble rather Brady's *T. tenera* than his *P. umbonata*. Moreover, the Arctic *Oridorsalis* specimen, like the Brady's figure of *T. tenera*, often lack the supplementary spiral sutural apertures characteristic of *O. umbonatus*.

In taxonomic works with illustrations of both morphotypes, *O. umbonatus* has more straight sutures on the spiral side, chambers of equal size in the last whorl, a trochoidal cross-sectional outline, whereas *O. tener* has curved sutures, a more rapid increase in chamber height, and a much more compressed outline (Bornmalm, 1997; Lohmann, 1978; Pflum et al., 1976; Corliss, 1979). It is also stated that *Oridorsalis umbonatus* has a more rounded periphery, is more inflated, and has a smaller rate of whorl expansion than *O. tener* (Lohmann, 1978; Corliss, 1979). Except for the difference in shell height and the common lack of visible secondary apertures, none of these differences are supported by the original descriptions of both species (Mead and Kennett, 1987). As both variants usually co-occur it is generally agreed that *O. umbonatus* has a certain morphological variability which includes *O. tener* (Bornmalm, 1997). The Arctic Ocean lacks *Oridorsalis* specimens with rounded periphery, and shows only occasionally supplementary apertures under the SEM (Suppl. Pl. 5i). They have always a compressed outline, and increase always rapidly in chamber height. Thus, although the first author agrees that the species descriptions of *O. tener* and *O. umbonatus* are very similar, she doubts that the Arctic *Oridorsalis* specimens are genetically identical to the large *O. umbonatus* specimens with significant shell height, small chamber height and rounded periphery found in the Norwegian Seas. However, at present although genetic differences between *O. umbonatus* specimens have recently been observed (Himmighofen et al., 2023), no assignments to different species have been made. Thus, based on today's state of knowledge all records of *O. tener* in the Arctic Ocean are reassigned to *O. umbonatus*.

A57 Geographic distribution

Worldwide (Holbourn et al., 2013).

A58 Stratigraphic range

Middle Paleocene to recent (Holbourn et al., 2013). In the Norwegian-Greenland Sea since the late Miocene (Osterman and Qvale, 1989)

A59 Bathymetric distribution

Lower neritic to abyssal (Holbourn et al., 2013)

***Pullenia bulloides* (d'Orbigny, 1846)**

Pl. A4, panels (l1)–(l2).

Nonionina bulloides d'Orbigny, 1846, Pl. 5, Figs. 9–10.

Pullenia sphaeroides Brady, 1884a, Pl. 84, Figs. 12–13.

Pullenia sphaeroides Goës, 1894, Pl. 14, Figs. 771–772.

Pullenia bulloides Feyling-Hanssen and Ulleberg, 1984, Pl. 1, Figs. 27–28.

Pullenia bulloides Wollenburg, 1992, Pl. 20, Fig. 2.

Pullenia bulloides Wollenburg and Mackensen 1998, Pl. 5, Figs. 9, 10.

Pullenia bulloides Hanslik, 2011, Pl. 1, Figs. 8–9.

Pullenia bulloides Chauhan et al., 2015, Figs. 3.23–24.

A60 Original description (d'Orbigny, 1846; translated into English)

Test spheric, almost as thick as broad, smooth, scope rounded; formed by 4 only very weakly convex, and only by weakly depressions separated chambers, which join in the centre leaving a hardly noticeable umbilical depression; the last flat and halfmoon-curved chamber is penetrated by very long linear opening.

A61 Discussion

In the sediment cores PS2185-6, PS72/340-5 and PS72/396-5, *Pullenia bulloides*, *P. quinqueloba* (Reuss, 1851) and *P. osloensis* Feyling-Hanssen (1954) have been occasionally observed (Figs. 3–5). In contrast, most records from the central Arctic Ocean list only *P. bulloides*. Because of only slight morphological differences, *P. quinqueloba* and *P. osloensis* may have been lumbed with *P. bulloides*. *P. quinqueloba* differs from *P. bulloides* in being much flatter and five-chambered, whereas *P. osloensis* is a small sub-sphaerical five-chambered species (Wollenburg, 1992; Feyling-Hanssen, 1964). Since the observed species *P. bulloides, P. quinqueloba* and *P. osloensis* occupy different habitats in modern Arctic Ocean sediments (Wollenburg and Mackensen, 1998a), most stratigraphic records from the Arctic Ocean require careful restudy to confirm taxonomic assignments.

A62 Geographic distribution

Worldwide (Holbourn et al., 2013); in the modern Arctic Ocean restricted to areas influenced by the inflow of Atlantic Water close to Fram Strait (Wollenburg and Mackensen, 1998b; Wollenburg et al., 2001).

A63 Stratigraphic range

Latest Paleocene to recent (Holbourn et al., 2013).

A64 Bathymetric distribution

Bathyal to abyssal (Holbourn et al., 2013).

***Pyrgo rotalaria* Loeblich and Tappan, 1953**

Pl. A5, panel (m).

Pyrgo rotalaria Loeblich and Tappan, 1953, Pl. 6, Figs. 5–6.

Biloculina murrhyna Schwager, Cushman, 1917, Pt. 6, Pl. 29, Figs. 1a–e.

Pyrgo rotalaria Lagoe, 1977, Pl. 2, Fig. 21.

A65 Original description (Loeblich and Tappan 1953)

Test free, circular in outline, much inflated, but with a distinctly carinate border, slightly produced at the aboral end; chamber development typically biloculine; wall calcareous, imperforate, surface

smooth; aperture nearly circular, with a broad tooth that is slightly notched to give a bifid appearance. Length of holotype 0.55 mm, greatest breadth 0.52 mm, thickness 0.31 mm. Length of figured paratype 0.57 mm, breadth 0.52 mm. Other specimens range from 0.47 to 0.86 mm in length.

A66 Taxonomic remarks

The species resembles *Pyrgo murrhyna* (Schwager) of some authors, but the type specimen of Schwager has two strong spines on either side of an indentation on the basal margin, and the peripheral margin of the test is grooved.

A67 Discussion

As noted by Belanger and Streeter (1980), specimens occur with two varieties of aperture, a round rather small aperture with indistinct bifid tooth as described by Loeblich and Tappan, and a large broad one with broad bifid tooth. Todd and Low (1980) had assigned varieties with a large aperture and large bifid tooth to *P. vespertilio* which, however, is less compressed, has a rounded border and fine rips on the test. In our samples the large aperture is just expressed in some adult tests, whereas all juveniles and also the majority of adult

tests show an aperture as described by Loeblich and Tappan (1953). It is not known whether this is an expression of sexual versus asexual generation. Size: 0.2–2 mm.

A68 Geographic distribution

Arctic Ocean, Norwegian-Greenland Sea.

A69 Stratigraphic range

In the Arctic Ocean to our knowledge restricted to the Pleistocene, the closely related species has its first occurrence in the middle Miocene (Holbourn et al., 2013).

A70 Bathymetric distribution

Bathyal to abyssal, mostly from depths > 600 m (Wollenburg and Mackensen, 1998b; Thies, 1991).

***Stetsonia horvathi* Green, 1959**

Pl. A4, panels (j)–(k).

Stetsonia horvathi Green, 1959 (Green, 1959), Pl. 1, Figs. 6a–b.

Stetsonia horvathi Lagoe, 1977, Pl. 4, Figs. 17, 22.

Stetsonia arctica Scott and Vilks, 1991, Pl. 3, Figs. 6–7, not 5, 8–14.

Stetsonia horvathi Wollenburg, 1995, Pl. 4, Figs. 9–11.

Stetsonia arctica Ishman and Foley, 1996, Pl. 2, Fig. 11.

Stetsonia horvathi Wollenburg and Mackensen 1998a, Pl. 4, Figs. 9–11.

Stetsonia arctica Adler et al., 2009, in parts, no images.

Stetsonia horvathi Jennings et al., 2020, Pl. 2, Figs. 3a–4b.

A71 Original description (Green, 1959)

Test small, generally quadrate in side view, generally glassy, may be opaque, planispiral involute, four to five chambers in the last whorl, test flat; edge subrounded; periphery smooth; sutures slightly depressed, slightly curved; aperture a high arched opening at the base of the last septal face, somewhat curved, situated in a depression. In the glassy specimens the previous whorls are clearly visible through the outer wall, causing the sutures to appear widen toward the umbilicus. Diameter of the holotype 0.10 mm, width of the holotype 0.04 mm. Diameter of the paratypes 0.07–0.10 mm, width of the paratype 0.03–0.04 mm. Geographic distribution: Arctic Ocean. Stratigraphic range: Pliocene to Pleistocene.

Bathymetric distribution: bathyal to abyssal.

A72 Discussion

Scott and Vilks (1991) stated that the trochospiral *E. arctica* and the planispiral *S. horvathi* would represent morphotypes of the same species that they called *S. arctica* . This contrasts with the involute chamber arrangement, one of the basic requirements of the genus *Stetsonia*, that is not expressed in *E. arctica* tests. Moreover, no trochospiral form with a high-arched aperture, and no planispiral form with inflated chamber, that could represent some transitional forms can be identified. In broken *E. arctica* (Pl. A4, panel (i)) it also becomes obvious that even juvenile *E. arctica* tests are trochospiral and that at no point in ontogeny a high-arched aperture is developed. However, many studies followed the approach of Scott and Vilks lumping both species (Pak et al., 1992; Müllen and McNeil, 1995; Bergsten, 1994). As other groups work on size fractions > 150 µm (Polyak et al., 2004; Adler et al., 2009) *Stetsonia horvathi*, like *E. arctica*, are often not recorded in Arctic studies since the average shell size for both species is 100 µm (Table B1). In shallower waters of the transition zone between the Fram Strait and the Arctic Ocean, both species may account for a smaller proportion of the fauna and thus may not be detected in studies using the > 100 µm size fraction (Chauhan et al., 2014, 2015).

A73 Geographic distribution

Arctic Ocean, Weddell Sea (Cornelius and Gooday, 2004).

A74 Stratigraphic range

?Pliocene, Pleistocene to recent (Müllen and McNeil, 1995). Due to lumping with *E. arctica* the first occurrence of *Stetsonia horvathi* is unclear.

A75 Bathymetric distribution

continental slope to abyssal (Wollenburg and Mackensen, 1998b).

Table A1. Benthic Foraminifera taxa.

Adercotryma glomerata Brady, 1878	*Cyclammina* sp.
Adelosina pulchella (d'Orbigny, 1826)	*Cystammina pauciloculata* Brady, 1879
Alabaminella weddellensis (Earland, 1936)	Deuterammina (Deuterammina) grisea (Earland, 1934)
Allomorphina fragilis Hofker, 1952	*Deuterammina (Deuterammina) grahami* Brönnimann and Whittaker, 1988
Ammodiscus gullmarensis Höglund, 1948	*Discorbinella bertheloti* (d'Orbigny, 1839)
Ammomarginulina ensis Wiesner, 1931	*Discorbis vilardeboanus* (d'Orbigny, 1839)
Archimerismus subnodosus (Brady, 1884)	*Earlandammina inconspicua* (Earland, 1934)
Aschemonella ramuliformis Brady, 1884	*Eggerelloides advenum* (Cushman, 1922) = *Verneuilina arctica* (Höglund, 1947) junior synonym
Aschemonella scabra Brady, 1879	*Eilohedra vitrea Parker, in Phleger et al., 1953*
Astacolus crepidula (Fichtel and Moll, 1798)	*Elphidium funderi Feyling-Hanssen, 1990*
Astacolus hyalacrulus Loeblich and Tappan, 1953	*Elphidiella groenlandica* (Cushman, 1933) = *E. gorbunovi* Shchedrina, 1946 junior synonym
Astrononion hamadaense Asano, 1950 = *A. gallowayi* Loeblich and Tappan, 1953 junior synonym	*Elphidiella rolfi* Gudina and Polovova, 1984
Bolivina arctica Herman, 1974	*Elphidium asklundi* Brotzen, 1943
Bolivina gramen (d'Orbigny, 1839)	*Elphidium bartletti* Cushman, 1933
Bolivina sp.	*Elphidiella groenlandica* (Cushman, 1933)
Bolivina robusta (Brady, 1881)	*Emayerella frigida* (Cushman, 1933)
Botuloides ittai (Loeblich and Tappan, 1953)	*Eoeponidella pulchella* (Parker, 1952)
Buccella floriformis Voloshinova, 1960 = *B. hannai arctica* Voloshinova, 1960 junior synonym (Hayward et al. 2023)	*Epistominella arctica* Green, 1959
Buccella frigida (Cushman, 1922)	*Epistominella exigua* (Brady, 1884)
Buccella tenerrima Bandy, 1950	*Favulina melo* (d'Orbigny, 1839)
Bulimina aculeata d'Orbigny, 1826	*Fissurina annectens* (Burrows and Holland, 1895
Buliminella hensoni Lagoe, 1977	*Fissurina bassensis* Parr, 1950
Cassidulina reniforme Nørvang, 1945	*Fissurina bimarginata* Parr, 1950
Cassidulina neoteretis Seidenkrantz, 1995	*Fissurina cucurbitasema* Loeblich and Tappan, 1953
Cassidulina teretis Loeblich and Tappan, 1953	*Fissurina danica* (Madsen, 1895)
Cassidulina obtusa Williamson, 1858	*Fissurina laevigata* (Reus, 1850)
Ceratobulimina arctica Green, 1960	*Fissurina lucida* (Williamson, 1848)
Chilostomella elongata Lagoe, 1977	*Fissurina marginata* (Montagu, 1803)
Cibicides refulgens Montfort, 1808	*Fissurina orbygniana* Serguenza, 1862
Cornuspira involvens Reuss, 1850	*Fissurina semimarginata* (Reuss, 1870)
Cornuspira planorbis Schultze, 1854	*Fissurina staphyllearia* (Schwager, 1866) = *F. kerguelensis* Parr, 1950 junior synonym
Cornuspiroides striolata (Brady, 1882)	*Fissurina* spp.

Table A1. Continued.

Cribroelphidium clavatum Cushman, 1930	*Fursenkoina complanata* (Egger, 1893)
Cryptoelphidiella asklundi Brotzen, 1943	*Galwayella trigonomarginata* (Parker and Jones, 1865)
Cryptoelphidiella bartletti Cushman, 1933	*Globobulimina auriculata* subsp. *arctica* Höglund, 1947
Cryptoelphidiella hallandensis (Brotzen, 1943)	*Globulina glacialis* (Cushman and Ozawa, 1930)
Cryptoelphidiella magellanica (Heron-Allen and Earland, 1932)	*Glomospira charoides* (Jones and Parker, 1860)
Cryptoelphidiella paucilocula (Cushman, 1944) = *C. albiumbilicatum* (Weiss, 1954) junior synonym	*Glomospira gordialis* (Jones and Parker, 1860)
Cryptoelphidiella/Cribroelphidium sp.	*Gyroidina subplanulata* Echols, 1971
Cribrostomoides jeffreysii (Williamson, 1858)	*Haplophragmoides bradyi* (Schwager, 1883)
Cribrostomoides sphaerilocula (Cushman, 1910)	*Haplophragmoides obscurus* O'Neill, 1981
Cribrostomoides subglobosus (Sars, 1868)	*Haplophragmoides pusillum* Höglund, 1947
Cuneata arctica (Brady, 1881)	*Haplophragmoides* sp.
Cyclammina orbicularis Brady, 1881	*Haynesina nivea* (Lafrenz, 1963)
Cyclammina trullissata (Brady, 1879)	*Haynesina orbicularis* (Brady, 1881)
Haynesina orbicularis (Brady, 1881)	*Nonionella iridea* Heron-Allen and Earland, 1932
Heronallenia sp.	*Nonionellina labradorica* (Dawson, 1860)
Homalohedra apiopleura (Loeblich and Tappan, 1953)	*Nuttallides umbonifera* (Cushman, 1933)
Hormosinella ovicula (Brady, 1879)	*Oolina borealis* Loeblich and Tappan, 1954
Hormosinelloides guttifer (Brady, 1881)	Oolina caudigera (Wiesner, 1931)
Hyalinea balthica (Schröter, 1783)	*Oolina globosa* (Montagu, 1803)
Hyalinonetrion gracillimum (Seguenza, 1862)	*Oolina stelligera* (Brady, 1881)
Hyperammina elongata Brady, 1878	*Oolina* spp.
Hyperammina laevigata Wright, 1891	*Oridorsalis umbonatus* (Reuss, 1851) = *O. tener* (Brady, 1884) junior synonym
Hyperammina sp.	*Parafissurina arctica* Green, 1960
Hyperammina/Jaculella/Psammosiphonella fragments	*Parafissurina fusiformis* (Wiesner, 1931)
Ioanella tumidula subsp. *horvathi* (Green, 1960)	*Parafissurina fusuliformis* Loeblich and Tappan, 1953
Islandiella algida (Cushman, 1944) = *I. islandica* (Nørvang, 1945) junior synonym	*Parafissurina groenlandica* Shchedrina, 1946
Islandiella helenae Feyling-Hanssen and Buzas, 1976	*Parafissurina lata* (Wiesner, 1931)
Islandiella norcrossi (Cushman, 1933)	*Parafissurina marginata* (Wiesner, 1931)
Jaculella acuta Brady, 1879	*Parafissurina obtusa* (Egger, 1857)
Jaculella obtusa Brady, 1882	*Parafissurina tectulostoma* Loeblich and Tappan, 1953
Laevidentalina advena (Cushman, 1923)	*Parafissurina* spp.
Laevidentalina baggi (Galloway and Wissler, 1927)	*Paratrochammina challengeri* Brönnimann and Whittaker, 1988
Laevidentalina communis (d'Orbigny, 1826)	*Patellina corrugata* Williamson, 1858
Laevidentalina drammenensis (Feyling-Hanssen, 1964)	Placopsilinella aurantiaca Earland, 1934

Table A1. Continued.

Laevidentalina frobisherensis (Loeblich and Tappan, 1953)	*Polymorphina* spp.
Laevidentalina elegans (d'Orbigny, 1846) = *D. pauperata* (d'Orbigny, 1846) junior synonym	*Procerolagena meridionalis* (Wiesner, 1931)
Laevidentalina sp.	*Psammatodendron arborescens* Norman in Brady, 1881
Lagena flatulenta Loeblich and Tappan, 1953	*Psammosiphonella cylindrica* (Glaessner, 1937)
Lagena hispida Reuss, 1863	*Psammosphaera fusca* Schulze, 1875
Lagena nebulosa Cushmani, 1923	*Psammosphaera* sp.
Lagena laevicostata Cushman and Gray, 1946	*Psammossiphonella discreta* (Brady, 1881)
Lagnea tenuistriatiformis (McCulloch, 1977) = *Fissurina lagenoides tenuistriata*	Pseudobolivina antarctica Wiesner, 1931
Lagena sp.	*Pseudonodosinella nodulosa* Brady, 1879
Lagenammina arenulata (Skinner, 1961)	*Pseudopolymorphina dawsoni* (Cushmani and Ozawa, 1930)
Lagenammina tubulata (Rhumbler, 1931)	*Pseudopolymorphina novangliae* (Cushman, 1923)
Laryngosigma lactea (Walter and Jacob, 1798)	*Pseudopolymorphina suboblonga* Cushman and Ozawa, 1930
Laryngosigma williamsoni (Terquem, 1878)	*Pullenia bulloides* (d'Orbigny, 1846)
Laryngosigma hyalascidea Loeblich and Tappan, 1953	*Pullenia quinqueloba* (Reuss, 1851)
Laryngosigma sp.	*Pyrgo rotalaria* Loeblich and Tappan, 1953
Lenticulina sp.	*Pyrgo williamsoni* Silvestri, 1923
Lepidoparatrochammina lepida Brönnimann and Whitaker, 1986	*Pyrgoella irregularis* (d'Orbigny, 1839)
Lobatula wuellerstorfi (Schwager, 1866)	*Pyrgoella sphaera* (d'Orbigny, 1839)
Lobatula lobatula (Walker and Jacob, 1798)	*Pyrulina cylindroides* (Roemer, 1838)
Lobatula lobatula subsp. grossa Ten Dam and Reinhold, 1941	*Pullenia bulloides* (d'Orbigny, 1846)
Marginulina similis d'Orbigny, 1826 = M. glabra (Parker, Jones and Brady, 1865) unaccepted nov. nudum	*Pullenia quinqueloba* (Reuss, 1851)
Marginulinopsis tenuis (Bornemann, 1855)	*Pyrgo rotalaria* Loeblich and Tappan, 1953
Melonis zaandami (van Voorthuysen, 1952)	*Pyrgo williamsoni* Silvestri, 1923
Miliolina pulchella (d'Orbigny, 1826)	*Pyrgoella irregularis* (d'Orbigny, 1839)
Miliolinella subrotunda (Montagu, 1803)	*Pyrgoella sphaera* (d'Orbigny, 1839)
Miliolinella chukchiensis Loeblich and Tappan, 1953	*Pyrulina cylindroides* (Roemer, 1838)
juv. Miliolids	*Parafissurina* spp.
Moncharmontzeiana paradoxa (Sidebottom, 1912)	*Paratrochammina challengeri* Brönnimann and Whittaker, 1988
Nodosaria doliolaris Parr, 1950	*Patellina corrugata* Williamson, 1858
Nodosaria sp.	Placopsilinella aurantiaca Earland, 1934
Nonion umbilicatulum (Walker and Jacob, 1798)	*Pyrgo rotalaria* Loeblich and Tappan, 1953

Table A1. Continued.

Pyrgo williamsoni Silvestri, 1923	*Sorosphaera confusa* Brady, 1879
Pyrgoella irregularis (d'Orbigny, 1839)	*Sphaeroidina* sp.
Pyrgoella sphaera (d'Orbigny, 1839)	*Stainforthia concava* Höglund, 1947
Pyrulina cylindroides (Roemer, 1838)	*Stainforthia feylingi* Knudsen and Seidenkrantz, 1994
Quinqueloculina akneriana d'Orbigny, 1846	*Stainforthia loeblichi* (Feyling-Hanssen, 1954)
Quinqueloculina arctica Cushman, 1933	*Stetsonia horvathi* Green, 1959
Quinqueloculina sadkovi (Bogdanowicz in Shchedrina, 1946)	*Subreophax aduncus* (Brady, 1882)
Quinqueloculina seminula (Linnaeus, 1758)	*Spiroplectammina biformis* Parker and Jones, 1865
Quinqueloculina stalkeri Loeblich and Tappan 1953	*Textularia earlandi* Parker, 1952
Quinqueloculina venusta Karrer, 1868	*Textularia torquata* Parker, 1952
Quinqueloculina nitida Nørvang, 1965	*Thalamophaga ramosa* Rhumbler, 1911
Quinqueloculina sp.	*Tholosina confusa* (Cushman, 1920)
Recurvoides laevigatum Höglund, 1947, despite Höglund's argumentation that this species is much more delicate than *R. contortus,* regarded by Kaminski and Gradstein (http://nhm2.uio.no/norges/atlas/index.htm, last access: 15 May 2026) as being identical	*Thurammina papillata* Brady, 1879
Reophax pilulifer Brady, 1884	*Toddinella incerta* (Williamson, 1858)
Reophax scorpiurus Montfort, 1808	*Toddinella ustulata* (Todd, 1957)
Reophax sp.	*Tolypammina schaudinni* Rhumbler, 1904
Resigella moniliformis (Resig, 1982)	*Tolypammina vagans* (Brady, 1979)
Reussoolina apiculata (Reuss, 1851)	*Triloculina elongata* d'Orbigny in Fornasini, 1905
Reusoolina laevis (Montagu, 1803)	*Triloculina frigida* Lagoe, 1977
Robertinoides charlottense (Cushman, 1925)	*Triloculina trigonula* (Lamarck, 1804)
Robertinoides pumilum Höglund, 1947	*Triloculina trihedra* Loeblich and Tappan, 1953
Rosalina sp.	*Triloculina tricarinata* d'Orbigny in Deshayes, 1832
Saccammina socialis Brady, 1884	*Trochammina japonica* Ishiwada, 1950
Saccammina sphaerica Brady, 1871	*Trochammina lomonosoviensis* Evans and Kaminski, 1998
Saccammina sp.	*Trochammina* sp.
Saccorhiza ramosa (Brady, 1879)	*Trochamminopsis pusilla* (Höglund, 1947)
Seabrokia pellucida Brady, 1890 = jun. Synonym of *S. earlandi* Wright, 1891	*Vaginulinopsis angulata* (Noth, 1951)
Sipholagena benevestita (Buchner, 1940)	*Valvulineria arctica* Green, 1959

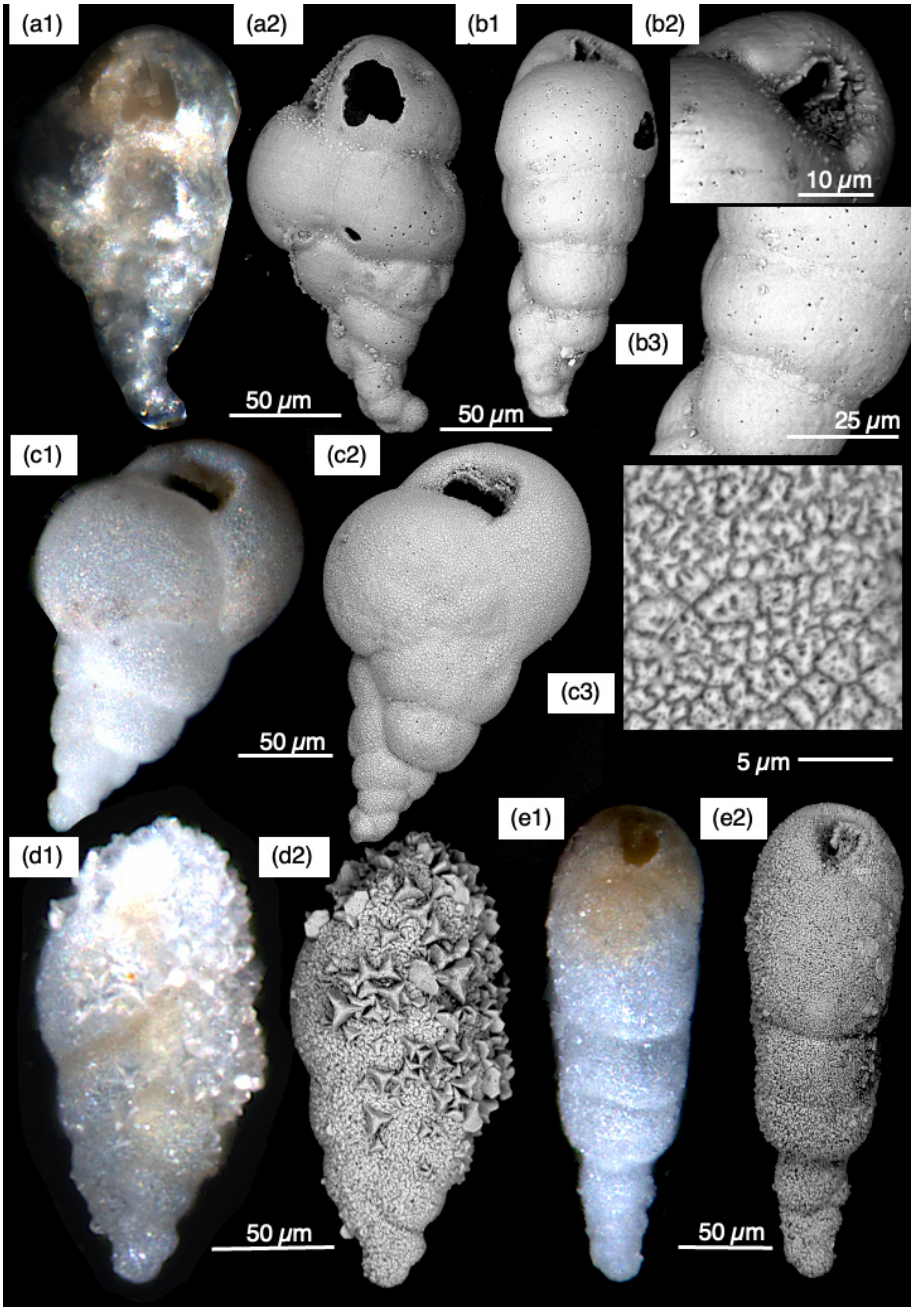

Plate A1. **(a)–(e)** *Bolivina arctica*; **(a)** Same specimen under light (a1) and scanning electron microscope (a2). (a1) Translucent well-preserved specimen; (a2) smooth shell surface with unevenly distributed pores; tubercles occur in the apertural face and along some sutures. **(b)** Specimen in side view. (b1) Whole specimen; (b2) close-up on the aperture situated in a depression, and surrounded by a serrated lip and multiple tubercles; (b3) close-up on the overlapping ribbon between two successive chambers. **(c)** Inflated specimen with triserial juvenile test part, wide aperture and a shell covered by a coat of porous authigenic overgrowth. (c1) Opaque and dull appearance of the shell caused by authigenic overgrowth; (c2–3) details of the porous authigenic overgrowth. **(d)** Same specimen heavily encrusted by authigenic overgrowth, light (d1) and scanning electron microscope images (d2). (d1) Opaque and dull shell with larger crystals sticking out from the shell; (d2) details of large authigenic idiomorphic calcite crystals formed on top of an authigenic overgrowth coat covering the shell, crystals oriented perpendicular to the shell surface. **(e)** Same specimen covered by small idiomorphic authigenic calcite crystals, light (e1) and scanning electron microscope images (e2). **(a–b)** PS2185-4, 0–1 cm; **(c)** PS72/396-5, 75 cm. **(d–e)** PS2185-6, 143.5 cm. (a1), (c1), (d1), (e1), Axiozoom images; (a2–b3), (c2–3), (d2), (e2), SEM images.

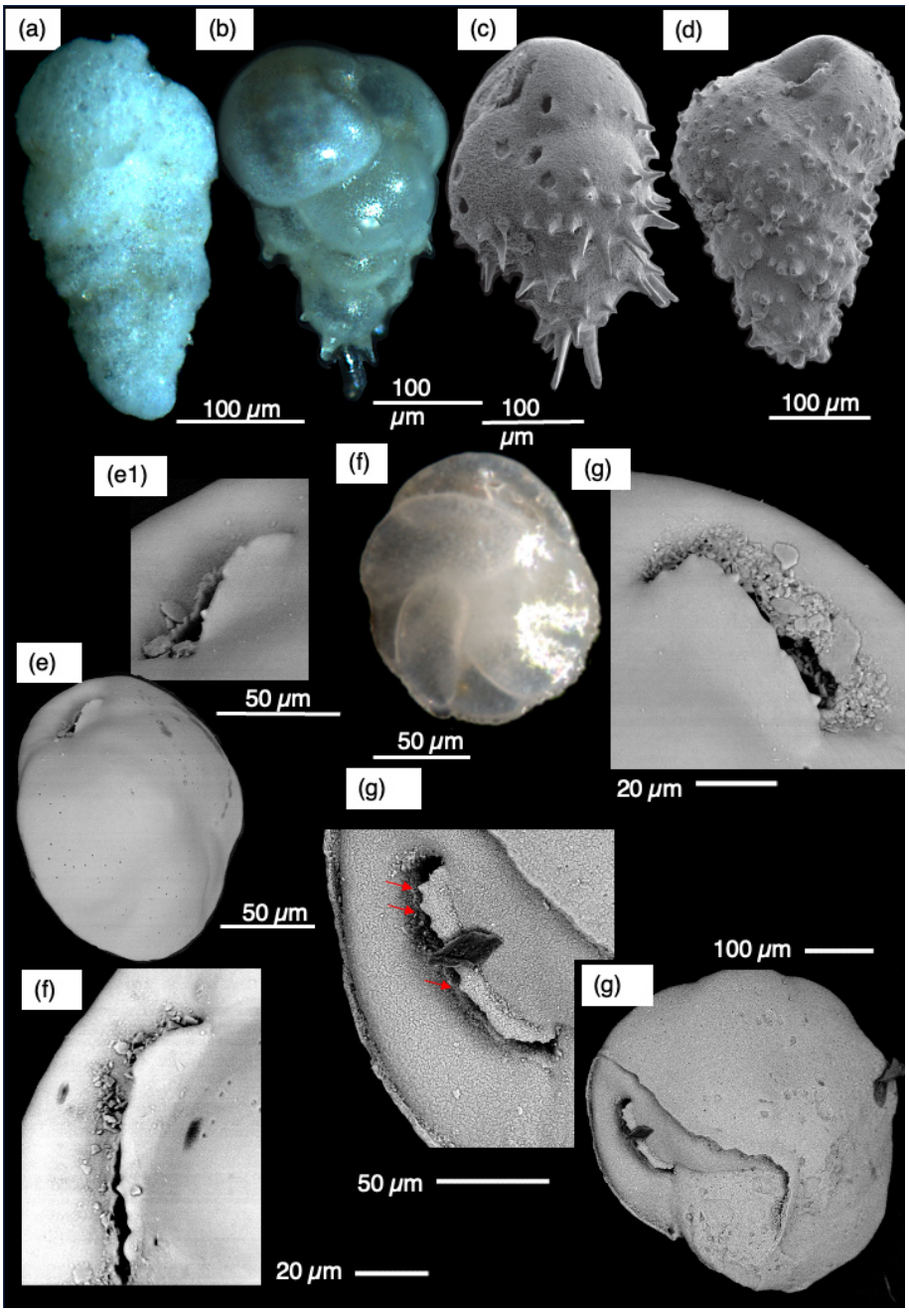

Plate A2. **(a)** *Siphotextularia rolshauseni* with its typical white appearance, biserial chamber arrangement, distinct neck, and coarse agglutination. **(b)** *Bulimina aculeata*, translucent shell of well-preserved specimen with long spines from upper bathyal water depth. **(c)** *Bulimina aculeata*, corroded specimen with long spines from middle bathyal water depth. **(d)** *Bulimina aculeata*, corroded specimen with multiple short blunt spines from lower deep bathyal depth. **(e)** *Cassidulina neoteretis,* well preserved specimens, showing the angular periphery, and slit-like aperture partly covered with a prominent smooth apertural plate; (e1) close-up showing the smooth apertural plate and the opposing serrated ridge. **(f)** *Cassidulina neoteretis*, well preserved specimens with translucent shell revealing the biserial chamber arrangement and milky umbilical area. **(g–h)** *Cassidulina neoteretis*, aperture covered by subtriangular apertural plate with a smooth edge, formed by the infolded chamber wall with 1–2 small serrata on the apertural plate. **(i)** *Cassidulina teretis*, corroded specimen with the last chamber missing; (i1) Close-up of the aperture covered by a crescentic, narrow serrated apertural plate. Red arrows point to the serrata. **(a)** PS2212-3, 90 cm (Wollenburg et al., 2001); **(b)** ODP910A-1H1, 135–136.5; **(c)** PS2185-6, 163.5 cm; **(d)** PS72/396-5, 33.5 cm; **(e)** PS2185-4, 0.5 cm; **(f)** PS2185-6, 237.5 cm; **(g–h)** PS2185-6, 223 cm; **(i)** PS72/396-5, 72.5 cm. **(a–b)**, **(f)** Axiozoom images; **(c–e)**, **(g–i)** SEM images.

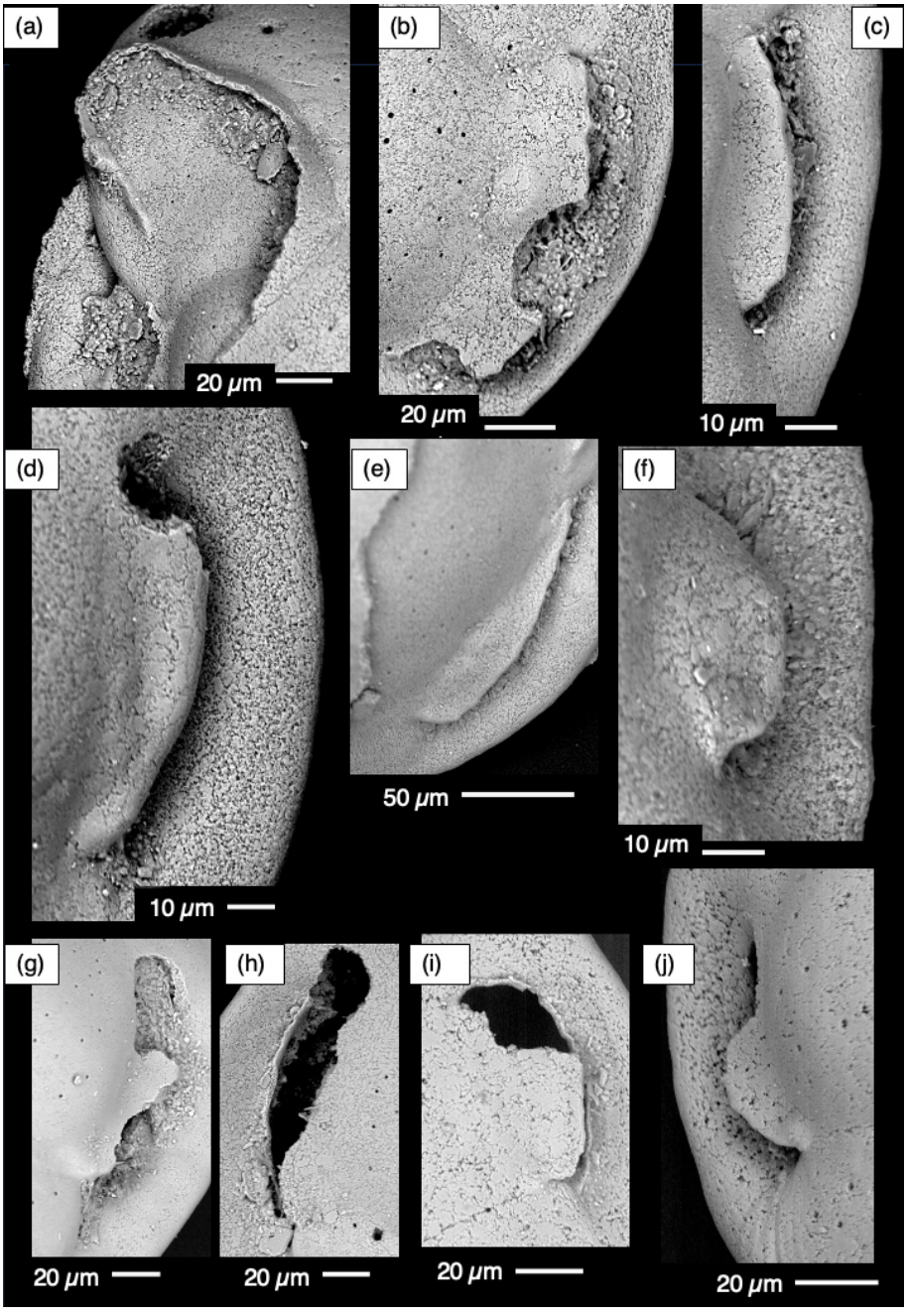

Plate A3. *Cassidulina neoteretis* apertural view of all specimens from a sample split of the coarse size fraction > 125 µm at 223.5 cm sediment depth in core PS2185-6. All specimens are heavily corroded. As the calcite shell dissolves on the surface, the sutures between adjacent calcite crystals become visible as so-called cogwheel structures **(a–d, f, h–j)**. Damaged apertural plate **(b)**, **(d)**, **(g–j)**. Although the apertural plate of most specimens is damaged, the broader subtriangular apertural plate with smooth rim (compared to *C. teretis*) allows to assign them to *C. neoteretis*. All SEM images.

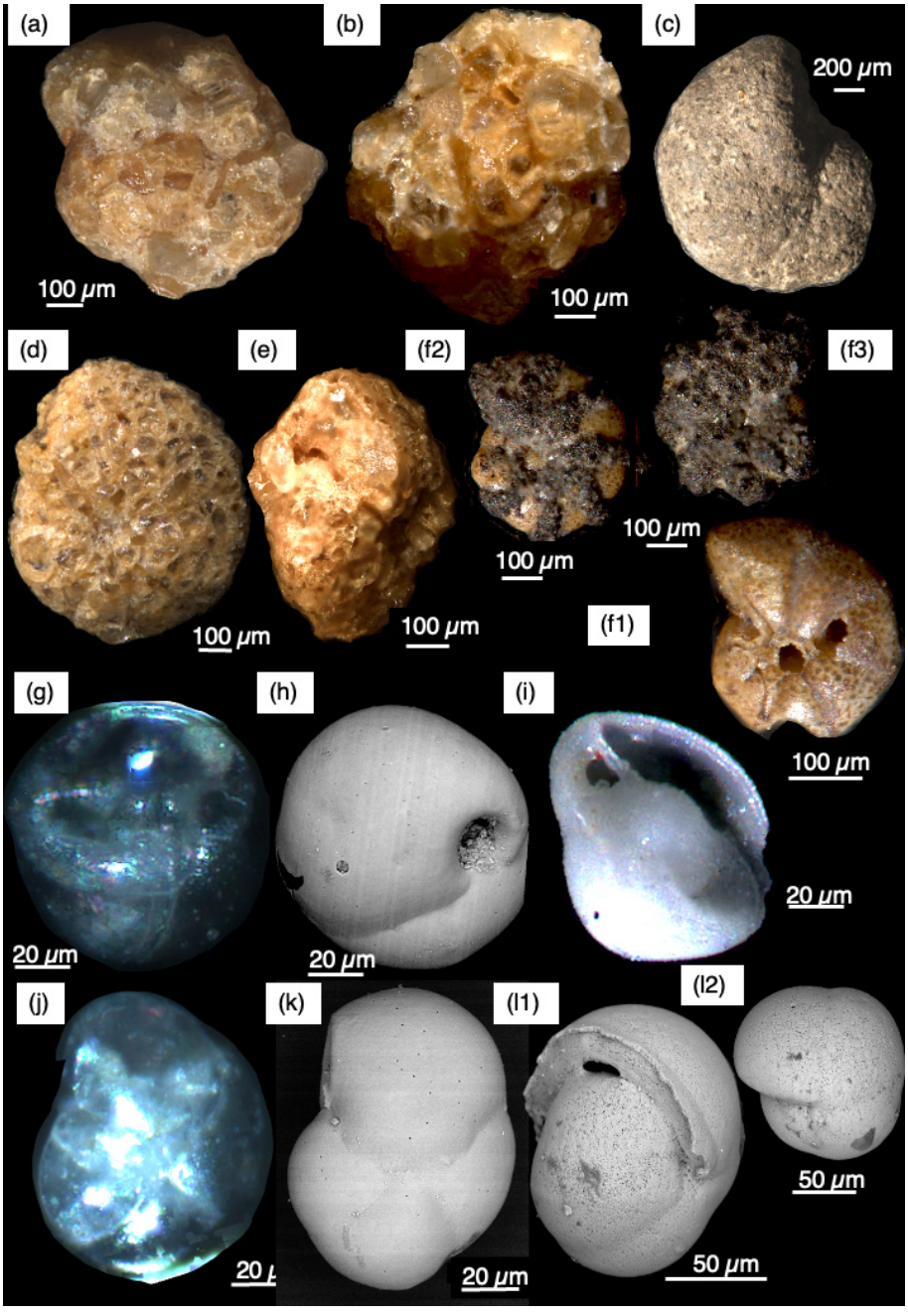

Plate A4. **(a–b)** *Cribrostomoides subglobosus* revealing the streptospiral coiling and large variability in grain-size used for agglutination; **(a)** side view; **(b)** apertural view showing the slite-like aperture of young specimen. **(c)** *Cyclammina orbicularis* side view of the thick planispiral test; agglutination obscured by iron-manganese coating. **(d–e)** *Haplophragmoides obscurus* revealing the variable grain-size used for agglutination and the numerous indistinct sutures of the shell; **(d)** Side view; **(e)** apertural view. (f1–3) *Cyclammina trullisata* with smooth shell surface but progressive coverage by iron-manganese overgrowth (f1–f3). **(g–i)** *Epistominella arctica.* **(g–h)** umbilical view of well-preserved specimens with thin, translucent shell; **(g)** with smooth, shiny test. **(h)** irregularly distributed pores. **(i)** Diagenetically altered specimen with broken final chamber revealing that only the final chamber of *E. arctica* is inflated and has a circular aperture on the umbilical side, in earlier chambers the aperture is positioned in a peripheral-umbilical positioned depression. **(j–k)** *Stetsonia horvathi,* well-preserved specimen; **(j)** translucent shell; **(k)** unevenly distributed pores. (l1–2) *Pullenia bulloides*, images of corroded specimens with visible cogwheel structure, (l1) revealing the subglobose 4-chambered shell composed of chambers increasing rapidly in length and width but only little in height, lateral view; (l2) apertural view, but slit-like aperture is not visible as last chamber missing. **(a)** PS2212-3 90 cm (Wollenburg et al., 2001); **(b)** PS2185-6, 150 cm; **(c–d)** PS2185-6, 223 cm; **(e)** PS2185-4, 379.5 cm; **(f–g)** PS2185-6, 166.5 cm; **(h–k)** PS2185-4, 0.5 cm. **(a–g)**, **(i–j)** Axiozoom photos. **(h)**, **(k–l)** SEM images.

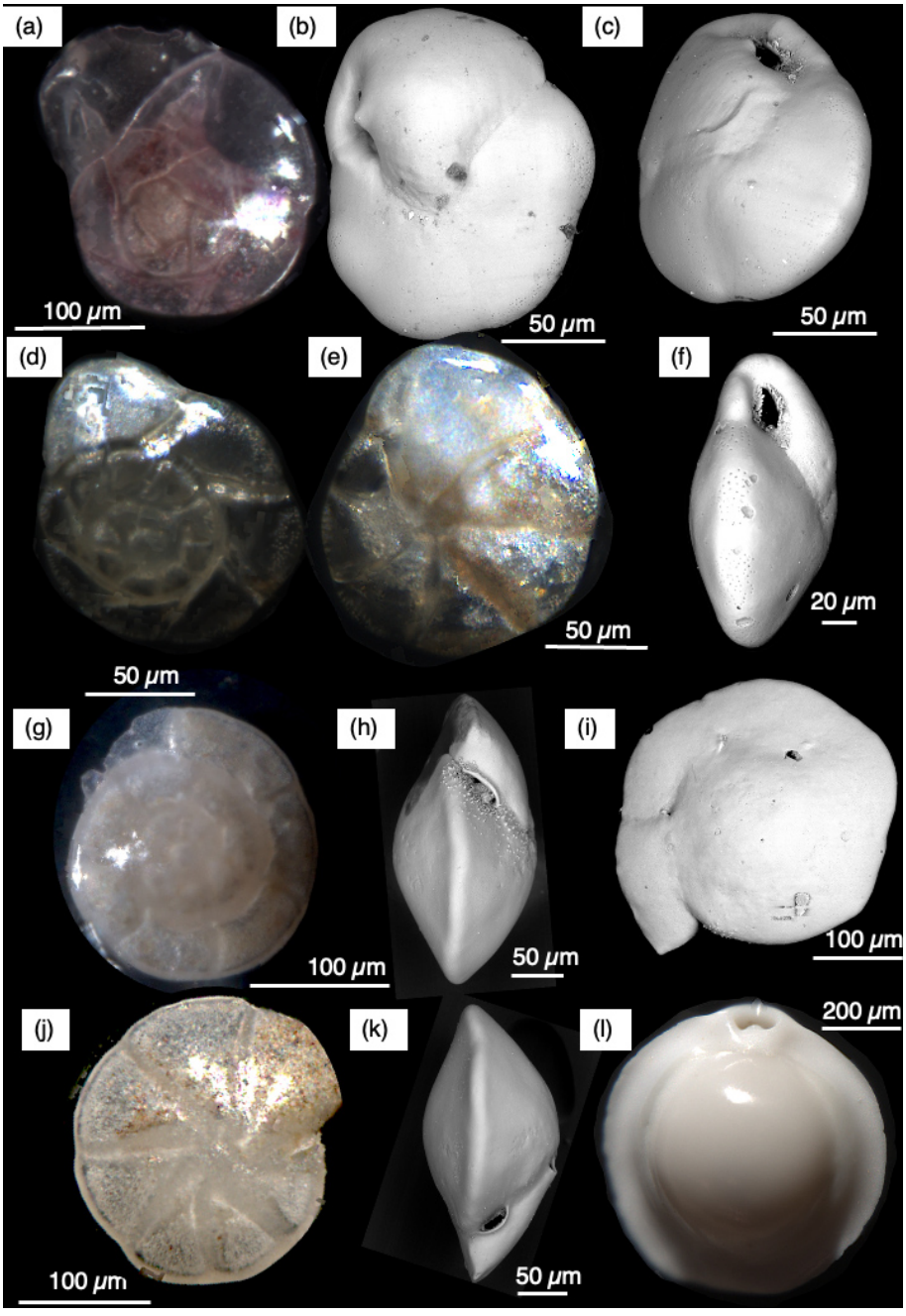

Plate A5. **(a–c)** *Epistominella* exigua, well preserved specimens; **(a)** Dorsal side of a specimen revealing the translucent shell, the curved sutures, and the rapidly increasing chamber size with 5 chambers in the last whorl; **(b)** umbilical view revealing the lack of a significant depression in the umbilical area, the smooth shell and the increasing porosity towards the periphery; **(c)** Tilted umbilical view revealing the lack of apertural lips bordering the elongated aperture, peripheral view. **(d–f)** *Eilohedra vitrea*; **(d)** dorsal view revealing the translucent shell, and 6 chambers in the last whorl separated by straight sutures; **(e)** umbilical view revealing 6.5 chambers in the last whorl separated by slightly curved sutures, a slightly depressed umbilicus; **(f)** peripheral view revealing details of the aperture composed of a short basal and elongated slit towards the periphery bordered by serrated lips. **(g–k)** *Oridorsalis umbonatus*; **(g)** dorsal view revealing the translucent shell with relatively straight sutures; **(h, k)** peripheral view showing the aperture and an either tuberculous **(h)** or smooth **(k)** basal area of the aperture, aperture surrounded by a lip on the last whorl; **(i)** Dorsal view revealing three Appendix apertures in the last chambers; **(j)** Umbilical view revealing the only slightly curved sutures and the non-depressed umbilical area. **(l)** *Pyrgo rotalaria*, specimen with small round aperture and small tooth, apertural view. **(a)** sediment surface from site PS2446-2, 2026 m water depth northern Barents Sea continental slope (Wollenburg and Mackensen, 1998c). **(b–c)** PS2185-6 229.5 cm. **(d–f)** ODP 910A 1H1 135 cm. **(g–k)** PS2185-4 0.5 cm **(a)**, **(d–f)**, **(g)**, **(j)**, **(l)** Axiozoom photos. **(c)**, **(f)**, **(h–i)**, **(j–k)**. SEM images.

Table B1. Ecology, shell characteristics, and preservation of main calcareous taxa.

(a) hhline Species	Habitat depth	Ecology	Size ø µm	No. whorls/Chambers
Epistominella arctica	phytodetritus/surface sediment layer	phytodetritus species, opportunistic, r-strategist	70	2/10
Epistominella exigua	phytodetritus/surface sediment layer	phytodetritus species; Atlantic species, r-strategist opportunistic	390	3/15
Stetsonia horvathi	shallow infaunal	low food demand, opportunistic	100	3/15
Ioanella tumidula subsp. *horvathi*	epifaunal, often epilithic	low to moderate food demand, opportunistic	140	3.5/ca. 20
Nonionella iridea	phytodetritus/surface sediment layer	phytodetritus species, eventually nourishing on associated bacteria, opportunistic, r-strategist	130	2.5/12-14
Eilohedra vitrea	shallow infaunal	able to respond to high food availability, opportunist	150	3/15
Alabaminella weddellensis	phytodetritus/surface sediment layer	phytodetritus species, opportunistic, r-strategist	160	4/20
Pyrgo rotalaria	epi- to shallow infaunal	ingest rapidly phytodetritus and nourish on its own cytoplasm during absent food fall, opportunistic, k-strategist	> 600	not available
Oridorsalis umbonatus	shallow infaunal	low to moderate food demand, opportunistic	400	3.5/ca. 25
Cassidulina neoteretis	shallow infaunal	able to nourish on bacteria associated with phytodetritus, opportunistic, r-strategist	300	8-10 Ch. Last whorl
Bolivina arctica	infauna	Today rare; k-strategist likely adapted to past environmental conditions	200	Biserial/12
Pullenia bulloides	infaunal in seasonally ice-free areas	Atlantic species, opportunistic, r-strategist	500	not known/4–5 in the final whorl
Bulimina aculeata	usually shallow but also deep infaunal	high labile organic carbon demand	2000	?4/?12

https://doi.org/10.5194/cp-22-1305-2026

Table B1. Continued.

(b)				
Species	Test shape	Shell thickness (µm)	Preservation potential	No. whorls/Chambers
Epistominella arctica	inflated trochospiral, biconvex, chambers increasing rapidly in size with growth	0.47	very low	(9); (18); (21); this study
Epistominella exigua	trochospiral, biconvex, periphery acute, chambers increasing rapidly in size with growth	1.37	low-very low	(3); (27); this study
Stetsonia horvathi	planispiral involute, biconvex	0.77	low	(9); (18); (21); this study
Ioanella tumidula subsp. *horvathi*	trochospiral planoconvex with high dorsal spire	1.45	low	(6); (18); this study
Nonionella iridea	trochospiral, biconvex, periphery rounded, chambers increasing rapidly in size with growth		low	(5); (17); (20); (22); (25); this study
Eilohedra vitrea	trochospiral, biconvex, periphery acute, chambers increasing rapidly in size with growth		low	(7); (13); (25); this study
Alabaminella weddellensis	trochospiral, biconvex	2.25	low-moderate	(6); (16); (20); (21); (23); (25); this study
Pyrgo rotalaria	miliolid, biserial, biconvex, peripheral keel	59.71	moderate-low	(7); (12); (18); this study
Oridorsalis umbonatus	trochospiral, biconvex, periphery acute, chambers increasing moderately in size	2.15	moderate	(4); (18); (19); (25); (26); this study
Cassidulina neoteretis	lenticular, umbilical boss on each side, biserial coiled, peripheral keel	2.64	moderate	(15); (18); (19); (22); this study
Bolivina arctica	elongated biserial, tapered twisted	1.14	moderate	(10); this study
Pullenia bulloides	planispiral involute, biconvex, subglobular, broad rounded periphery	2.59	moderate	(2); (19); this study
Bulimina aculeata	elongated triserial inflated, spinose	5.16	high	(1); (27); (28); (29)

Data availability. All utilized datasets are available via the PANGAEA online repository: https://doi.org/10.1594/PANGAEA.988969 (Wollenburg and Matthiessen, 2026a), https://doi.org/10.1594/PANGAEA.988971 (Wollenburg and Matthiessen, 2026b), and https://doi.org/10.1594/PANGAEA.988973 (Wollenburg and Matthiessen, 2026c).

Author contributions. JW and JM conceptualized the study, sampled the sediment cores, interpreted the data set and wrote the manuscript. JW performed the benthic foraminifera analysis.

Competing interests. The contact author has declared that none of the authors has any competing interests.

Disclaimer. Publisher's note: Copernicus Publications remains neutral with regard to jurisdictional claims made in the text, published maps, institutional affiliations, or any other geographical representation in this paper. The authors bear the ultimate responsibility for providing appropriate place names. Views expressed in the text are those of the authors and do not necessarily reflect the views of the publisher.

Acknowledgements. We thank the *Polarstern* Core Repository for providing the samples used in this study. We are grateful to Stefanie Kaboth-Bahr, Jörg Wagner, Matthias Feldtmann, Matthias Heinze, Leonie Peti who, over the years helped in picking foraminifera from these cores. We thank two anonymous reviewers for their comments that helped to improve the manuscript.

Financial support. The article processing charges for this open-access publication were covered by the Alfred-Wegener-Institut Helmholtz-Zentrum für Polar- und Meeresforschung.

Review statement. This paper was edited by Antje Voelker and reviewed by two anonymous referees.

References

Adler, R. E., Polyak, L., Ortiz, J. D., Kaufman, D. S., Channell, J. E. T., Xuan, C., Grottoli, A. G., Sellen, E., and Crawford, K. A.: Sediment record from the western Arctic Ocean with an improved late Quaternary age resolution: HOTRAX core HLY0503-8JPC, Mendeleev Ridge, Glob. Planet. Change, 68, 18–29, https://doi.org/10.1016/j.gloplacha.2009.03.026, 2009.

Aksu, A. E.: Paleomagnetic stratigraphy of the CESAR cores, in: Initial geological report on CESAR – the Canadian expedition to study the Alpha Ridge, Arctic Ocean, edited by: Jackson, H. R., Mudie, P. J., and Blasco, S. M., Geol. Surv. Can. Pap., 101–114, https://doi.org/10.4095/120315, 1985.

Alexanderson, H., Backman, J., Cronin, T. M., Funder, S., Ingólfsson, Ó., Jakobsson, M., Landvik, J. Y., Löwemark, L., Mangerud, J., März, C., Möller, P., O'Regan, M., and Spielhagen, R. F.: An Arctic perspective on dating Mid-Late Pleistocene environmental history, Quat. Sci. Rev., 92, 9–31, https://doi.org/10.1016/j.quascirev.2013.09.023, 2014.

Altenbach, A. V.: Short term processes and patterns in the foraminiferal response to organic flux rates, Mar. Micropaleontol., 19, 119–129, https://doi.org/10.1016/0377-8398(92)90024-E, 1992.

Alve, E.: Colonization of new habitats by benthic foraminifera: a review, Earth Sci. Rev., 46, 167–185, https://doi.org/10.1016/S0012-8252(99)00016-1, 1999.

Alve, E. and Goldstein, S. T.: Propagule transport as a key method of dispersal in benthic foraminifera (Protista), Limnol. Oceanogr., 48, 2163–2170, https://doi.org/10.4319/lo.2003.48.6.2163, 2003.

Alve, E. and Goldstein, S. T.: Dispersal, survival and delayed growth of benthic foraminiferal propagules, J. Sea Res., 63, 36–51, https://doi.org/10.1016/j.seares.2009.09.003, 2010.

Alve, E. and Goldstein, S.: The propagule method as an experimental tool in foraminiferal ecology, in: Approaches to Study Living Foraminifera. Environmental Science and Engineering, edited by: Kitazato, H. and Bernhard, M., J., Springer, Tokyo, 1–12, https://doi.org/10.1007/978-4-431-54388-6_1, 2014.

Anderson, L. G., Jones, E. P., and Swift, J. H.: Export production in the central Arctic Ocean evaluated from phosphate deficits, J. Geophys. Res.-Oceans, 108, 3199, https://doi.org/10.1029/2001JC001057, 2003.

Anthonissen, D. E. and Ogg, J. G.: Appendix 3: Cenozoic and Cretaceous biochronology of planktonic foraminifera and calcareous nannofossils, in: The Geologic Time Scale 2012, edited by: Gradstein, F., Ogg, J. G., Schmitz, M. D., and Ogg, G. M., Elsevier, Amsterdam, 1083–1127, https://doi.org/10.1016/B978-0-444-59425-9.15003-6, 2012.

Backman, J., Jakobsson, M., Løvlie, R., Polyak, L., and Febo, L. A.: Is the central Arctic Ocean a sediment starved basin?, Quat. Sci. Rev., 23, 1435–1454, https://doi.org/10.1016/j.quascirev.2003.12.005, 2004.

Backman, J., Fornaciari, E., and Rio, D.: Biochronology and paleoceanography of late Pleistocene and Holocene calcareous nannofossil abundances across the Arctic Basin, Mar. Micropaleontol., 72, 86–98, https://doi.org/10.1016/j.marmicro.2009.04.001, 2009.

Backman, J., Raffi, I., Rio, D., Fornaciari, E., and Pälike, H.: Biozonation and biochronology of Miocene through Pleistocene calcareous nannofossils from low and middle latitudes, Newslett. Stratigr., 45, 221–244, https://doi.org/10.1127/0078-0421/2012/0022, 2012.

Barker, R. W.: Taxonomic notes on the species figured by H. B. Brady in his report on the foraminifera dredged by H. M. S. Challenger during the years 1873–1876, SEPM Spec. Publ., 9, 1–238, 1960.

Bazhenova, E.: Reconstruction of late Quaternary sedimentary environments at the southern Mendeleev Ridge (Arctic Ocean), Ph.D. thesis, University of Bremen, Germany, 91 pp., https://nbn-resolving.de/urn:nbn:de:gbv:46-00102884-17 (last access: 20 July 2026), 2012.

Bazhenova, E., Fagel, N., and Stein, R.: North American origin of "pink–white" layers at the Mendeleev Ridge (Arctic Ocean): New insights from lead and neodymium isotope composition of detrital sediment component, Mar. Geol., 386, 44–55, https://doi.org/10.1016/j.margeo.2017.01.010, 2017.

Belanger, P. E. and Streeter, S. S.: Distribution and ecology of benthic foraminifera in the Norwegian-Greenland Sea, Mar. Micropaleontol., 5, 401–428, https://doi.org/10.1016/0377-8398(80)90020-1, 1980.

Belyaeva, N. V. and Khusid, T. A.: Benthonic and planktonic foraminifera in the Pleistocene sediments of the Arctic Ocean: Evolution of communities and of the environment, Dokl. Akad. Nauk SSSR, 309, 1472–1475, 1989.

Bender, H.: Gehäuseaufbau, Gehäusegenese und Biologie agglutinierter Foraminiferen (Sarcodina, Textulariina), Jb. Geol. B.-A., 132, 259–347, 1989.

Bendif, E. M., Probert, I., Archontikis, O. A., Young, J. R., Beaufort, L., Rickaby, R. E., and Filatov, D.: Rapid diversification underlying the global dominance of a cosmopolitan phytoplankton, The ISME J., 17, 630–640, https://doi.org/10.1038/s41396-023-01365-5, 2023.

Bergmann, U.: Physical properties of sediment core PS2185-6, PANGAEA [data set], https://doi.org/10.1594/PANGAEA.50137, 1996.

Bergsten, H.: Recent benthic foraminifera of a transect from the North Pole to the Yermak Plateau, eastern central Arctic Ocean, Mar. Geol., 119, 251–267, https://doi.org/10.1016/0025-3227(94)90184-8, 1994.

Bingham-Koslowski, N., Pufahl, P., Boggild, K., Kong, M., and Priv, D.: Mysteries of the deep: Exploring the origin of carbonate hardgrounds from the Alpha Ridge, Arctic Ocean, Geosci. Can., 52, 99, https://doi.org/10.12789/geocanj.2025.52.223, 2025.

Bornmalm, L.: Taxonomy and paleoecology of late Neogene benthic foraminifera from the Caribbean Sea and eastern equatorial Pacific Ocean, Fossils Strata, 41, 1–96, https://doi.org/10.18261/8200376664-1997-01, 1997.

Brady, H. B.: Report on the foraminifera dredged by H.M.S. Challenger during the years 1873-1876, Report on the Scientific Results of the voyage of H.M.S. Challenger during the years 1873–76, Zoology 9, Part XXII, 814 pp., 1884.

Burgess, M. V. and Schnitker, D.: Morphometry of *Bulimina aculeata* Orbigny and *Bulimina marginata* Orbigny, J. Foraminifer. Res., 20, 37–49, https://doi.org/10.2113/gsjfr.20.1.37, 1990.

Buzas, M. A. and Culver, S. J.: Biogeographic and evolutionary patterns of continental margin benthic foraminifera, Paleobiology, 15, 11–19, https://doi.org/10.1017/S0094837300009143, 1989.

Buzas, M. A. and Culver, S. J.: Species diversity and dispersal of benthic foraminifera: Analysis of extant organisms and fossils of the waters around North America, BioScience, 41, 483–489, https://doi.org/10.2307/1311806, 1991.

Cage, A., Pieńkowski, A., Jennings, A., Knudsen, K., and Seidenkrantz, M.-S.: Comparative analysis of six common foraminiferal species of the genera *Cassidulina*, *Paracassidulina*, and *Islandiella* from the Arctic–North Atlantic domain, J. Micropalaeontol., 40, 37–60, https://doi.org/10.5194/jm-40-37-2021, 2021.

Carstens, J. and Wefer, G.: Recent distribution of planktonic foraminifera in the Nansen Basin, Arctic Ocean, Deep-Sea Res. I, 39, 507–524, https://doi.org/10.1016/S0198-0149(06)80018-X, 1992.

Chauhan, T., Rasmussen, T. L., Noormets, R., Jakobsson, M., and Hogan, K. A.: Glacial history and paleoceanography of the southern Yermak Plateau since 132 ka BP, Quat. Sci. Rev., 92, 155–169, https://doi.org/10.1016/j.quascirev.2013.10.023, 2014.

Chauhan, T., Rasmussen, T., and Noormets, R.: Palaeoceanography of the Barents Sea continental margin, north of Nordaustlandet, Svalbard, during the last 74 ka, Boreas, 45, https://doi.org/10.1111/bor.12135, 2015.

Clark, D. L., Whitman, R. R., Morgan, K. A., and Mackey, S. D.: Stratigraphy and glacial-marine sediments of the Amerasian Basin, Central Arctic Ocean, Geol. Soc. Am. Spec. Pap., 181, 57 pp., https://doi.org/10.1130/SPE181-p1, 1980.

Clark, D. L., Chern, L. A., Hogler, J. A., Mennicke, C. M., and Atkins, E. D.: Late Neogene climate evolution of the Central Arctic Ocean, Mar. Geol., 93, 69–94, https://doi.org/10.1016/0025-3227(90)90078-X, 1990.

Collins, L. S.: Relationship of environmental gradients to morphologic variation within *Bulimina aculeata* and *Bulimina marginata*, Gulf of Maine area, J. Foraminifer. Res., 19, 222–234, https://doi.org/10.2113/gsjfr.19.3.222, 1989.

Collins, L. S.: Regional versus physiographic effects on morphologic variability within *Bulimina aculeata* and *B. marginata*, Mar. Micropaleontol., 17, 155–170, https://doi.org/10.1016/0377-8398(91)90026-3, 1991.

Corliss, B. H.: Recent deep-sea benthonic foraminiferal distributions in the southeast Indian Ocean: Inferred bottom-water routes and ecological implications, Mar. Geol., 31, 115–138, https://doi.org/10.1016/0025-3227(79)90059-8, 1979.

Corliss, B. H. and Honjo, S.: Dissolution of deep-sea benthonic foraminifera, Micropaleontology, 27, 358–378, https://doi.org/10.2307/1485191, 1981.

Cornelius, N. and Gooday, A. J.: 'Live' (stained) deep-sea benthic foraminiferans in the western Weddell Sea: trends in abundance, diversity and taxonomic composition along a depth transect, Deep-Sea Res. II: Top. Stud. Oceanogr., 51, 1571–1602, https://doi.org/10.1016/j.dsr2.2004.06.024, 2004.

Cronin, T. M., Smith, S. A., Eynaud, F., O'Regan, M., and King, J.: Quaternary paleoceanography of the central Arctic based on Integrated Ocean Drilling Program Arctic Coring Expedition 302 foraminiferal assemblages, Paleoceanography, 23, PA1S18, https://doi.org/10.1029/2007PA001484, 2008.

Cronin, T. M., Polyak, L., Reed, D., Kandiano, E. S., Marzen, R. E., and Council, E. A.: A 600-ka Arctic sea-ice record from Mendeleev Ridge based on ostracodes, Quat. Sci. Rev., 79, 157–167, https://doi.org/10.1016/j.quascirev.2012.12.010, 2013.

Cronin, T. M., DeNinno, L. H., Polyak, L., Caverly, E. K., Poore, R. Z., Brenner, A., Rodriguez-Lazaro, J., and Marzen, R. E.: Quaternary ostracode and foraminiferal biostratigraphy and paleoceanography in the western Arctic Ocean, Mar. Micropaleontol., 111, 118–133, https://doi.org/10.1016/j.marmicro.2014.05.001, 2014.

Cronin, T. M., Keller, K. J., Farmer, J. R., Schaller, M. F., O'Regan, M., Poirier, R., Coxall, H., Dwyer, G. S., Bauch, H., Kindstedt, I. G., Jakobsson, M., Marzen, R., and Santin, E.: Interglacial Paleoclimate in the Arctic, Paleoceanogr. Paleoclimatol., 34, 1959–1979, https://doi.org/10.1029/2019PA003708, 2019a.

Cronin, T., Seidenstein, J., Keller, K., McDougall, K., Ruefer, A., and Gemery, L.: The benthic foraminifera *Cassidulina* from the Arctic Ocean: Application to paleoceanography and biostratigraphy, Micropaleontology, 65, 105–125, https://doi.org/0.47894/mpal.65.2.02, Cronin2019b.

Cushman, J. A.: A monograph of the foraminifera of the North Pacific Ocean. Part I. Astrorhizidae and Lituolidae, U. S. Natl. Mus. Bull., 71, 1–134, https://doi.org/10.5479/SI.03629236.71.I, 1910.

Cushman, J. A.: The foraminifera of the Atlantic Ocean, U. S. Natl. Mus. Bull., 10, 1–179, https://doi.org/10.5479/si.03629236.104.7, 1931.

Cushman, J. A. and Parker, F. L.: *Bulimina* and related foraminiferal genera, U. S. Geol. Surv. Prof. Pap., 210-D, 55–176, https://doi.org/10.3133/pp210D, 1947.

Darby, D. A., Naidu, A. S., Mowatt, T. C., and Jones, G.: Sediment composition and sedimentary processes in the Arctic Ocean, in: The Arctic Seas: Climatology, Oceanography, Geology, and Biology, edited by: Herman, Y., Van Nostrand Reinhold Company, New York, 657–720, https://doi.org/10.1007/978-1-4613-0677-1_24, 1989.

Darby, D. A., Bischof, J. F., Spielhagen, R. F., Marshall, S. A., and Herman, S. W.: Arctic ice export events and their potential impact on global climate during the late Pleistocene, Paleoceanography, 17, 1025, https://doi.org/10.1029/2001PA000639, 2002.

De Schepper, S. and Head, M. J.: Age calibration of dinoflagellate cyst and acritarch events in the Pliocene–Pleistocene of the eastern North Atlantic (DSDP Hole 610A), Stratigraphy, 5, 137–161, https://doi.org/10.29041/strat.05.2.02, 2008.

Devendra, D., Łącka, M., Telesiński, M., Rasmussen, T., Sztybor, K., and Zajączkowski, M.: Paleoceanography of the northwestern Greenland Sea and Return Atlantic Current evolution, 35–4 kyr BP, Global Planet. Change, 103947, https://doi.org/10.1016/j.gloplacha.2022.103947, 2022.

Devendra, D., Łącka, M., Szymańska, N., Szymczak-Żyła, M., Krajewska, M., Weiner, A. K. M., De Schepper, S., Simon, M. H., and Zajączkowski, M.: The development of ocean currents and the response of the cryosphere on the Southwest Svalbard shelf over the Holocene, Global Planet. Change, 228, 104213, https://doi.org/10.1016/j.gloplacha.2023.104213, 2023.

Dipre, G. R., Polyak, L., Kuznetsov, A. B., Oti, E. A., Ortiz, J. D., Brachfeld, S. A., Xuan, C., Lazar, K. B., and Cook, A. E.: Plio-Pleistocene sedimentary record from the Northwind Ridge: new insights into paleoclimatic evolution of the western Arctic Ocean for the last 5 Ma, Arktos, 4, 1–23, https://doi.org/10.1007/s41063-018-0054-y, 2018.

Domanov, M., Khusid, T., and Libina, N.: Benthic foraminifera in deep trenches of the Kara Sea and the relation of S*accorhiza ramosa* (Brady) to the distribution of natural radionuclides, Biol. Bull., 44, 187–192, https://doi.org/10.1134/S1062359017020054, 2017.

d'Orbigny, A. D.: Tableu méthodique de la classe des Céphalopodes, Ann. Sci. Nat., 1, 245–314, 1826.

Dong, L., Polyak, L., Liu, Y., Shi, X., Zhang, J., and Huang, Y.: Isotopic fingerprints of ice-rafted debris offer new constraints on Mid to Late Quaternary Arctic circulation and glacial history, Geochem. Geophys. Geosyst., 21, https://doi.org/10.1029/2020GC009019, 2020.

Ellis, B. F. and Messina, A. R.: Catalogue of foraminifera online, Micropaleontology Press, https://doi.org/10.1661/0026-2803(2002)048[0092:EAMCO]2.0.CO;2, 1940-2025.

Elkina, D. V., Piskarev, A. L., and Bezumov, D. V.: Sedimentation in the Central Arctic submarine elevations: Results of comprehensive analysis of paleomagnetic and seismoacoustic data, Geotectonics, 57, Suppl. 1, S100–S111, https://doi.org/10.1134/S0016852123070063, 2023.

Enge, A. J., Nomaki, H., Ogawa, N. O., Witte, U., Moeseneder, M. M., Lavik, G., Ohkouchi, N., Kitazato, H., Kučera, M., and Heinz, P.: Response of the benthic foraminiferal community to a simulated short-term phytodetritus pulse in the abyssal North Pacific, Mar. Ecol. Prog. Ser., 438, 129–142, https://doi.org/10.3354/meps09298, 2011.

Evans, J. R. and Kaminski, M. A.: Pliocene and Pleistocene chronostratigraphy and paleoenvironment of the central Arctic Ocean, using deep water agglutinated foraminifera, Micropaleontology, 44, 109–130, https://doi.org/10.2307/1486065, 1998.

Evans, J. R., Kaminski, M. A., Cronin, T. M., and Fütterer, D. K.: Pleistocene agglutinated foraminifera from the Lomonosov Ridge and Amundsen Basin, Arctic Basin. Initial report on piston cores 2177-5 (KAL) and 2176-3 (KAL), Mar. Micropaleontol., 26, 245–253, https://doi.org/10.1016/0377-8398(95)00016-X, 1995.

Eynaud, F., Cronin, T., Smith, S., Zaragosi, S., Mavel, J., Mary, Y., Mas, V., and Pujol, C.: Morphological variability of the planktonic foraminifera *Neogloboquadrina pachyderma* from ACEX cores: Implications for Late Pleistocene circulation in the Arctic Ocean, Micropaleontology, 55, https://doi.org/10.47894/mpal.55.2.02, 2009.

Faizieva, K., Wollenburg, J. E., Nagy, M., Berndt, C., and Heinz, P.: Benthic foraminiferal colonisation of phytodetritus during spring bloom within the marginal sea ice zone off Northern Svalbard continental margin. Sci. Rep. 16, 10889, https://doi.org/10.1038/s41598-026-45090-3, 2026.

Feyling-Hanssen, R. W.: Late-Pleistocene foraminifera from the Oslofjord Area, Southeast Norway, Norw. J. Geol., 33, 109–151, 1954.

Feyling-Hanssen, R. W.: Foraminifera in Late Quaternay deposits from the Oslofjord area, Norges Geologiske Undersøkelse, 225, 383 pp., http://www.ngu.no/filearchive/NGUPublikasjoner/NGUnr_225_FeylingHanssen.pdf (last access: 20 July 2026), 1964.

Feyling-Hanssen, R. W. and Ullberg, K.: A Tertiary-Quaternary section at Sarsbukta, Spitsbergen, Svalbard, and its foraminifera., Polar Res., 2, 77–106, https://doi.org/10.3402/polar.v2i1.6963 1984.

Feyling-Hanssen, R. W., Funder, S., and Petersen, K. S.: The Lodin Elv Formation, a Plio-Pleistocene occurrence in Greenland, Bull. Geol. Soc. Denmark, 31, 81–106, https:/doi.org/10.37570/bgsd-1982-31-07, 1983.

Fontanier, C., Jorissen, F. J., Licari, L., Alexandre, A., Anschutz, P., and Carbonel, P.: Live benthic foraminiferal faunas from the Bay of Biscay: faunal density, composition, and microhabitats, Deep-Sea Res. I: Oceanogr. Res. Pap, 49, 751–785, https://doi.org/10.1016/S0967-0637(01)00078-4, 2002.

Frank, M., Backman, J., Jakobsson, M., Moran, K., O'Regan, M., King, J., Haley, B., Kubik, P., and Garbe-Schönberg, D.: Beryllium isotopes in central Arctic Ocean sediments

over the past 12.3 million years: Stratigraphic and paleoclimatic implications, Paleoceanography, 23, PA1S01, https://doi.org/10.1029/2007PA001478, 2008.

Gaździcki, A. and Majewski, W.: Foraminifera from the Eocene La Meseta Formation of Isla Marambio (Seymour Island), Antarctic Peninsula, Antarct. Sci., 24, 408–416, https//-doi.org/10.1017/S095410201200020X, 2012.

Geibert, W., Matthiessen, J., Stimac, I., Wollenburg, J., and Stein, R.: Glacial episodes of a freshwater Arctic Ocean covered by a thick ice shelf, Nature, 590, 97–102, https://doi.org/10.1038/s41586-021-03186-y, 2021.

Goës, A. T.: A synopsis of Arctic and Scandinavian recent marine Foraminifera hitherto discovered, K. Svensk. Vetensk. Akad. Handlingar. XXV, 1893-4, No. 9, 127 p., https://doi.org/10.5962/bhl.title.14885, 1894.

Gooday, A. J.: A response by benthic foraminifera to the deposition of phytodetritus in the deep sea, Nature, 332, 70–73, https://doi.org/10.1038/332070a0, 1988.

Gooday, A. J. and Jorissen, F. J.: Benthic foraminiferal biogeography: Controls on global distribution patterns in deep-water settings, Annu. Rev. Mar. Sci., 4, 237–262, https://doi.org/10.1146/annurev-marine-120709-142737, 2012.

Gooday, A. and Lambshead, P. J.: Influence of seasonally deposited phytodetritus on benthic foraminiferal populations in the bathyal northeast Atlantic: The species response, Mar. Ecol. Prog. Ser., 58, 53–67, https://doi.org/10.3354/meps058053, 1989.

Gooday, A. J., Nomaki, H., and Kitazato, H.: Modern deep-sea benthic foraminifera: a brief review of their morphology-based biodiversity and trophic diversity, Geol. Soc. Spec. Publ., 303, 97–119, https://doi.org/10.1144/SP303.8, 2008a.

Gooday, A., Todo, Y., Uematsu, K., and Kitazato, H.: New organic-walled foraminifera (Protista) from the ocean's deepest point, the Challenger Deep (western Pacific Ocean), Zool. J. Linn. Soc., 153, 399–423, https://doi.org/10.1111/j.1096-3642.2008.00393.x, 2008b.

Green, K. E.: Ecology of some Arctic foraminifera, in Scientific Studies at Fletcher's Ice Island, T-3, 1952–1955, Volume 1, edited by: Bushnell, V., Terrestrial Sciences Laboratory, Geophysics Research Directorate, Air Force Cambridge Research Center, Air Research and Development Command, U.S. Air Force. Geophysical Research Papers no. 63, 59–81, 1959.

Green, K. E.: Ecology of some Arctic Foraminifera, Micropaleontology, 6, 57–78, https://doi.org/10.2307/1484317, 1960.

Grobe, H. and Fütterer, D. K.: Documentation of sediment core PS2185-6, PANGAEA [data set], https://doi.org/10.1594/PANGAEA.115184, 2003.

Gupta Sen, B. K.: Modern Foraminifera, Kluwer Academic Publishers, 368 pp., https://doi.org/10.1007/0-306-48104-9, 2003.

Haake, F.-W., Erlenkeuser, H., and Pflaumann, U.: *Pullenia bulloides* (Orbigny) in sediments of the Norwegian/Greenland Sea and the northeastern Atlantic Ocean: paleo-oceanographic evidence, in Studies in Benthic Foraminifera, International Symposium (Benthos∼ 90), Sendai, Tokai University Press, 235–244, 1992.

Hald, M. and Korsun, S.: Distribution of modern benthic foraminifera from fjords of Svalbard, European Arctic, J. Foraminifer. Res., 27, 101–122, https://doi.org/10.2113/gsjfr.27.2.101, 1997.

Hanslik, D.: Late Quaternary biostratigraphy and paleoceanography of the central Arctic Ocean, Ph.D. thesis, Stockholm University, Sweden, Meddelanden från Stockholms Universitets Institution för Geologiska Vetenskaper, 345, 32 pp., urn:nbn:se:su:diva-57245, 2011.

Hanslik, D., Löwemark, L., and Jakobsson, M.: Biogenic and detrital-rich intervals in central Arctic Ocean cores identified using x-ray fluorescence scanning, Polar Res., 32, 18386, https://doi.org/10.3402/polar.v32i0.18386, 2013.

Harada, N.: Review: Potential catastrophic reduction of sea ice in the western Arctic Ocean: Its impact on biogeochemical cycles and marine ecosystems, Glob. Planet. Change., 136, 1–17, https://doi.org/10.1016/j.gloplacha.2015.11.005, 2016.

Hayward, B. W.: Global deep-sea extinctions during the Pleistocene ice ages, Geology, 29, 599–602, https://doi.org/10.1130/0091-7613(2001)029<0599:GDSEDT>2.0.CO;2, 2001.

Hayward, B. W.: Late Pliocene to middle Pleistocene extinctions of deep-sea benthic foraminifera ("*Stilostomella* extinction") in the southwest Pacific, J. Foraminifer. Res., 32, 274–307, https://doi.org/10.2113/32.3.274, 2002.

Hayward, B. W., Kawagata, S., Grenfell, H. R., Sabaa, A. T., and O'Neill, T.: Last global extinction in the deep sea during the mid-Pleistocene climate transition, Paleoceanography, 22, 267–291, https://doi.org/10.1016/j.palaeo.2005.03.001, 2007.

Hayward, B. W., Johnson, K., Sabaa, A. T., Kawagata, S., and Thomas, E.: Cenozoic record of elongate, cylindrical, deep-sea benthic foraminifera in the North Atlantic and equatorial Pacific Oceans, Mar. Micropaleontol., 74, 75–95, https://doi.org/10.1016/j.marmicro.2010.01.001, 2010.

Hayward, B. W., Kawagata, S., Sabaa, T. A., Grenfell, H., Van Kerckhoven, L., Johnson, K., and Thomas, E.: The last global extinction (Mid-Pleistocene) of deep-sea benthic foraminifera (Chrysalogoniidae, Ellipsoidinidae, Glandulonodosariidae, Plectofrondicularиidae, Pleurostomellidae, Stilostomellidae), their Late Cretaceous-Cenozoic history and taxonomy, Cush. Found. Spec. Publ., 43, 408 pp., https://www.researchgate.net/publication/256078664 (last access: 20 July 2026), 2012.

Hayward, B. W., Le Coze, F., Vachard, D., and Gross, O.: World Foraminifera Database, https://doi.org/10.14284/305, https://www.marinespecies.org/foraminifera, last access: 17 November 2025.

Head, M. J., Pillans, B., Zalasiewicz, J. A. and the ICS Subcommission on Quaternary Stratigraphy: Formal ratification of subseries for the Pleistocene Series of the Quaternary System, Episodes, 44, 241–247, https://doi.org/10.18814/epiiugs/2020/020084, 2021.

Hedley, R. H.: Cement and iron in the arenaceous foraminifera, Micropaleontology, 9, 433–441, https://doi.org/10.2307/1484505, 1963.

Herman, Y.: Temperate water planktonic foraminifera in Quaternary sediments of the Arctic Ocean, Nature, 201, 386–387, https://doi.org/10.1038/201386a0, 1964.

Herman, Y.: *Bolivina arctica*, a new benthonic foraminifera from Arctic Ocean sediments, J. Foraminifer. Res., 3, 137–141, https://doi.org/10.2113/gsjfr.3.3.137, 1973.

Herman, Y.: Arctic Ocean sediments, microfauna, and the climatic record in late Cenozoic time, in: Marine Geology and Oceanography of the Arctic Seas, edited by: Herman, Y., Springer, Berlin,

Heidelberg, 283–348, https://doi.org/10.1007/978-3-642-87411-6_13, 1974.

Herman, Y., Osmond, J. K., and Somayajulu, B. L. K.: Late Neogene Arctic paleoceanography: micropaleontology, stable isotopes, and chronology, in: The Arctic Seas, edited by: Herman, Y., Van Nostrand Reinhold Company, New York, 581–655, https://doi.org/10.1007/978-1-4613-0677, 1989.

Hillaire-Marcel, C., Ghaleb, B., de Vernal, A., Maccali, J., Cuny, K., Jacobel, A., Le Duc, C., and McManus, J.: A new chronology of late Quaternary sequences from the central Arctic Ocean based on " extinction ages" of their excesses in ^{231}Pa and ^{230}Th, Geochem. Geophys. Geosyst, 18, 4573–4585, https://doi.org/10.1002/2017/GC007050, 2017.

Himmighofen, O., Holzmann, M., Barrenechea, I., Pawlowski, J., and Gooday, A.: An integrative taxonomic survey of benthic foraminiferal species (Protista, Rhizaria) from the eastern Clarion-Clipperton Zone, J. Mar. Sci. Eng., 11, 2038, https://doi.org/10.3390/jmse11112038, 2023.

Höglund, H. G.: Foraminifera in the Gullmar Fjord and the Skagerrak, Zoologiska bidrag från Uppsala, 26, 1–328, 1947.

Holbourn, A., Henderson, A., and MacLeod, N.: Atlas of Benthic Foraminifera, John Wiley & Sons, London, 642 pp., https://doi.org/10.1002/9781118452493, 2013.

Honjo, S., Manganini, S. J., Krishfield, R. A., and Francois, R.: Particulate organic carbon fluxes to the ocean interior and factors controlling the biological pump: A synthesis of global sediment trap programs since 1983, Progr. Oceanogr, 76, 217–285, https://doi.org/10.1016/j.pocean.2007.11.003, 2008.

Hottinger, L.: Processes determining the distribution of larger foraminifera in space and time, Utrecht Micropaleontol. Bull., 30, 239–253, 1983.

Hunkins, K., Bé, A. W. H., Opdyke, N. D., and Mathieu, G.: The late Cenozoic history of the Arctic Ocean, in: The late Cenozoic glacial ages, edited by: Turekian, K. K., Yale University Press, New Haven, 215–237, 1971.

Husum, K. and Hald, M.: Modern foraminiferal distribution in the subarctic Malangen Fjord and adjoining shelf, Northern Norway, J. Foraminifer. Res., 34, 34–48, https://doi.org/10.2113/0340034, 2004.

Husum, K., Hald, M., Stein, R., and Weißschnur, M.: Recent benthic foraminifera in the Arctic Ocean and Kara Sea continental margin, Arktos, 1, 5, https://doi.org/10.1007/s41063-015-0005-9, 2015.

Ishman, S. E. I. and Foley, K. M.: Modern benthic foraminifera distribution in the Amerasian Basin, Arctic Ocean, Micropaleontology, 42, 206–220, https://doi.org/10.2307/1485871, 1996.

Ishman, S. E., Polyak, L. V., and Poore, R. Z.: Expanded record of Quaternary oceanographic change: Amerasian Arctic Ocean, Geology, 24, 139–142, https://doi.org/10.1130/0091-7613(1996)024<0139:EROQOC>2.3.CO;2, 1996.

Jakobsson, M., Løvlie, R., Al-Hanbali, H., Arnold, E., Backman, J., and Mörth, M.: Manganese and color cycles in Arctic Ocean sediments constrain Pleistocene chronology, Geology, 28, 23–26, https://doi.org/10.1130/0091-7613(2000)28<23:MACCIA>2.0.CO;2, 2000.

Jakobsson, M., Løvlie, R., Arnold, E. M., Backman, J., Polyak, L., Knutsen, J.-O., and Musatov, E.: Pleistocene stratigraphy and paleoenvironmental variation from Lomonosov Ridge sediments, central Arctic Ocean, Glob. Planet. Change, 31, 1–22, https://doi.org/10.1016/S0921-8181(01)00110-2, 2001.

Jakobsson, M., Backman, J., Murray, A., and Løvlie, R.: Optically stimulated luminescence dating supports central Arctic Ocean cm-scale sedimentation rates, Geochem. Geophys. Geosyst., 4, 1016, https://doi.org/1016, 10.1029/2002GC000423, 2003.

Jennings, A., Reilly, B., Andrews, J., Hogan, K., Walcak, M., Jakobsson, M., Stoner, J., Mix, A., Nicholls, K. W., O'Regan, M., Prins, M. A., and Troelstra, S. R.: Modern and early Holocene ice shelf sediment facies from Petermann Fjord and northern Nares Strait, northwest Greenland, Quat. Sci. Rev., 283, 107460, https://doi.org/10.1016/j.quascirev.2022.107460, 2022.

Jennings, A. E., Andrews, J. T., Ó Cofaigh, C., Onge, G. S., Sheldon, C., Belt, S. T., Cabedo-Sanz, P., and Hillaire-Marcel, C.: Ocean forcing of Ice Sheet retreat in central west Greenland from LGM to the early Holocene, Earth Planet. Sci. Lett., 472, 1–13, https://doi.org/10.1016/j.epsl.2017.05.007, 2017.

Jones, G. A.: The central Arctic Ocean sediment record: Current progress in moving from a litho- to a chronostratigraphy, Polar Res., 5, 309–311, https://doi.org/10.3402/polar.v5i3.6898, 1987.

Jones, R. W.: The Challenger Foraminifera, 1995, Oxford University Press, Oxford, 149 pp., https://doi.org/10.1017/S0025315400018452, 1994.

Jones, R. W., Bender, H., Charnock, M. A., Kaminski, M. A., and Whittaker, J. E.: Emendation of the foraminiferal genus *Cribrostomoides* Cushman, 1910, and its taxonomic implications. J. Micropalaeontol., 12, 181–193, https://doi/org.10.1144/jm.12.2.181, 1993.

Jorissen, F. J.: Benthic foraminiferal microhabitats below the sediment-water interface, in: Modern Foraminifera, edited by: Sen Gupta, B. K., Springer Netherlands, Dordrecht, 161–179, https://doi.org/10.1007/0-306-48104-9_10, 2003.

Jorissen, F. J., de Stigter, H. C., and Widmark, J. G. V.: A conceptual model explaining benthic foraminiferal microhabitats, Mar. Micropaleontol., 26, 3–15, https://doi.org/10.1016/0377-8398(95)00047-X, 1995.

Kaithwar, A., Singh, D. P., and Saraswat, R.: A highly diverse living benthic foraminiferal assemblage in the oxygen deficient zone of the southeastern Arabian Sea, Biodiv. Conserv., 29, 3925–3958, https://doi.org/10.1007/s10531-020-02056-9, 2020.

Kaminski, M. A., Silye, L., and Kender, S.: Miocene deep-water agglutinated foraminifera from IODP Hole M0002A, Lomonosov Ridge: faunal constraints for the opening of the Fram Strait, Micropaleontology, 55, 117–135, https://doi.org/10.47894/mpal.55.2.03, 2009.

Kaparulina, E., Strand, K., and Lunkka, J. P.: Provenance analysis of central Arctic Ocean sediments: Implications for circum-Arctic ice sheet dynamics and ocean circulation during Late Pleistocene, Quat. Sci. Rev., 147, 210–220, https://doi.org/0.1016/j.quascirev.2015.09.017, 2016.

Kaufman, D. S., Polyak, L., Adler, R., Channell, J. E. T., and Xuan, C.: Dating late Quaternary planktonic foraminifera *Neogloboquadrina pachyderma* from the Arctic Ocean using amino acid racemization, Paleoceanography, 23, PA3224, https://doi.org/10.1029/2008PA001618, 2008.

Kawagata, S., Hayward, B. W., Grenfell, H. R., and Sabaa, A.: Mid-Pleistocene extinction of deep-sea foraminifera in the North Atlantic Gateway (ODP sites 980 and 982),

Palaeogeogr. Palaeoclimatol. Palaeoecol., 221, 267–291, https://doi.org/10.1016/j.palaeo.2005.03.001, 2005.

Kawagata, S., Hayward, B. W., and Kuhnt, W.: Extinction of deep-sea foraminifera as a result of Pliocene–Pleistocene deep-sea circulation changes in the South China Sea (ODP Sites 1143 and 1146), Quat. Sci. Rev., 26, 808–827, https://doi.org/10.1016/j.quascirev.2006.10.011, 2007.

Kender, S. and Kaminski, M. A.: Arctic Ocean benthic foraminiferal faunal change associated with the onset of perennial sea ice in the Middle Miocene, J. Foraminifer. Res., 43, 99–109, https://doi.org/10.2113/gsjfr.43.1.99, 2013.

Kender, S., McClymont, E. L., Elmore, A. C., Emanuele, D., Leng, M. J., and Elderfield, H.: Mid Pleistocene foraminiferal mass extinction coupled with phytoplankton evolution, Nature Comm., 7, 11970, https://doi.org/10.1038/ncomms11970, 2016.

Kireenko, L., Tikhonova, A., Kozina, N., and Matul, A.: Image dataset of benthic foraminifera in multicorer and gravity corer sediments from north-western Scotland shelf (North Atlantic Ocean), Biodiv. Data J., 10, e87457, https://doi.org/10.3897/BDJ.10.e87457, 2022.

Kniazeva, O. and Korsun, S.: Seasonal data on Rose Bengal stained foraminifera in the head of Kongsfjorden, Svalbard, Data Brief, 25, 104040, https://doi.org/10.1016/j.dib.2019.104040, 2019.

Koho, K. A., de Nooijer, L. J., and Reichart, G. J.: Combining benthic foraminiferal ecology and shell Mn/Ca to deconvolve past bottom water oxygenation and paleoproductivity, Geochim. Cosmochim. Acta, 165, 294–306, https://doi.org/10.1016/j.gca.2015.06.003, 2015.

Lagoe, M. B.: Recent benthic foraminifera from the central Arctic Ocean, J. Foraminifer. Res., 7, 106–129, https://doi.org/10.2113/gsjfr.7.2.106, 1977.

Lazar, K. B. and Polyak, L.: Pleistocene benthic foraminifers in the Arctic Ocean: Implications for sea-ice and circulation history, Mar. Micropaleontol., 126, 19–30, https://doi.org/10.1016/j.marmicro.2016.04.004, 2016.

Lazar, K., Polyak, L., and Dipre, G.: Re-examination of the use of *Cassidulina neoteretis* as a Pleistocene biostratigraphic marker in the Arctic Ocean, J. Foraminifer. Res., 46, 115–123, https://doi.org/10.2113/gsjfr.46.2.115, 2016.

Lecroq, B., Gooday, A., and Pawlowski, J.: Global genetic homogeneity in the deep-sea foraminiferan *Epistominella exigua* (Rotaliida: Pseudoparrellidae), Zootaxa, 2096, 23–32, https://doi.org/10.11646/zootaxa.2096.1.4, 2009.

Lee, A. J. and Anderson, O. R. (Eds.): The Biology of Foraminifera, Academic Press, London, England, 368 pp., https://doi.org/10.1016/S0932-4739(11)80246-4, 1991.

Linke, P.: Metabolic adaptations of deep-sea benthic foraminifera to seasonally varying food input, Mar. Ecol. Prog. Ser., 81, 51–63, https://doi.org/10.3354/meps081051, 1992.

Linke, P. and Lutze, G. F.: Microhabitat preferences of benthic foraminifera – a static concept or a dynamic adaptation to optimize food acquisition?, Mar. Micropaleontol., 20, 215–234, https://doi.org/10.1016/0377-8398(93)90034-U, 1993.

Linke, P., Altenbach, A.V., Graf, G., and Heeger, T.: Response of deep-sea foraminifera to a simulated sedimentation event, J. Foraminifer. Res., 25, 75–92, https://doi.org/10.2113/gsjfr.25.1.75, 1995.

Lohmann, G. P.: Abyssal benthonic foraminifera as hydrographic indicators in the western South Atlantic Ocean, J. Foraminifer. Res., 8, 6–34, https//doi.org/10.2113/gsjfr.8.1.6, 1978.

Loubere, P. and Rayray, S.: Benthic foraminiferal assemblage formation: theory and observation for the European Arctic margin, Deep-Sea Research Part I: Oceanogr. Res. Pap., 115, 36–47, https://doi.org/10.1016/j.dsr.2016.05.004, 2016.

Loubere, P., Gary, A., and Lagoe, M.: Generation of the benthic foraminiferal assemblage: Theory and preliminary data, Mar. Micropaleontol., 20, 165–181, https://doi.org/10.1016/0377-8398(93)90031-R, 1993.

Löwemark, L., März, C., O'Regan, M., and Gyllencreutz, R.: Arctic Ocean Mn-stratigraphy: genesis, synthesis and inter-basin correlation, Quat. Sci. Rev., 92, 97–111, https://doi.org/10.1016/j.quascirev.2013.11.018, 2014.

Mackensen, A. and Hald, M.: *Cassidulina teretis* Tappan and *C. laevigata* d'Orbigny; their modern and late Quaternary distribution in northern seas, J. Foraminifer. Res., 18, 16–24, https://doi.org/10.2113/gsjfr.18.1.16, 1988.

Mackensen, A., Sejrup, H. P., and Jansen, E.: The distribution of living benthic foraminifera on the continental slope and rise off southwest Norway, Mar. Micropaleontol., 9, 275–306, https://doi.org/10.1016/0377-8398(85)90001-5, 1985.

Mackensen, A., Grobe, H., Kuhn, G., and Fütterer, D. K.: Benthic foraminiferal assemblages from the eastern Weddell Sea between 68 and 73° S: Distribution, ecology and fossilization potential, Mar. Micropaleontol., 16, 241–283, https://doi.org/10.1016/0377-8398(90)90006-8, 1990.

Mackensen, A., Schumacher, S., Radke, J., and Schmidt, D. N.: Microhabitat preferences and stable carbon isotopes of endobenthic foraminifera: clue to quantitative reconstruction of oceanic new production?, Mar. Micropaleontol., 40, 233–258, https://doi.org/10.1016/S0377-8398(00)00040-2, 2000.

Mancin, N., Hayward, B. W., Trattenero, I., Cobianchi, M., and Lupi, C.: Can the morphology of deep-sea benthic foraminifera reveal what caused their extinction during the mid-Pleistocene climate transition?, Mar. Micropaleontol., 104, 53–70, https://doi.org/10.1016/j.marmicro.2013.09.004, 2013.

Mar, F.-M.: Primary productivity in Arctic sea ice and ocean, Ph.D. thesis, University Bremen, Bremen, Germany, 289 pp., https://nbn-resolving.de/urn:nbn:de:gbv:46-00104070-11 (last access: 20 July 2026), 2014.

Martin, R. E.: Taphonomy and temporal resolution of foraminiferal assemblages, in: Modern Foraminifera, Kluwer Academic Publishers New York, Boston, Dordrecht, London, Moscow, edited by: Sen Gupta, B. K., 281–298, https://doi.org/10.1007/0-306-48104-9_16, 2003.

März, C., Stratmann, A., Matthiessen, J., Meinhardt, A. K., Eckert, S., Schnetger, B., Vogt, C., Stein, R., and Brumsack, H. J.: Manganese-rich brown layers in Arctic Ocean sediments: Composition, formation mechanisms, and diagenetic overprint, Geochim. Cosmochim. Acta, 75, 7668–7687, https://doi.org/10.1016/j.gca.2011.09.046, 2011.

Matthiessen, J.: Linescanner images of sediment core PS72/340-5, PANGAEA [data set], https://doi.org/10.1594/PANGAEA.817500, 2013a.

Matthiessen, J.: Linescanner images of sediment core PS72/396-5, PANGAEA [data set], https://doi.org/10.1594/PANGAEA.817507, 2013b.

Matthiessen, J., Niessen, F., Stein, R., and Naafs, B. D. A.: Pleistocene Glacial Marine Sedimentary Environments at the Eastern Mendeleev Ridge, Arctic Ocean, Polarforsch. 79, 123–137, 2010.

Matthiessen, J., Schreck, M., De Schepper, S., Zorzi, C., and de Vernal, A.: Quaternary dinoflagellate cysts in the Arctic Ocean: Potential and limitations for stratigraphy and paleoenvironmental reconstructions, Quat. Sci. Rev., 192, 1–26, https://doi.org/10.1016/j.quascirev.2017.12.020, 2018.

McKinney, M. L.: Taxonomic selectivity and continuous variation in mass and background extinctions of marine taxa, Nature, 325, 143–145, https://doi.org/10.1038/325143a0, 1987.

McNeill, D. H.: New foraminifera from the Upper Cretaceous and Cenozoic of the Beaufort-Mackenzie Basin of Arctic Canada, Cushm. Found. Foram. Res. Spec. Publ. 35, 95 p., 1997.

Mead, G. A. and Kennett, J. P.: The distribution of Recent benthic foraminifera in the Polar Front region, southwest Atlantic, Mar. Micropaleontol., 11, 343–360, https://doi.org/10.1016/0377-8398(87)90006-5, 1987.

Minicucci, D. A. and Clark, D. L. C.: A late Cenozoic stratigraphy for glacial-marine sediments of the eastern Alpha Cordillera, Central Arctic Ocean, in: Glacial-marine sedimentation, edited by: Molnia, B. F., Springer, Boston, MA, 331–365, https://doi.org/10.1007/978-1-4613-3793-5_8, 1983.

Moodley, L., Middelburg, J., Boschker, H., Duineveld, G., Pel, R., Herman, P., and Heip, C.: Bacteria and foraminifera: key players in a short-term deep-sea benthic response to phytodetritus, Mar. Ecol. Prog. Ser., 236, 23–29, https://doi.org/10.3354/meps236023, 2002.

Morris, T. H., Clark, D. L., and Blasco, S. M.: Sediments of the Lomonosov Ridge and Makarov Basin: a Pleistocene stratigraphy for the North Pole, Geol. Soc. Amer. Bull., 96, 901–910, https://doi.org/10.1130/0016-7606(1985)96<901:sotlra>2.0.co;2, 1985.

Mudie, P. J.: Palynology of the Cesar cores, Alpha Ridge, in: Initial geological report on CESAR – the Canadian expedition to study the Alpha Ridge, Arctic Ocean, edited by: Jackson, H. R., Mudie, P. J., and Blasco, S. M., Geol. Surv. Can. Pap., 84–22, 149–174, https://doi.org/10.4095/120315, 1985.

Mudie, P. J. and Blasco, S. M.: Lithostratigraphy of the Cesar cores, in: Initial geological report on CESAR - the Canadian expedition to study the Alpha Ridge, Arctic Ocean, edited by: Jackson, H. R., Mudie, P. J., and Blasco, S. M., Geol. Surv. Can. Pap., 84–22, 59–99, https://doi.org/10.4095/120315, 1985.

Mullen, M. W. and McNeil, D. H.: Biostratigraphic and paleoclimatic significance of a new Pliocene foraminiferal fauna from the central Arctic Ocean, Mar. Micropaleontol., 26, 273–280, https://doi.org/10.1016/0377-8398(96)87758-9, 1995.

Murray, J.: An illustrated guide to the benthic foraminifera of the Hebridean Shelf, west of Scotland, with notes on their mode of life, Palaeontologia Electronica 5, 1, 31 pp, https://palaeo-electronica.org/2002_2/guide/guide.pdf (last access: 20 July 2026), 2003.

Murray, J. and Alve, E.: The distribution of agglutinated foraminifera in NW European seas: Baseline data for the interpretation of fossil assemblages, Palaeontologia Electronica 14.2.14A, 41 p, https://palaeo-electronica.org/2011_2/248/248.pdf (last access: 20 July 2026), 2011.

Murray, J. W.: Ecology and palaeoecology of benthic Foraminifera, Logman Scientific & Technical, London, 71, 397 pp., https://doi.org/10.4324/9781315846101, 1991.

Murray, J. W.: Ecology and Applications of Benthic Foraminifera, Cambridge University Press, Cambridge, 27–60 pp., https://doi.org/10.1017/CBO9780511535529, 2006.

Nees, S.: High-resolution benthic foraminiferal records of the last glacial termination in the northern North Atlantic, in: Contributions to the Micropaleontology and Paleoceanography of the Northern North Atlantic, edited by: Hass, H. C. and Kaminski, M. A., Gryzbowski Found. Spec, Publ., 5, pp. 167–197, https://doi.org/10.1130/0091-7613(1997)025<0659:HRROFR>2.3.CO;2, 1997.

Nees, S. and Struck, U.: The biostratigraphic and paleoceanographic significance of *Siphotextularia rolshauseni* Phleger and Parker in Norwegian-Greenland Sea sediments, J. Foraminifer. Res., 24, 233–240, https://doi.org/10.2113/gsjfr.24.4.233, 1994.

Nguyen, N.-L.: Metabarcoding reveals high diversity of benthic foraminifera linked to water masses circulation at coastal Svalbard, Geobiology, 21, 1–18, https://doi.org/10.1111/gbi.12530, 2022.

Nguyen, N.-L., Pawłowska, J., Szymańska, N., Zajączkowski, M., Weiner, A., De Schepper, S., and Pawlowski, J.: Assessing the passive dispersal of benthic foraminifera through environmental DNA, Limnol. Oceanogr., 71, e70294, https://doi.org/10.1002/lno.70294, 2025.

Niessen, F.: Physical properties of sediment core PS72/340-5, PANGAEA [data set], https://doi.org/10.1594/PANGAEA.737861, 2010a.

Niessen, F.: Physical properties of sediment core PS72/396-5, PANGAEA [data set], https://doi.org/10.1594/PANGAEA.737871, 2010b.

Nørgaard-Pedersen, N., Mikkelsen, N., and Kristoffersen, Y.: Arctic Ocean record of last two glacial-interglacial cycles off North Greenland/Ellesmere Island – Implications for glacial history, Mar. Geol., 244, 93–108, https://doi.org/10.1016/j.margeo.2007.06.008, 2007a.

Nørgaard-Pedersen, N., Mikkelsen, N., Lassen, S. J., Kristoffersen, Y., and Sheldon, E.: Reduced sea ice concentrations in the Arctic Ocean during the last interglacial period revealed by sediment cores off northern Greenland, Paleoceanography, 22, PA1218, https://doi.org/10.1029/2006PA001283, 2007b.

Nowicki, M., DeVries, T., and Siegel, D. A.: Quantifying the carbon export and sequestration pathways of the Ocean's biological carbon pump, Global Biogeochem. Cycle, 36, e2021GB007083, https://doi.org/10.1029/2021GB007083, 2022.

O'Neill, B. J.: Pliocene and Pleistocene benthic foraminifera from the central Arctic Ocean, J. Paleontol., 55, 1141–1170, https://www.jstor.org/stable/1304546 (last access: 20 July 2026), 1981.

O'Regan, M., Coxall, H. K., Cronin, T. M., Gyllencreutz, R., Jakobsson, M., Kaboth, S., Löwemark, L., Wiers, S., and West, G.: Stratigraphic occurrences of sub-polar planktic foraminifera in Pleistocene sediments on the Lomonosov Ridge, Arctic Ocean, Front. Earth Sci., 7, https://doi.org/10.3389/feart.2019.00071, 2019.

O'Regan, M., Jakobsson, M., and Moran, K.: Did the central Arctic became a sediment-starved basin in the Quaternary? Mar. Geol., 494, 1107729, https://doi.org/10.1016/j.margeo.2026.107729, 2026.

Osterman, L. E.: Pliocene and Quaternary benthic foraminiferal biostratigraphy from Site 910, Yermak Plateau, in: Proc. Ocean Drilling Progr., Sci. Res., edited by: Thiede, J., Myhre, A., Firth, J. V., Johnson, G. L., and Ruddiman, W. F., ODP, College Station, 187–195, https://doi.org/10.2973/odp.proc.sr.151.107.1996, 1996.

Osterman, L. E. and Qvale, G.: Benthic foraminifers from the Vøring Plateau (ODP Leg 104), in: Proc. ODP, Sci. Results, edited by: Eldholm, O., Thiede, J., Taylor, E., and Barton, C., College Station, TX (ODP), 745–768, https://doi.org/10.2973/odp.proc.sr.104.159.1989, 1989.

Osterman, L. E., Poore, R. Z., and Foley, K. M.: Distribution of benthic foraminifers (> 125 µm) in the surface sediments of the Arctic Ocean, U.S. Geol. Surv. Bull. 2164, 1–28, https://doi.org/10.3133/b2164, 1999.

Pak, D. K., Clark, D. L., and Blasco, S. M.: Late Pleistocene stratigraphy and micropaleontology of a part of the Eurasian basin (=Fram Basin), central Arctic Ocean, Mar. Micropaleontol., 20, 1–22, https://doi.org/10.1016/0377-8398(92)90006-6, 1992.

Park, K., Kim, J.-H., Asahi, H., Polyak, L., Khim, B.-K., Schreck, M., Niessen, F., Kong, G. S., and Nam, S.-I.: Cyclostratigraphic age constraining for Quaternary sediments in the Makarov Basin of the western Arctic Ocean using manganese variability, Quat. Geochronol., 55, 101021, https://doi.org/10.1016/j.quageo.2019.101021, 2020.

Parker, F. L., Phleger, F. B., and Peirson, J. F.: Ecology of Foraminifera from San Antonio Bay and Environs, Southwest Texas, Cushman Found. Foraminifer. Res. Spec. Publ., 2, 75 pp., 1953.

Parker, W. K., Jones, T. R., and Brady, H. B.: On the nomenclature of the Foraminifera. Part XIV. The species enumerated by D'Orbigny in the 'Annales des Sciences Naturelles,' 1826, vol. vii.–iv. The species founded upon the figures in Soldani's "Testaceographia ac Zoophytogeographia", [Cont. from vol. iv. p. 392.], Ann. Mag. Nat. Hist., 29–40, 1871.

Pawlowski, J., Bowser, S. S., and Gooday, A. J.: A note on the genetic similarity between shallow- and deep-water *Epistominella vitrea* (Foraminifera) in the Antarctic, Deep-Sea Res. II: Top. Stud. Oceanogr., 54, 1720–1726, https://doi.org/10.1016/j.dsr2.2007.07.016, 2007.

Pflum, C. E. an dFrerichs, W. E.: Gulf of Mexico deep-water foraminifers, Cushman Found. Foraminifer. Res. Spec. Publ., 14, 124 pp., 1976.

Phillips, R. L. and Grantz, A.: Quaternary history of sea ice and paleoclimate in the Amerasia basin, Arctic Ocean, as recorded in the cyclical strata of Northwind Ridge, Geol. Soc. Am. Bull., 109, 1101–1115, https://doi.org/10.1130/0016-7606(1997)109<1101:QHOSIA>2.3.CO;2, 1997.

Phleger, F. B., Parker, F. L., and Pierson, J. F.: North Atlantic foraminifera, Reports of the Swedish Deep-Sea Expedition, 1947–1948, 7, 3–122, 1953.

Poirier, R. K., Gaetano, M. Q., Acevedo, K., Schaller, M. F., Raymo, M. E., and Kozdon, R.: Quantifying diagenesis, contributing factors, and resulting isotopic bias in benthic foraminifera using the foraminiferal preservation index: Implications for geochemical proxy records, Paleoceanogr. Paleoclimatol., 36, e2020PA004110, https://doi.org/10.1029/2020PA004110, 2021.

Polyak, L. and Solheim, A.: Late- and postglacial environments in the northern Barents Sea west of Franz Josef Land, Polar Res., 13, 197–207, https://doi.org/10.3402/polar.v13i2.6693, 1994.

Polyak, L., Korsun, S., Febo, L. A., Stanovoy, V., Khusid, T., Hald, M., Paulsen, B. E., and Lubinski, D. J.: Benthic foraminiferal assemblages from the southern Kara Sea, a river-influenced arctic marine environment, J. Foraminifer. Res., 32, 252–273, https://doi.org/10.2113/32.3.252, 2002.

Polyak, L., Curry, W. B., Darby, D. A., Bischof, J., and Cronin, T. M.: Contrasting glacial/interglacial regimes in the western Arctic Ocean as exemplified by a sedimentary record from the Mendeleev Ridge, Palaeogeogr. Palaeoclimatol. Palaeoecol., 203, 73–93, https://doi.org/10.1016/S0031-0182(03)00661-8, 2004.

Polyak, L., Alley, R. B., Andrews, J. T., Brigham-Grette, J., Cronin, T. M., Darby, D. A., Dyke, A. S., Fitzpatrick, J. J., Funder, S., Holland, M., Jennings, A. E., Miller, G. H., O'Regan, M., Savelle, J., Serreze, M., St. John, K., White, J. W. C., and Wolff, E.: History of sea ice in the Arctic, Quat. Sci. Rev., 29, 1757–1778, https://doi.org/10.1016/j.quascirev.2010.02.010, 2010.

Polyak, L., Best, K. M., Crawford, K. A., Council, E. A., and St-Onge, G.: Quaternary history of sea ice in the western Arctic Ocean based on foraminifera, Quat. Sci. Rev., 79, 145–156, https://doi.org/10.1016/j.quascirev.2012.12.018, 2013.

Poore, R. Z., Phillips, R. L., and Rieck, H. J.: Paleoclimatic record for Northwind Ridge, western Arctic Ocean, Paleoceanography, 8, 149–159, https://doi.org/10.1029/93PA00146, 1993.

Poore, R. Z., Ishman, S. E., Phillips, R. L., and McNeil, D. H.: Quaternary stratigraphy and paleoceanography of the Canada Basin, western Arctic Ocean, Bull. U.S. Geol. Surv., 2080, 32 pp., https://doi.org/10.3133/b2080, 1994.

Rasmussen, J. A. and Sheldon, E.: Microfossil biostratigraphy of the Palaeogene succession in the Davis Strait, offshore West Greenland, Mar. Pet. Geol., 20, 1017–1030, https://doi.org/10.1016/S0264-8172(02)00114-9, 2003.

Rasmussen, T. L. and Thomsen, E.: Warm Atlantic surface water inflow to the Nordic seas 34–10 calibrated ka B.P, Paleoceanography, 23, PA1201, https://doi.org/10.1029/2007pa001453, 2008.

Rasmussen, T. L., Thomsen, E., and Nielsen, T.: Water mass exchange between the Nordic seas and the Arctic Ocean on millennial timescale during MIS 4–MIS 2, Geochem. Geophys. Geosyst., 15, 530–544, https://doi.org/10.1002/2013GC005020, 2014.

Rasmussen, T. L., Oppo, D. W., Thomsen, E., and Lehman, S. J.: Deep sea records from the southeast Labrador Sea: Ocean circulation changes and ice-rafting events during the last 160,000 years, Paleoceanography, 18, 1018, https://doi.org/10.1029/2001pa000736, 2003a.

Rasmussen, T. L., Thomsen, E., Kuijpers, A., and Wastegard, S.: Late warming and early cooling of the sea surface in the Nordic seas during MIS 5e (Eemian Interglacial), Quat. Sci. Rev., 22, 809–821, https://doi.org/10.1016/S0277-3791(02)00254-8, 2003b.

Rasmussen, T. L., Thomsen, E., Slubowska, M. A., Jessen, S., Solheim, A., and Koc, N.: Paleoceanographic evolution of the SW Svalbard margin (76°N) since 20,000 14C yr BP, Quat. Res., 67, 100–114, https://doi.org/10.1016/j.yqres.2006.07.002, 2007.

Razmjooei, M. J., Henderiks, J., Coxall, H. K., Baumann, K.-H., Vermassen, F., Jakobsson, M., Niessen, F., and O'Regan, M.:

Revision of the Quaternary calcareous nannofossil biochronology of Arctic Ocean sediments, Quat. Sci. Rev., 321, 108382, https://doi.org/10.1016/j.quascirev.2023.108382, 2023.

Reuss, A. E.: Ueber die fossilen Foraminiferen und Entomostraceen der Septarienthone der Umgegend von Berlin, Zeitschr. Deut. Geol. Gesell., 3, 49–92, 1851.

Roca-Martí, M., Puigcorbé, V., Loeff, M., Katlein, C., Fernández-Méndez, M., Peeken, I., and Masqué, P.: Carbon export fluxes and export efficiency in the central Arctic during the record sea-ice minimum in 2012: a joint $^{234}Th/^{238}U$ and $^{210}Po/^{210}Pb$ study, J. Geophys. Res.-Oceans, 121, 5030–5049, https://doi.org/10.1002/2016JC011816, 2016.

Rudels, B. and Carmack, E.: Arctic Ocean water mass structure and circulation, Oceanography, 35, 3–4, 52–65, https://doi.org/10.5670/oceanog.2022.116, 2022.

Saidova, K. M.: Deep-water foraminifera communities of the Arctic Ocean, Oceanology, 51, 60–68, https://doi.org/10.1134/S0001437011010152, 2011.

Saraswat, R., Kurtarkar, S. R., Saalim, S. M., Bhadra, S. R., and Gawas, A. M.: Freeze – drying partially affects dead benthic foraminiferal shells in estuarine sediments, J. Palaeontol. Soc. India, 65, 178–184, https://doi.org/10.1177/0971102320200205, 2020.

Schmiedl, G., Mitschele, A., Beck, S., Emeis, K.-C., Hemleben, C., Schulz, H., Sperling, M., and Weldeab, S.: Benthic foraminiferal record of ecosystem variability in the eastern Mediterranean Sea during times of sapropel S5 and S6 deposition, Palaeogeogr. Palaeoclimatol. Palaeoecol., 190, 139–164, https://doi.org/10.1016/S0031-0182(02)00603-X, 2003.

Schneider, C. A., Rasband, W. S., and Eliceiri, K. W.: NIH Image to ImageJ: 25 years of image analysis, Nature Meth., 9, 671, https://doi.org/10.1038/nmeth.2089, 2012.

Schoster, F.: Geochemistry of sediment core PS2185-6, PANGAEA [data set], https://doi.org/10.1594/PANGAEA.227857, 2005.

Sperling, M., Weldeab, S., and Schmiedl, G.: Drying of samples may alter foraminiferal isotopic ratios and faunistic composition, Micropaleontology, 48, 87–91, https://doi.org/10.1661/0026-2803(2002)048[0087:DOSMAF]2.0.CO;2, 2002.

Schröder, C.: Subsurface preservation of agglutinated foraminifera in the northwest Atlantic Ocean, Abh. Geol. B.-A., 41, 325–336, 1988.

Schröder, C. J.: Deep-water Arenaceous Foraminifera in the Northwest Atlantic Ocean, Canadian Technical Rep. Hydrogr. Ocean Sci, 71, 205 pp., http://hdl.handle.net/10222/75109 (last access: 20 July 2026), 1986.

Schroeder, C. J., Scott, D. B., and Medioli, F. S.: Can smaller benthic foraminifera be ignored in paleoenvironmental analyses?, J. Foraminifer. Res., 17, 101–105, https://doi.org/10.2113/gsjfr.17.2.101, 1987.

Scott, D. B. and Vilks, G.: Benthic foraminifera in the surface sediments of the deep-sea Arctic Ocean, J. Foraminifer. Res., 21, 20–38, https://doi.org/10.2113/gsjfr.21.1.20, 1991.

Scott, D. B., Mudie, P. J., Baki, V., MacKinnon, K. E., and Cole, F. E.: Biostratigraphy and late Cenozoic paleoceanography of the Arctic Ocean: Foraminiferal, lithostratigraphic, and isotopic evidence, Geol. Soc. Am. Bull., 101, 260–277, https://doi.org/10.1130/0016-7606(1989)101<0260:BALCPO>2.3.CO;2, 1989.

Scott, D. B., Schell, T., Rochon, A., and Blasco, S.: Benthic foraminifera in the surface sediments of the Beaufort Shelf and slope, Beaufort Sea, Canada: Applications and implications for past sea-ice conditions, J. Mar. Syst., 74, 840–863, https://doi.org/10.1016/j.jmarsys.2008.01.008, 2008.

Scott, D. B., Schell, T., St-Onge, G., Rochon, A., and Blasco, S.: Foraminiferal assemblage changes over the last 15,000 years on the Mackenzie-Beaufort Sea Slope and Amundsen Gulf, Canada: Implications for past sea ice conditions, Paleoceanography, 24, PA2219, https://doi.org/10.1029/2007PA001575, 2009.

Seidenkrantz, M. S.: *Cassidulina teretis* Tappan and *Cassidulina neoteretis* new species (Foraminifera): stratigraphic markers for deep sea and outer shelf areas, J. Micropalaeontol., 14, 145–157, https://doi.org/10.1144/jm.14.2.145, 1995.

Seidenkrantz, M.-S.: Benthic foraminifera as palaeo sea-ice indicators in the subarctic realm – examples from the Labrador Sea–Baffin Bay region, Quat. Sci. Rev., 79, 135–144, https://doi.org/10.1016/j.quascirev.2013.03.014, 2013.

Sellén, E., Jakobsson, M., and Backman, J.: Sedimentary regimes in Arctic's Amerasian and Eurasian Basins: Clues to differences in sedimentation rates, Glob. Planet. Change., 61, 275–284, https://doi.org/10.1016/j.gloplacha.2007.10.007, 2008.

Sellén, E., O'Regan, M., and Jakobsson, M.: Spatial and temporal Arctic Ocean depositional regimes: a key to the evolution of ice drift and current patterns, Quat. Sci. Rev., 29, 3644–3664, https://doi.org/10.1016/j.quascirev.2010.06.005, 2010.

Sirenko, B. I., Burhinskaja, G. N., Andriashev, A. P., Balushkin, A. V., Neyelov, A. V., Markhaseva, E. L., Stepanjants, S. D., and Lukina, T. G., Alimov, A. F. (Eds.): List of species of free-living invertebrates of Eurasian Arctic Seas and adjacent deep water, Explorations of the fauna of the seas, 51 (59), edited by: Sirenko, B. I., St.-Petersburg, 129 pp., 2001.

Song, T., Hillaire-Marcel, C., Liu, Y., Ghaleb, B., and de Vernal, A.: Cycling and behavior of ^{230}Th in the Arctic Ocean: Insights from sedimentary archives, Earth Sci. Rev., 244, 104514, https://doi.org/10.1016/j.earscirev.2023.104514, 2023.

Spezzaferri, S., Rüggeberg, A., Stalder, C., and Margreth, S.: Benthic foraminifer assemblages from Norwegian cold-water coral reefs, J. Foraminifer. Res., 43, 21–39, https://doi.org/10.2113/gsjfr.43.1.21, 2013.

Spielhagen, R. F., Bonani, G., Eisenhauer, A., Frank, M., Frederichs, T., Kassens, H., Kubik, P. W., Mangini, A., Nørgaard-Pedersen, N., Nowaczyk, N. R., Schäper, S., Stein, R., Thiede, J., Tiedemann, R., and Wahsner, M.: Arctic Ocean evidence for late Quaternary initiation of northern Eurasian ice sheets, Geology, 25, 783–786, https://doi.org/10.1130/0091-7613(1997)025<0783:AOEFLQ>2.3.CO;2, 1997a.

Spielhagen, R. F., Bonani, G., Eisenhauer, A., Frank, M., Frederichs, T., Kassens, H., Kubik, P. W., Mangini, A., Nørgaard-Pedersen, N., Nowaczyk, N. R., Schäper, S., Stein, R., Thiede, J., Tiedemann, R., and Wahsner, M.: Figure 2. Sedimentology of core PS2185-6, PANGAEA [data set], https://doi.org/10.1594/PANGAEA.713859, 1997b.

Spielhagen, R. F., Baumann, K.-H., Erlenkeuser, H., Nowaczyk, N. R., Nørgaard-Pedersen, N., Vogt, C., and Weiel, D.: Arctic Ocean deep-sea record of northern Eurasian ice sheet history, Quat. Sci. Rev., 23, 1455–1483, https://doi.org/10.1016/j.quascirev.2003.12.015, 2004.

Stärz, M.: Stratigraphie und Paläoumwelt im Arktischen Ozean während des mittleren Pleistozäns: Rekonstruktion aus Sedimentabfolgen vom Lomonosov-Rücken, Fakultät für Geowissenschaften, Geotechnik und Bergbau der Technischen Universität Bergakademie Freiberg, 105 pp., 2008.

Stein, R., Matthiessen, J., and Niessen, F.: Re-coring at Ice Island T3 site of key core FL-224 (Nautilus Basin, Amerasian Arctic): sediment characteristics and stratigraphic framework, Polarforsch., 79, 81–96, https://doi.org/10.2312/polarforschung.79.2.81, 2010a.

Stein, R., Matthiessen, J., Niessen, F., Krylov, R., Nam, S., and Bazhenova, E.: Towards a better (litho-) stratigraphy and reconstruction of Quaternary paleoenvironment in the Amerasian Basin (Arctic Ocean), Polarforsch., 79, 97–121, 2010b.

Steinsund, P. I. and Hald, M.: Recent calcium carbonate dissolution in the Barents Sea: Paleoceanographic applications, Mar. Geol., 117, 303–316, https://doi.org/10.1016/0025-3227(94)90022-1, 1994.

Struck, U.: Stepwise postglacial migration of benthic foraminifera into the abyssal northeastern Norwegian Sea, Mar. Micropaleontol., 26, 207–213, https://doi.org/10.1016/0377-8398(95)00034-8, 1995.

Swoboda, S., Krumpen, T., Nöthig, E.-M., Metfies, K., Ramondenc, S., Wollenburg, J., Fahl, K., Peeken, I., and Iversen, M.: Release of ballast material during sea-ice melt enhances carbon export in the Arctic Ocean, PNAS Nexus, 3, pgae081, https://doi.org/10.1093/pnasnexus/pgae081, 2024.

Sztybor, K. and Rasmussen, T.: Late glacial and deglacial palaeoceanographic changes at Vestnesa Ridge, Fram Strait: Methane seep versus non-seep environments, Palaeogeogr. Palaeoclimatol. Palaeoecol., 476, 77–89, https://doi.org/10.1016/j.palaeo.2017.04.001, 2017.

Thies, A.: Die Benthos-Foraminiferen im Europäischen Nordmeer, Ber. SFB 313, Kiel, Germany, 144, https://doi.org/10.2312/reports-sfb313.1991.31, 1991.

Thomas, E.: Cenozoic mass extinctions in the deep sea; what disturbs the largest habitat on Earth?, in: Large Ecosystem Perturbations: Causes and Consequences, edited by: Monechi, S., Coccioni, R., and Rampino, M., Geol. Soc. Amer. Spec. Pap. 424, 23 pp., https://doi.org/10.1130/2007.2424(01), 2007.

Thomas, E., Booth, L., Maslin, M., and Shackleton, N. J.: Northeastern Atlantic benthic foraminifera during the last 45,000 years: Changes in productivity seen from the bottom up, Paleoceanography, 10, 545–562, https://doi.org/10.1029/94PA03056, 1995.

Timmermans, M.-L. and Marshall, J.: Understanding Arctic Ocean circulation: A review of ocean dynamics in a changing climate, J. Geophys. Res.-Oceans, 125, e2018JC014378, https://doi.org/10.1029/2018JC014378, 2020.

Todd, R. and Low, D.: Foraminifera from the Kara and Greenland Seas, and review of arctic studies, U.S. Geol. Surv. Prof. Paper 1070, 30 pp., https://doi.org/10.3133/pp1070, 1980.

Tsuchiya, M., Tazume, M., and Kitazato, H.: Molecular characterization of the non-costate morphotypes of buliminid foraminifers based on internal transcribed region of ribosomal DNA (ITS rDNA) sequence data, Mar. Micropaleontol., 69, 212–224, https://doi.org/10.1016/j.marmicro.2008.07.008, 2008.

Van Morkhoven, F. P. C. M., Berggren, W. A., and Edwards, A. S.: Cenozoic Cosmopolitan Deep-water Benthic Foraminifera, Bull. Centr. Rech. Expl.-Prod. Elf-Aquitaine, Mem., 11, 423 pp., 1986.

Vermassen, F., O'Regan, M., West, G., Cronin, T. M., and Coxall, H. K.: Testing the stratigraphic consistency of Pleistocene microfossil bioevents identified on the Alpha and Lomonosov ridges, Arctic Ocean, Arctic, Antarctic, Alpine Res., 53, 309–323, https:/doi.org/10.1080/15230430.2021.1988356, 2021.

Wang, R., Polyak, L., Xiao, W., Wu, L., Zhang, T., Sun, Y., and Xu, X.: Late-Middle Quaternary lithostratigraphy and sedimentation patterns on the Alpha Ridge, central Arctic Ocean: Implications for Arctic climate variability on orbital time scales, Quat. Sci. Rev., 181, 93–108, https://doi.org/10.1016/j.quascirev.2017.12.006, 2018.

Wang, W., Zhao, M., Yang, J., Xiao, W., Wang, H., and Liu, Y.: The marine environmental evolution in the northern Norwegian Sea revealed by foraminifera during the last 60 ka, Adv. Polar Sci., 32, 210–220, https://doi.org/10.13679/j.advps.2021.0020, 2021.

Wefing, A. M., Casacuberta, N., Christl, M., Gruber, N., and Smith, J. N.: Circulation timescales of Atlantic Water in the Arctic Ocean determined from anthropogenic radionuclides, Ocean Sci., 17, 111–129, https://doi.org/10.5194/os-17-111-2021, 2021.

West, G., Kaufman, D. S., Jakobsson, M., and O'Regan, M.: Amino acid racemization in *Neogloboquadrina pachyderma* and *Cibicidoides wuellerstorfi* from the Arctic Ocean and its implications for age models, Geochronology, 5, 285–299, https://doi.org/10.5194/gchron-5-285-2023, 2023.

Williamson, W. C.: On the recent Foraminifera of Great Britain, The Ray Society, London, 1–107, 1858.

Wollenburg, J.: Taxonomic notes on recent benthic foraminifera from Nansen Basin, Arctic Ocean, Ber. Polarforsch., 112, 136 pp., https://doi.org/10.2312/BzP_0112_1992, 1992.

Wollenburg, J. E.: Benthic foraminiferal assemblages in the Arctic Ocean: indicators for water mass distribution, productivity, and sea ice drift, Ber. Polarforsch., 179, 227 pp., https://doi.org/10.2312/BzP_0179_1995, 1995.

Wollenburg, J. E. and Kuhnt, W.: The response of benthic foraminifers to carbon flux and primary production in the Arctic Ocean, Mar. Micropaleontol., 40, 189–231, https://doi.org/10.1016/S0377-8398(00)00039-6, 2000.

Wollenburg, J. E. and Mackensen, A.: Living benthic foraminifers from the central Arctic Ocean: faunal composition, standing stock and diversity, Mar. Micropaleontol., 34, 153–185, https://doi.org/10.1016/S0377-8398(98)00007-3, 1998a.

Wollenburg, J. E. and Mackensen, A.: On the vertical distribution of living (rose bengal stained) benthic foraminifers in the Arctic Ocean, J. Foraminifer. Res., 28, 268–285, https://doi.org/10.2113/gsjfr.28.4.268, 1998b.

Wollenburg, J. E. and Mackensen, A.: The ecology and distribution of benthic foraminifera at the Håkon Mosby mud volcano (SW Barents Sea slope), Deep Sea Res. Part I: Oceanographic Res. Pap., 56, 1336–1370, https://doi.org/10.1016/j.dsr.2009.02.004, 2009.

Wollenburg, J. E. and Matthiessen, J.: Benthic foraminiferal counts > 63 µm, and grain-size fractions absolute and relative abundances in sediment core PS72/396-5, PANGAEA [data set], https://doi.org/10.1594/PANGAEA.988969, 2026a.

Wollenburg, J. E. and Matthiessen, J.: Benthic foraminiferal counts > 63 µm, absolute and relative abundances in sediment core PS2185-6, PANGAEA [data set], https://doi.org/10.1594/PANGAEA.988971, 2026b.

Wollenburg, J. E. and Matthiessen, J.: Benthic foraminiferal counts > 63 µm, and grain-size fractions absolute and relative abundances in sediment core PS72/340-5, PANGAEA [data set], https://doi.org/10.1594/PANGAEA.988973, 2026c.

Wollenburg, J. E., Knies, J., and Mackensen, A.: High-resolution paleoproductivity fluctuations during the past 24 kyr as indicated by benthic foraminifera in the marginal Arctic Ocean, Palaeogeogr. Plaeoclimatol. Paleoecol., 204, 209–238, https://doi.org/10.1016/S0031-0182(03)00726-0, 2004.

Wollenburg, J. E., Kuhnt, W., and Mackensen, A.: (Table 2) Distribution of benthic foraminifers of sediment core PS2138-1, PANGAEA [data set], https://doi.org/10.1594/PANGAEA.56208, 2001a.

Wollenburg, J. E., Kuhnt, W., and Mackensen, A.: Changes in Arctic Ocean paleoproductivity and hydrography during the last 145 kyr: the benthic foraminiferal record, Paleoceanography, 16, 65–77, https://doi.org/10.1029/1999PA000454, 2001b.

Wollenburg, J. E., Kuhnt, W., and Mackensen, A.: (Table 4a) Distribution of benthic foraminifera of sediment core PS2212-3, PANGAEA [data set], https://doi.org/10.1594/PANGAEA.56209, 2001c.

Wollenburg, J. E., Kuhnt, W., and Mackensen, A.: (Table 4b) Distribution of benthic foraminifera of sediment core PS2212-3, PANGAEA [data set], https://doi.org/10.1594/PANGAEA.56213, 2001d.

Wollenburg, J. E., Mackensen, A., and Kuhnt, W.: Benthic foraminiferal biodiversity response to a changing Arctic palaeoclimate in the last 24.000 years, Palaeogeogr. Plaeoclimatol. Paleoecol., 255, 195–222, https://doi.org/10.1016/j.palaeo.2007.05.007, 2007.

Wollenburg, J. E., Raitzsch, M., and Tiedemann, R.: Novel high-pressure culture experiments on deep-sea benthic foraminifera – Evidence for methane seepage-related $\delta^{13}C$ of *Cibicides wuellerstorfi*, Mar. Micropaleontol., 117, 47–64, https://doi.org/10.1016/j.marmicro.2015.04.003, 2015.

Wollenburg, J. E., Matthiessen, J., Vogt, C., Nehrke, G., Grotheer, H., Wilhelms-Dick, D., Geibert, W., and Mollenhauer, G.: Omnipresent authigenic calcite distorts Arctic radiocarbon chronology, Commun. Earth Environ., 4, 136, https://doi.org/10.1038/s43247-023-00802-9, 2023a.

Wollenburg, J. E., Matthiessen, J., Vogt, C., Nehrke, G., Grotheer, H., Wilhelms-Dick, D., and Mollenhauer, G.: Omnipresent authigenic carbonates distort Arctic radiocarbon chronology, PANGAEA [data set], https://doi.org/10.1594/PANGAEA.938246, 2023b.

Xiao, W., Polyak, L., Wang, R., Löwemark, L., Mei, J., You, D., Wang, W., Wu, L., and Jin, X.: Middle to Late Pleistocene Arctic paleoceanographic changes based on sedimentary records from Mendeleev Ridge and Makarov Basin, Quat. Sci. Rev., 228, 106105, https://doi.org/10.1016/j.quascirev.2019.106105, 2020.

Yurco, L. N., Ortiz, J. D., Polyak, L., Darby, D. A., and Crawford, K. A.: Clay mineral cycles identified by diffuse spectral reflectance in Quaternary sediments from the Northwind Ridge: implications for glacial–interglacial sedimentation patterns in the Arctic Ocean, Polar Res., 29, 176–197, https://doi.org/10.1111/j.1751-8369.2010.00160.x, 2010.

Zhao, S., Dong, L., Shi, X., Polyak, L., Zou, X., Wang, W., and Wu, D.: Sedimentary record of glacial impacts and melt water discharge off the East Siberian Continental Margin, Arctic Ocean, J. Geophys. Res.-Oceans, 127, e2021JC017650, https://doi.org/10.1029/2021JC017650, 2022.